A spinal cord neuroprosthesis for locomotor deficits due to Parkinson's disease

Tomislav Milekovic, Eduardo Martin Moraud, Nicolo Macellari, Charlotte Moerman, Flavio Raschellà, Shiqi Sun, Matthew G Perich, Camille Varescon, Robin Demesmaeker, Alice Bruel, et al.

nature medicine

Article

https://doi.org/10.1038/s41591-023-02584-1

A spinal cord neuroprosthesis for locomotor deficits due to Parkinson's disease

Received: 6 July 2023

Accepted: 8 September 2023

Published online: 06 November 2023

Check for updates

A list of authors and their affiliations appears at the end of the paper

People with late-stage Parkinson's disease (PD) often suffer from debilitating locomotor deficits that are resistant to currently available therapies. To alleviate these deficits, we developed a neuroprosthesis operating in closed loop that targets the dorsal root entry zones innervating lumbosacral segments to reproduce the natural spatiotemporal activation of the lumbosacral spinal cord during walking. We first developed this neuroprosthesis in a non-human primate model that replicates locomotor deficits due to PD. This neuroprosthesis not only alleviated locomotor deficits but also restored skilled walking in this model. We then implanted the neuroprosthesis in a 62-year-old male with a 30-year history of PD who presented with severe gait impairments and frequent falls that were medically refractory to currently available therapies. We found that the neuroprosthesis interacted synergistically with deep brain stimulation of the subthalamic nucleus and dopaminergic replacement therapies to alleviate asymmetry and promote longer steps, improve balance and reduce freezing of gait. This neuroprosthesis opens new perspectives to reduce the severity of locomotor deficits in people with PD.

Approximately 90% of people with advanced Parkinson's disease (PD) experience locomotor deficits, which include gait impairments, balance problems and freezing-of-gait episodes[1,2]. These deficits severely reduce quality of life and increase comorbid conditions[3]. Unfortunately, these deficits respond poorly to currently available therapies, such as dopamine replacement strategies and deep brain stimulation (DBS) of the subthalamic nucleus[4–8]. These therapies often improve certain features of gait patterns but have limited impact on dopa-resistant components, such as gait initiation, balance, postural instability and freezing of gait[7]. An alternative strategy involves the delivery of continuous electrical stimulation over the cervical or thoracic segments of the spinal cord[9–14]. This stimulation aims to recruit ascending afferent fibers nested in the dorsal columns to modulate the activity of the basal ganglia and cerebral cortex[15,16]. Despite a reduction of locomotor deficits in some people with PD, the broader application of this strategy led to variable and unsatisfying outcomes[17–19]. Consequently, the identification of complementary therapies to alleviate locomotor deficits is defined as a priority for people with late-stage PD[7].

Although currently available therapies focus on the regions of the brain that are directly affected by the loss of dopamine-producing neurons, an alternative strategy may instead target the regions of the lumbosacral spinal cord that ultimately produce walking and is a priori not directly affected by PD. We, thus, hypothesized that strategies modulating the activity of the lumbosacral spinal cord may be effective to alleviate locomotor deficits due to PD.

Targeted epidural electrical stimulation (EES) of the lumbosacral spinal cord modulates the activity of motor neurons through the activation of large-diameter afferents where they enter the spinal cord through the dorsal root entry zones[20,21]. This physiological principle enables real-time control over the activity of leg motor neurons. Concretely, the individual dorsal root entry zones innervating lumbosacral segments are targeted with a precise timing that reproduces the natural spatiotemporal activation pattern of leg motor neurons[22,23]. This strategy restored standing, walking, cycling and even swimming in people with paralysis due to spinal cord injury[24–26]. We reasoned that this strategy can be adapted to the specific context of PD to conceive a neuroprosthesis that alleviates locomotor deficits due to PD.

Results

PD model shows gait deficits similar to people with PD

The development of a neuroprosthesis to alleviate locomotor deficits due to PD required establishing a preclinical model that replicates

e-mail: jocelyne.bloch@chuv.ch; erwan.bezard@u-bordeaux.fr; gregoire.courtine@epfl.ch

https://doi.org/10.1038/s41591-023-02584-1

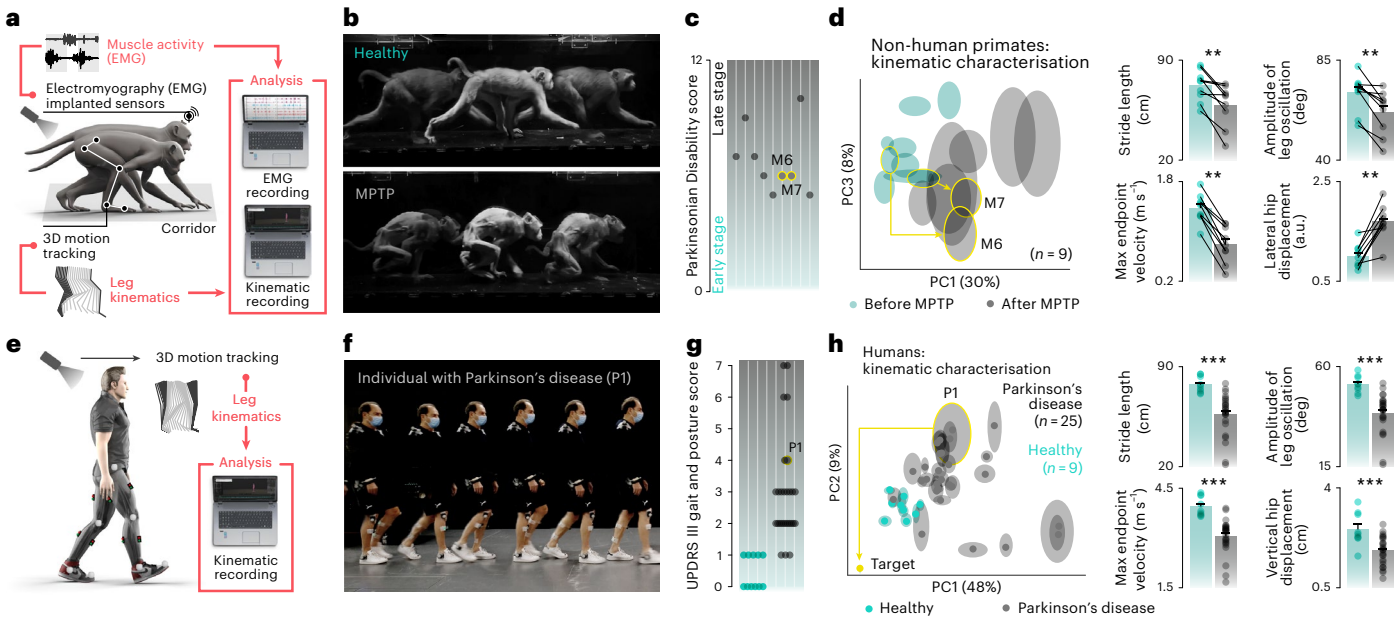

Fig. 1 | Locomotor deficits in MPTP-treated NHPs and people with PD. **a**, Recording platform for NHPs. **b**, Chronophotographs illustrating locomotor deficits in MPTP-treated NHPs. **c**, Distribution of PD scores for nine MPTP-treated NHPs. **d**, A PC analysis was applied on 83 parameters calculated for each gait cycle. Balloons show mean ± s.d. of all gait cycles projected in the space spanned by two of the three leading PCs. Bar plots report the mean values for four gait parameters highly correlated with PC1. **e**, Recording platform for people with PD. **f**, Chronophotographs illustrating locomotor deficits in a person with PD. **g**, UPDRS scores (gait) of nine healthy people and 25 people with PD. **h**, Same analysis as in **d** for people, including for P1 and its target gait (yellow), as explained in the section on the clinical trial in the human participant. ** and ***, $P < 0.01$ and $P < 0.001$, respectively, using two-sided Wilcoxon signed-rank or rank-sum tests. Error bars, s.e.m. deg, degrees.

the key components of gait impairments and balance problems observed in humans with PD. The non-human primate (NHP) treated with 1-methyl-4-phenyl-1,2,3,6-tetrahydropyridine (MPTP) is the most established preclinical model of PD[27]. However, the locomotor deficits of MPTP-treated NHPs have not yet been characterized with comprehensive kinematic analyses. Therefore, it remains unclear whether the deficits observed during quadrupedal walking in MPTP-treated NHPs resemble those observed during bipedal walking in people with PD.

To enable this comparison, we established comparable recording platforms for NHPs and humans to capture whole-body kinematics during natural walking in both species[28] (Fig. 1 and Supplementary Movie 1).

We first recorded walking in nine rhesus monkeys before and after an MPTP treatment that modeled a late stage of Parkinsonism (Fig. 1a–c), coinciding with the severe depletion of striatal dopaminergic terminals and nigral neurons (Extended Data Fig. 1a). We calculated an ensemble of kinematic variables that captured the key features of gait (Supplementary Table 3). We then implemented principal component (PC) analysis as an unbiased method to score locomotor performance and identify the more prominent variables to account for gait impairments[29]. PC1 and PC3 segregated gait patterns quantified before versus after MPTP treatment (Fig. 1d). Extraction of variables with the highest correlation with PC1 revealed that MPTP led to reduced stride length and slow movements ($P < 0.05$; Extended Data Fig. 1b,c). PC3 identified excessively flexed postures and impaired trunk movements ($P < 0.01$; Extended Data Fig. 1b,c).

To assess whether people with PD exhibited similar deficits, we quantified gait patterns of 25 people with PD whose neurological status covered a broad spectrum of impairments (Supplementary Table 4) and nine healthy age-matched people (Fig. 1e–g). PC analysis applied on kinematic variables (Supplementary Table 5) revealed that most gait impairments and balance problems observed in MPTP-treated NHPs were similar to those quantified in people with PD (Fig. 1h and Extended Data Fig. 1d).

These results show that MPTP-treated NHPs displayed gait impairments and balance problems that share many features commonly observed in people with PD. We concluded that the MPTP-treated NHP is an appropriate preclinical model for the development of a neuroprosthesis to alleviate gait impairments and balance problems due to PD.

Requirements to alleviate gait deficits due to PD

We sought to develop a neuroprosthesis based on EES[22–24] to restore the natural spatiotemporal activation of leg motor neurons that is disrupted during walking in people with PD. Therefore, we first determined the natural activation of leg motor neurons in healthy NHPs and how the administration of MPTP alters this activation.

To record muscle activity, we developed a head-mounted system that enabled wireless recordings of electromyographic (EMG) signals from implanted leg muscles while NHPs walked without constraints or tethered electronics. We then visualized motor neuron activity by projecting the recorded EMG signals onto the known anatomical location of the motor neurons that produce these signals (Fig. 2a)[22,23,30].

The resulting spatiotemporal maps of leg motor neuron activation revealed that walking involves the sequential activation of six well-defined hotspots located in the left and right hemicords. The sequential activation of these hotspots reflected the biomechanics of walking[30], successively ensuring weight acceptance, propulsion and leg lift (Fig. 2a and Extended Data Fig. 2a).

Comparison of maps recorded before and after the administration of MPTP revealed that locomotor deficits resulted from diverse alterations in the timing, duration and amplitude of each hotspot (Fig. 2a and Extended Data Fig. 2b). We, thus, reasoned that the ensemble of dorsal root entry zones projecting to these six hotspots must be targeted to alleviate gait impairments and balance problems.

Tailored implants target relevant pools of leg motor neurons

We aimed to develop implants with electrode configurations that are optimized to target the dorsal root entry zones projecting to the spinal segments wherein each hotspot is located.

To guide this development, we studied the anatomy of the rhesus monkey spinal cord. We identified a spatial distribution of electrodes to access all the targeted dorsal root entry zones (Fig. 2b), which informed the design of two eight-electrode arrays that we fabricated using AirRay[31] and electronic dura mater technologies[32,33] (Extended Data Fig. 3a).

These electrode arrays were implanted in four NHPs. The arrays were first advanced to the planned anatomical locations, covering the upper or lower region of the lumbosacral spinal cord (Extended Data Fig. 3b). We then delivered single pulses of EES to elicit muscle responses and leg movements and monitored these responses to fine-tune the final placement of the arrays. Postmortem anatomical evaluations confirmed the appropriate and stable location of the electrode arrays.

To deliver EES, we interfaced the electrode arrays with the Activa RC implantable pulse generator (IPG) that we upgraded with wireless communication modules[23]. Recordings of muscle responses when delivering single pulses of EES confirmed that the electrodes selectively recruited the dorsal root entry zones associated with each of the six targeted hotspots (Fig. 2c and Extended Data Fig. 3c).

We concluded that the newly designed electrode arrays possessed the necessary specificity to access the ensembles of hotspots responsible for locomotor deficits of MPTP-treated NHPs.

Cortical activity enables decoding of gait events in NHP

We aimed to recruit the individual dorsal root entry zones innervating lumbosacral segments with the appropriate timing to reproduce the natural activation of the spinal cord during walking. Concretely, the timing and location of EES bursts must coincide with the activation of the six identified hotspots that produce walking. This neuroprosthesis was contingent upon the identification of motor intentions to synchronize EES with the ongoing movements.

Motor intentions can be detected using various technologies, including manually pressed clickers[25], inertial measurement units (IMUs) attached to the limbs[24] and even primary motor cortex activity[23,33–38]. Compared to alternative technologies, detection of motor intentions from motor cortex activity is the only viable strategy in freely moving NHPs[23,28,36]. However, various studies reported that PD may alter motor cortex activity[10,39–44], suggesting that decoding motor intentions from this region may be compromised. We, thus, asked whether the timing appropriate to synchronize EES with the activity of the relevant hotspots based on the ongoing movement can be decoded from primary motor cortex activity in MPTP-treated NHPs.

To record neural activity, we inserted microelectrode arrays into the leg region of the primary motor cortex in two MPTP-treated NHPs (M6 and M7). We interfaced the microelectrode arrays with a wireless data transmission module[28] that enabled broadband recording of neural activity synchronized with EMG and kinematic data[23,36]. Despite pronounced locomotor deficits, both NHPs displayed neuronal firing patterns that were highly regular and phase locked to gait cycles (Fig. 2d).

We reasoned that these neuronal firing patterns must permit real-time detection of events linked to the activation of the identified hotspots. Because alterations of muscle activity occurred during weight acceptance, propulsion and leg lift, the three hotspots associated with these gait phases had to be targeted with EES in each hemicord. Consequently, we devised a strategy to decode the timing of events that coincided with the activation of these six hotspots.

To validate this strategy, we performed longitudinal recordings in M6 and M7 once they had reached stable gait impairments after the administration of MPTP. We configured a regularized linear discriminant analysis (rLDA) algorithm that accurately detected the activation of these hotspots using motor cortex activity[23,33,35,36,45]. The rLDA algorithm maintained accurate detection of the events associated with each hotspot across four sessions spanning a period of several weeks (Fig. 2d).

We concluded that motor intentions can be reliably decoded from motor cortex activity during walking in our NHP model of PD and that these predictions are suitable to synchronize the timing and location of EES bursts to alleviate locomotor deficits.

Brain-controlled neuroprosthesis reduces gait deficits in NHP

We then interfaced motor cortex activity with the timing and location of EES bursts to conceive a wireless brain-controlled neuroprosthesis operating in closed loop and asked whether this brain-controlled neuroprosthesis alleviates gait impairments and balance problems observed in MPTP-treated NHPs.

Three NHPs (M8, M9 and M11) had developed gait impairments and balance problems after the administration of MPTP. In a single neurosurgical intervention, we inserted two microelectrode arrays in the left and right motor cortex, two electrode arrays over the spinal cord, an IPG in the abdomen and EMG electrodes into selected leg muscles (Fig. 3a and Extended Data Fig. 3d). We configured a control computer that acquired the neural signals, detected events from cortical activity (Extended Data Fig. 4a) and sent updated sequences of EES bursts to the IPG to translate motor intentions into the activation of the six hotspots to facilitate walking. This ensemble of neurotechnologies established a digital bridge between the brain and spinal cord that operated wirelessly and in real time.

We noticed that the delivery of EES led to responses in the motor cortex. To mitigate the impact of these responses on the decoding of gait events, we calibrated the decoders using 2 min of neural activity without and with EES[23] (Extended Data Fig. 4b). This approach enabled accurate detection of movement intentions even in the presence of EES (Fig. 3b and Extended Data Fig. 5a,b).

This brain-controlled neuroprosthesis immediately alleviated gait impairments and balance problems in the three tested MPTP-treated NHPs (Extended Data Fig. 5b,c and Supplementary Movie 2). The NHPs

Fig. 2 | Design of the spinal cord neuroprosthesis in NHP. a, From left to right: EMG recordings from leg muscles during one gait cycle: iliopsoas (IPS), rectus femoris (RF), semitendinosus (ST), gastrocnemius medialis (MG), flexor hallucis longus (FHL), gluteus (GLU), extensor digitorum longus (EDL) and tibialis anterior (TA); location of IL and TA motor pools along the lumbosacral spinal cord (L1–L7)[14]; projection of EMG signals onto these locations to elaborate a spatial map of motor neuron activation during the highlighted period of the stance phase; average spatiotemporal map of motor neuron activation throughout the entire duration of the gait cycle ($n = 20$ gait cycles); three hotspots of the right hemicord extracted by fitting a Gaussian model: weight acceptance, propulsion and leg lift that comprises anatomically separated ankle and hip flexion motor neuron activations; and changes in the map after MPTP ($n = 17$ gait cycles). **b**, CT scan of the spine determining the design of two eight-electrode arrays that target the three hotspots from each side, highlighted by specific colors in the vertical bars near the spinal cord. **c**, Spatial maps of activation evoked by EES (left) and of the targeted hotspot (right). Bar plots report the correlations between the maps evoked by EES and the three targeted hotspots. **d**, Wireless modules are screwed onto skull-mounted pedestals to transmit wide-band neural activity recorded using microelectrode arrays inserted into the leg region of left and right motor cortex. Raster plots of neural activity and concomitant probability of activation of weight acceptance and leg lift hotspots over three successive gait cycles calculated by the rLDA algorithm (M6 after MPTP administration). Dots indicate moments when the probability crosses the detection threshold. The pie charts show the mean ± s.e.m. accuracy of the detections for M6 (178 events) and M7 (256 events) calculated by offline analysis using cross-validation.

https://doi.org/10.1038/s41591-023-02584-1

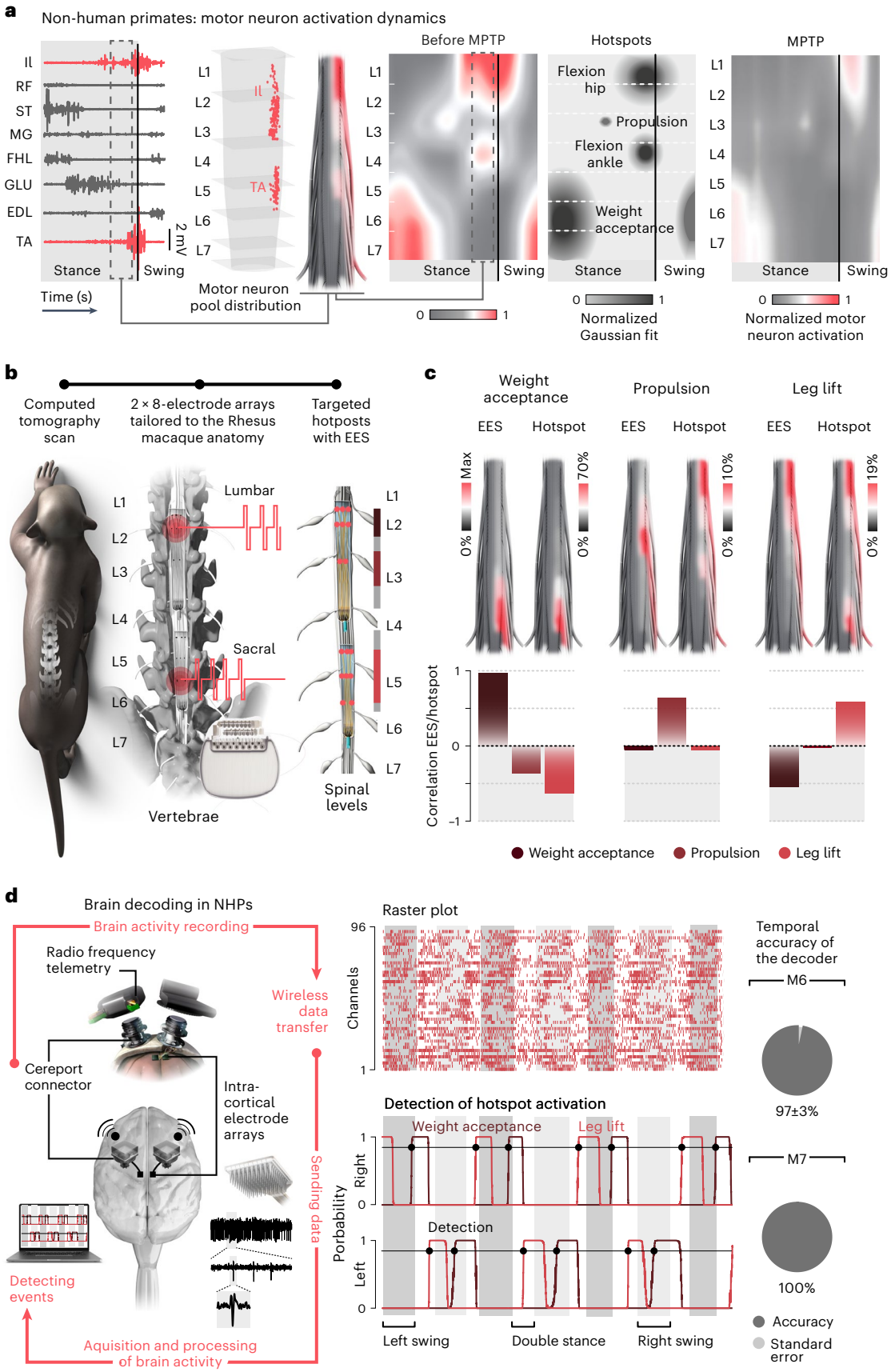

https://doi.org/10.1038/s41591-023-02584-1

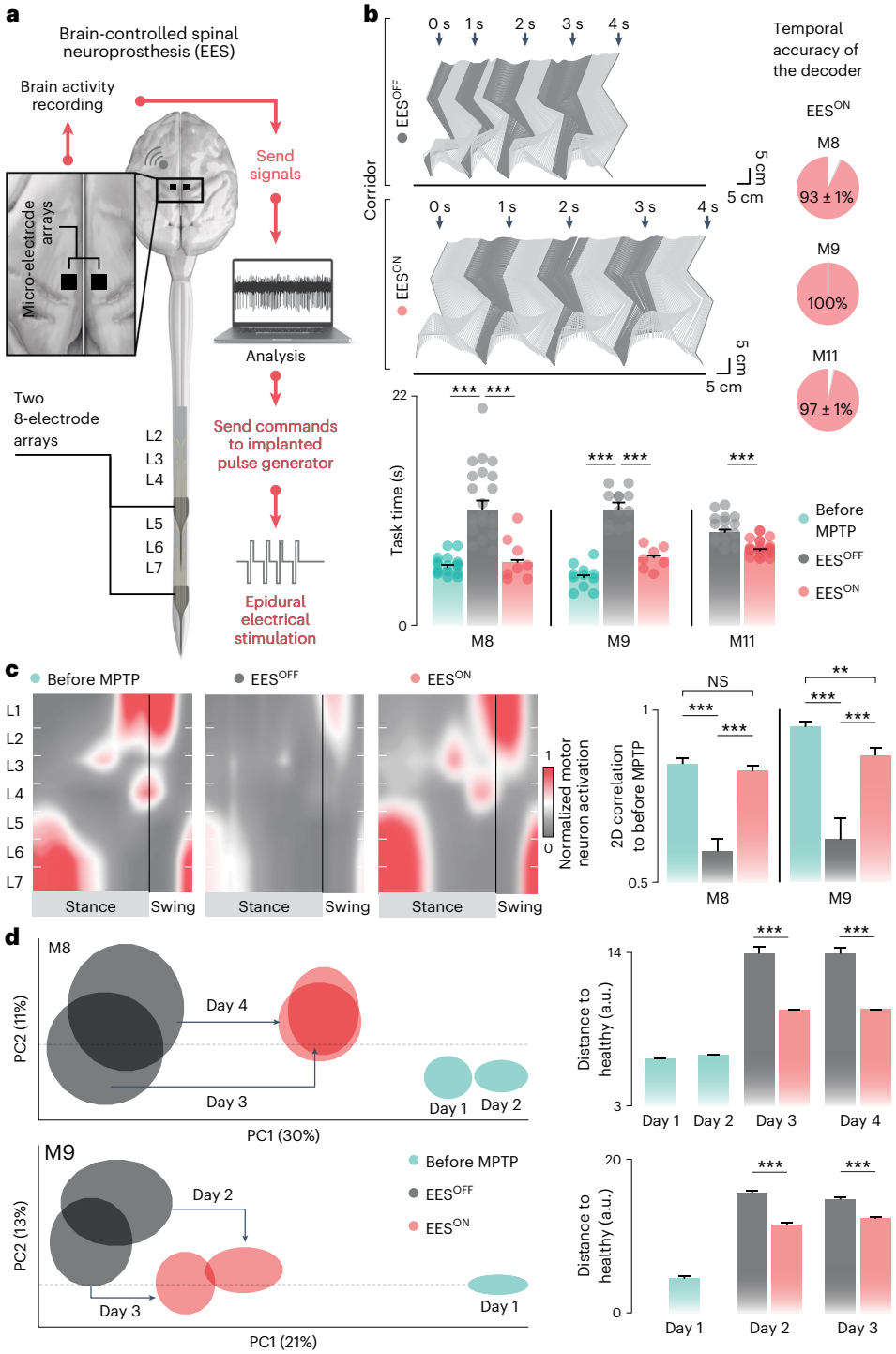

Fig. 3 | The neuroprosthesis alleviates gait impairments and balance problems in MPTP-treated NHPs. a, Scheme of the brain-controlled neuroprosthesis. **b**, Stick diagram decomposition of leg kinematics during 4 s of locomotion (animal M9) after MPTP administration without (EES^{OFF}) and with (EES^{ON}) the neuroprosthesis. Pie charts report the accuracy of the decoder (n = 516, 618 and 612 events for M8, M9 and M11, respectively) during walking. Bar plots report the average task time when crossing a 3m-long straight corridor (n = 16, 21 and 8 trials for M8; 11, 12 and 7 trials for M9; and 15 and 22 trials for M11 across conditions from left to right). **c**, Spatiotemporal maps of motor neuron activation for M8. Bar plots report the surface correlation between motor neuron activation maps for the various conditions (n = 17, 39 and 33 steps for M8 and 11, 26 and 34 steps for M9 across conditions from left to right). The maps were normalized to 1 using the 95th percentile of the envelope over the entire session (EES^{OFF} and EES^{ON} datasets were recorded in the same session, before the MPTP dataset was recorded in a separate session). **d**, PC analysis of gait kinematics, as in Fig. 1. The balloons show mean ± s.d. of all gait cycles of one of the experimental conditions. Bar plots report the Euclidean distance in the full 83-dimensional space between each gait cycle and the mean values across all the gait cycles recorded before MPTP administration (n = 26, 51, 27, 81, 50 and 45 gait cycles for M8 and 63, 62, 45, 140 and 55 gait cycles for M9 across conditions from left to right). Gait patterns from M8 were recorded in 2 d before the MPTP treatment (days 1 and 2) and 2 d after the treatment (days 3 and 4). For M9, gait patterns were recorded in 1 d before the MPTP treatment (day 1) and 2 d after the treatment (days 2 and 3). *, ** and *** indicate significant difference at $P < 0.05$, $P < 0.01$ and $P < 0.001$, respectively, using two-sided Wilcoxon rank-sum test or the one-sided Monte Carlo permutation test. NS, not significant ($P \geq 0.05$) according to the same tests. Error bars, s.e.m. 2D, two-dimensional.

walked across the corridor as rapidly as before the administration of MPTP (Fig. 3b). As intended, the neuroprosthesis restored the natural activation of leg motor neurons during walking (Fig. 3c), which translated into improvements of gait quality (Fig. 3d and Extended Data Fig. 5b) and balance (Extended Data Fig. 5b).

The neuroprosthesis also improved posture. To quantify these improvements, we transformed computed tomography (CT) scans into a tri-dimensional biomechanical model of NHPs onto which we morphed whole-body kinematics. This morphing procedure revealed a decrease in spine curvature during walking with the neuroprosthesis (Extended Data Fig. 5d).

The neuroprosthesis additionally improved gait and balance during skilled locomotion. M8 and M11 progressed slowly and even fell when negotiating the rungs of a horizontal ladder. The neuroprosthesis restored a natural progression along the ladder and reduced falls to nearly zero (Extended Data Fig. 5e and Supplementary Movie 2).

These results were reproduced over successive days, during which we implemented the same decoder and EES protocols without recalibration (Fig. 3d and Extended Data Fig. 5b,c,e).

The location (Extended Data Fig. 3c) and timing (Extended Data Fig. 6) of EES were critical to mediate improvement, because changing any of these parameters reduced the efficacy of the neuroprosthesis.

The neuroprosthesis complements DBS in MPTP-treated NHP

DBS is the primary neurosurgical intervention to alleviate motor signs of PD, but benefits on walking have been variable, if not detrimental[4–8]. We, thus, asked whether our neuroprosthesis can complement DBS to address the entire range of motor signs associated with PD.

To answer this question, we implanted electrodes into the left and right subthalamic nuclei in addition to the brain-controlled neuroprosthesis in M9. Structural magnetic resonance imaging (MRI) confirmed the accurate location of electrodes (Fig. 4a). DBS delivered at the known therapeutic frequency of 125 Hz (but not 20 Hz) improved general mobility and alertness, which translated into a higher number of completed trials and faster walking speeds (Extended Data Fig. 7a–c). However, kinematic quantifications revealed that the legs remained exaggeratedly flexed during the stance phase, indicating a lack of extension and propulsion that restricted the length and height of steps (Extended Data Fig. 7d).

When the neuroprosthesis and DBS were turned on concomitantly, M9 not only showed increased alertness (Fig. 4b) but also exhibited walking speeds closer to those quantified before the administration of MPTP (Fig. 4c) and gait improvements that enabled higher steps (Fig. 4d,e). Decoding of events to synchronize EES bursts to ongoing movements remained accurate during the use of DBS (Fig. 4f).

Together, these experiments revealed that the brain-controlled neuroprosthesis complements DBS of the subthalamic nucleus to alleviate gait impairments and balance problems due to the loss of dopamine-producing cells in NHPs. These observations compelled us to test this treatment in people with PD.

Cortical activity enables decoding of gait in people with PD

We previously established the technological feasibility of implementing a brain-controlled neuroprosthesis to restore walking in humans with paralysis[34]. However, the possibility of decoding motor intentions from cortical activity in people with PD remained unknown. Indeed, PD involves a widespread, slow-evolving alteration of neuronal circuits that may not be entirely reproduced using administration of MPTP over restricted time windows in NHPs. Therefore, we sought to verify the feasibility of detecting events from motor cortex activity in people with PD to synchronize EES with the ongoing movements.

Under the framework of a physician-sponsored clinical study (Investigational Device Exemption (IDE) protocol G180097), two participants with idiopathic PD and motor fluctuations received bilateral subdural electrode arrays over the primary motor cortex[46]. The arrays were interfaced to Summit RC+S implanted pulse generators, which enabled wireless streaming of electrocorticogram (ECoG) signals to an external computer.

We implemented the same event detection strategy as used previously in NHPs[23,33,36] and people[35,38] to detect events associated with the activation of hotspots from ECoG signals (Extended Data Fig. 8a,b). In both participants, P2 and P3, the algorithm detected the events linked to leg lift with high accuracy (Extended Data Fig. 8c,d).

These results demonstrated the feasibility of decoding events from primary motor cortex activity to synchronize EES to the ongoing movements in people with PD.

Design of a neuroprosthesis to alleviate gait deficits in humans

Finally, we enrolled a 62-year-old male (P1) who presented with a 30-year history of PD in the first-in-human STIMO-PARK clinical trial (ClinicalTrials.gov ID: NCT04956770). Although DBS and finely tuned dopaminergic replacement therapies improved cardinal signs of PD, he had developed severe locomotor deficits that led to 2–3 falls per day. P1 exhibited the common locomotor deficits observed in our cohort of people with PD (Fig. 1h), including marked gait asymmetry, reduced stride length, balance problems as well as episodes of freezing of gait and frequent falls. We, thus, asked whether the neuroprosthesis could complement DBS and dopaminergic replacement therapies to alleviate his persistent locomotor deficits.

The neuroprosthesis aims to re-establish the natural activation of leg motor neurons during walking. Contrary to NHPs that acted as their own control, we could not record the natural spatiotemporal activation of leg motor neurons underlying walking before the onset of PD in P1. To remedy this limitation, we generated a personalized neurobiomechanical model[47] actuated by a reflex-based circuit that allowed us to estimate the optimal activation of muscles during walking that was expected by P1 in the absence of PD (Fig. 5a and Extended Data Fig. 9a). As in NHPs, the occurrence of weight acceptance, propulsion and leg lift coincided with the activation of six hotspots that emerged in specific regions of the spinal cord (Fig. 5b). Compared to simulations, we detected changes in the timing, location and amplitude of these six hotspots (Fig. 5b). We concluded that the ensemble of dorsal root entry zones projecting to the six hotspots had to be targeted with EES.

To target these dorsal root entry zones, we repurposed a clinically approved electrode array commonly used to treat neurogenic pain[24]. The neurosurgical implantation of this array was guided by a personalized anatomical model of the spine that we generated using high-resolution CT and MRI[25] (Fig. 5c). This model determined the optimal location of the electrode array to recruit the targeted dorsal root entry zones. Under general anesthesia, the electrode array was advanced to the planned location (Extended Data Fig. 9b). We then delivered single pulses of EES to elicit responses in leg muscles and, thus, confirmed the ability of the electrode array to recruit the six targeted hotspots specifically (Fig. 5d). We interfaced the electrode array with the Activa RC IPG, which we upgraded with wireless communication modules[25], as in NHPs[23].

The neuroprosthesis alleviates gait deficits in a person with PD

Unlike NHPs, people tolerate wearable sensors attached to their limbs[48]. Signals from wearable sensors are suitable to synchronize EES to ongoing movements[24,25]. Before considering the surgical implantation of a system to record cortical activity[34], we asked whether this non-invasive approach was sufficient to control the neuroprosthesis in P1.

We developed clinical-grade software running on a tablet that acquired signals from IMUs attached to the left and right legs; detected events associated with the onset of the relevant hotspots based on the same rLDA algorithm as in NHPs and people with PD; and sent updated sequences of EES bursts to the implanted pulse generator (Extended Data Fig. 3d). This chain of hardware and software translated the detection of motor intentions from IMUs into the modulation of EES (Fig. 6a).

https://doi.org/10.1038/s41591-023-02584-1

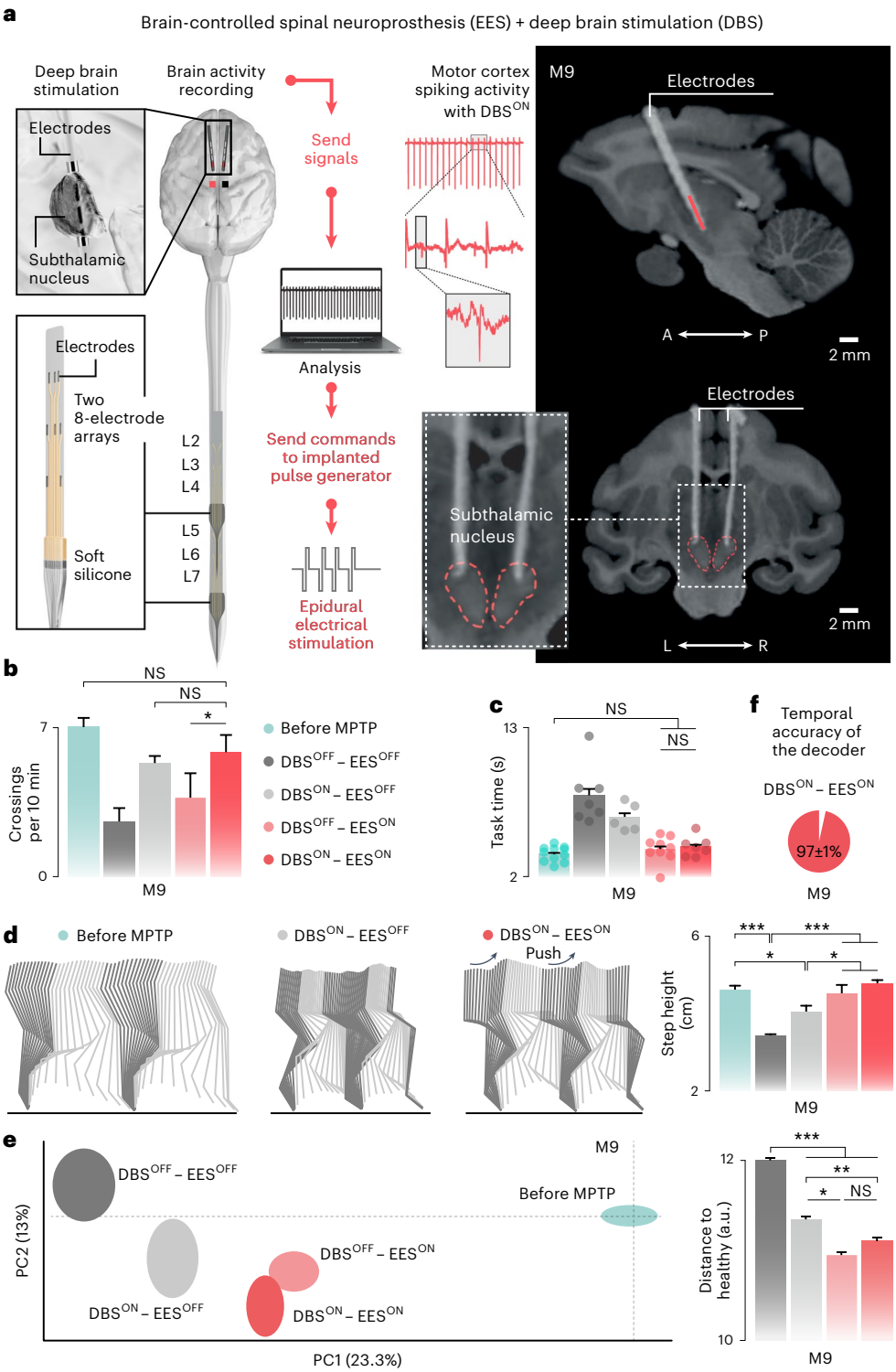

Fig. 4 | The neuroprosthesis complements DBS of the subthalamic nucleus to alleviate locomotor deficits in MPTP-treated NHPs. a, Scheme illustrating the insertion of DBS electrodes in the subthalamic nucleus of M9 and anatomical location of DBS implants as shown on postmortem MRI. **b**, Bar plots reporting the number of corridor crossings within 10 min (number of trials, before MPTP: 24; after MPTP: 19; DBS: 17; BSI: 19; BSI + DBS: 22). **c**, The bar plots report the task time (number of gait cycles, before MPTP: 11; after MPTP: $DBS^{OFF} – EES^{OFF}$: 7; $DBS^{ON} – EES^{OFF}$: 5; $DBS^{OFF} – EES^{ON}$: 9; $DBS^{ON} – EES^{ON}$: 7). **d**, Stick decomposition illustrating the changes in leg kinematics in M9 induced by EES when combined with DBS after the MPTP treatment, as compared to DBS alone and to before the MPTP treatment. Bar plots indicate the average step height across conditions (number of gait cycles, before MPTP: 39; after MPTP: $DBS^{OFF} – EES^{OFF}$: 47; $DBS^{ON} – EES^{OFF}$: 37; $DBS^{OFF} – EES^{ON}$: 60; $DBS^{ON} – EES^{ON}$: 43). **e**, PC analysis of gait kinematics, as in Fig. 3, under the various combinations of EES and DBS on or off (number of gait cycles same as in **e**). The balloons show mean ± s.d. of all gait cycles of one of the experimental conditions. The bar plot reports the Euclidean distance in the full 83-dimensional space between each gait cycle and the mean values across all the gait cycles recorded before MPTP administration. **f**, Pie chart reports the accuracy of the decoder during $DBS^{ON} – EES^{ON}$ trials ($n = 145$ events) measured during the online use of the neuroprosthesis. *, ** and *** indicate significant difference at $P < 0.05$, $P < 0.01$ and $P < 0.001$, respectively, using two-sided Wilcoxon rank-sum test or the one-sided Monte Carlo permutation test. NS, not significant ($P \geq 0.05$) according to the same tests. Error bars, s.e.m.

https://doi.org/10.1038/s41591-023-02584-1

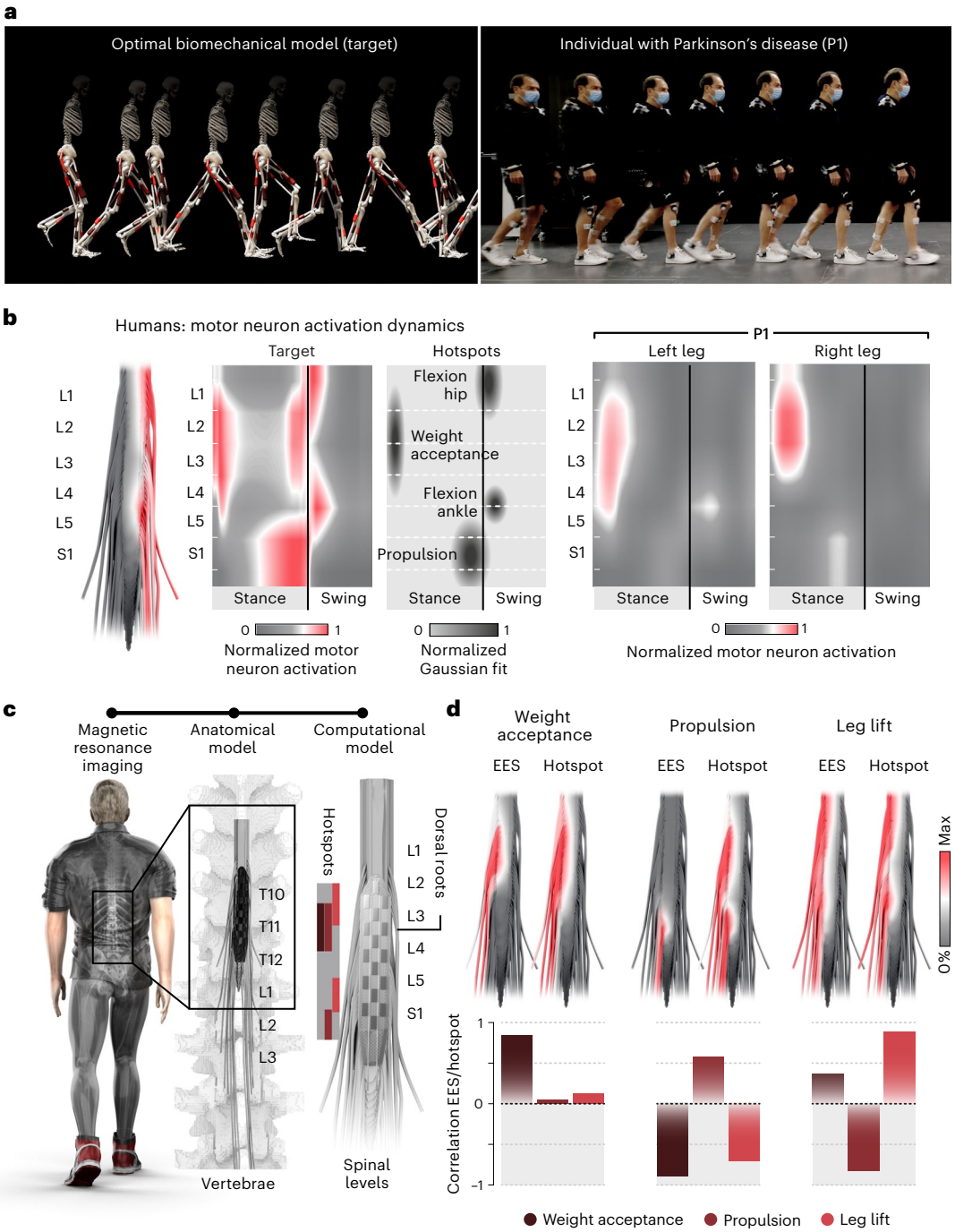

Fig. 5 | Design of the neuroprosthesis for people with PD. a, Chronophotographs illustrating an optimal gait for P1 based on a personalized OpenSim neurobiomechanical model (target gait) and gait deficits of P1, also reported in Fig. 1. **b**, Same analysis as in Fig. 2a here for P1, including spatiotemporal activation of leg motor neurons for P1's target gait. **c**, The illustration shows the anatomical model of P1's spine reconstructed from MRI and CT. This model was used to determine the surgical placement of a 16-electrode array as shown in the illustration on the right. The color-coded matrix shows the caudo-rostral locations of the three hotspots for each hemicord. **d**, Same analysis as in Fig. 2c here for P1.

We first quantified the impact of this neuroprosthesis in the presence of the best therapeutic strategy for P1, which involved dopamine replacement therapy and DBS. The neuroprosthesis restored the natural spatiotemporal activation of leg motor neurons during walking, which translated into improvements of gait and balance (Fig. 6b–e, Extended Data Fig. 10a–d and Supplementary Movies 2 and 3). Concretely, the neuroprosthesis restored gait symmetry by reinforcing the activity of muscles from the most affected leg (Extended Data Fig. 10b,c). In addition, EES bursts augmented the activation of propulsion hotspots, which produced longer and higher foot trajectories (Extended Data Fig. 10a–d). Lastly, EES bursts targeting weight acceptance hotspots reinforced stability during stance, which improved balance (Extended Data Fig. 10a–d).

To assess whether gait patterns from P1 were more similar to those of people with PD or to healthy people, we implemented a classification using an LDA decoder[26]. We calibrated this decoder on gait parameters calculated from kinematic recordings of 25 people with PD and nine healthy age-matched controls. We then used the decoder to classify

https://doi.org/10.1038/s41591-023-02584-1

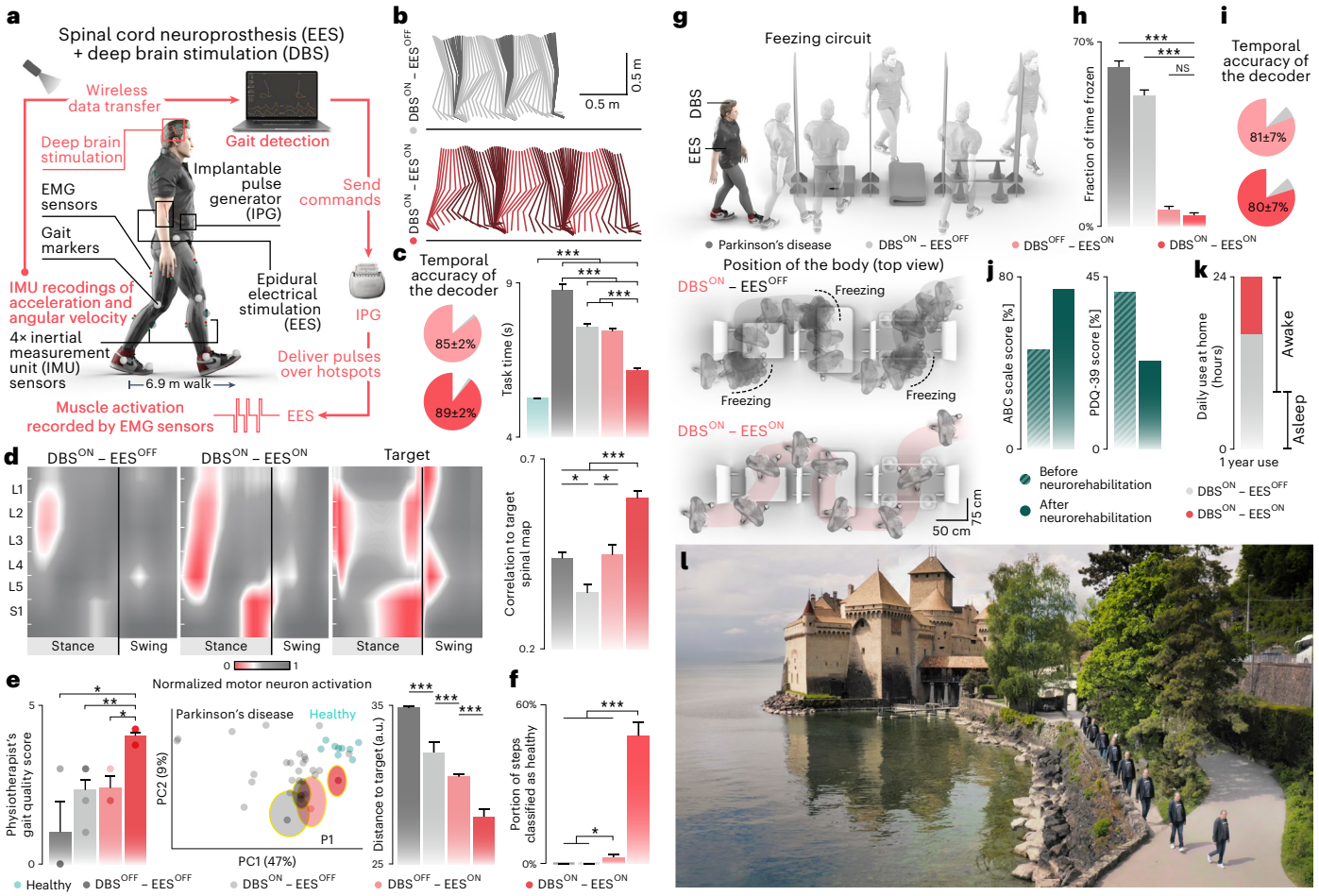

Fig. 6 | The neuroprosthesis alleviates gait impairments, improves balance, reduces the frequency of freezing of gait, increases quality of life and supports mobility in community settings in a person with PD. a, Scheme illustrating the neuroprosthesis combined with DBS of the subthalamic nucleus in P1. **b**, Stick diagram decomposition of leg kinematics during 3 s of locomotion with DBS^{ON} – EES^{OFF} and DBS^{ON} – EES^{ON}. **c**, Pie charts report the accuracy of the decoder during DBS^{OFF} – EES^{ON} (n = 462 events) and DBS^{ON} – EES^{ON} (n = 328 events) while P1 walks overground measured during the online use of the neuroprosthesis. Bar plot reports task time (number of trials: DBS^{OFF} – EES^{OFF}: 25; DBS^{ON} – EES^{OFF}: 24; DBS^{OFF} – EES^{ON}: 38; DBS^{ON} – EES^{ON}: 32). **d**, Spatiotemporal maps of motor neuron activation and bar plots reporting the surface correlation between motor neuron activation maps during DBS^{ON} – EES^{OFF} (n = 66 gait cycles) and DBS^{ON} – EES^{ON} (n = 91 gait cycles) compared to the map from the target gait (n = 168 gait cycles). s.e.m. was calculated using bootstrapping. **e**, Bar plots report gait quality score evaluated by physiotherapists (number of trials: DBS^{OFF} – EES^{OFF}: 2; DBS^{ON} – EES^{OFF}: 2; DBS^{OFF} – EES^{ON}: 5; DBS^{ON} – EES^{ON}: 5). The scatter plot shows the PC analysis of gait kinematics applied on 39 parameters. The balloons show mean ± s.d. of all gait cycles of P1 in one of the experimental conditions (number of gait cycles: DBS^{OFF} – EES^{OFF}: 255; DBS^{ON} – EES^{OFF}: 105; DBS^{OFF} – EES^{ON}: 317; DBS^{ON} – EES^{ON}: 172) projected in the space spanned by PC analysis of kinematics of nine healthy people and 25 people with PD shown in Fig. 1h. Each dot shows the mean of all gait cycles of one of the nine healthy people (gray) and 25 people with PD (green). Bar plots report the mean Euclidean distance in the full 39-dimensional space between each gait cycle in a given condition and the mean gait cycle of the target gait. **f**, Bar plots report the portion of gait cycles classified as healthy using an LDA decoder calibrated on all the steps from 25 people with PD and nine healthy age-matched people (number of gait cycles as reported in **e**). **g**, Scheme illustrating a circuit that comprises three narrow passages with obstacles that provoked freezing of gait in P1. Below is shown the successive position of the body while P1 navigates along this circuit with DBS^{ON} – EES^{OFF} and DBS^{ON} – EES^{ON}. Broken lines denote the occurrence of freezing of gait events. **h**, The bar plots report the fraction of time during which P1 experienced freezing (measurement duration: DBS^{OFF} – EES^{OFF}: 39.0 s; DBS^{ON} – EES^{OFF}: 51.3 s; DBS^{OFF} – EES^{ON}: 27.7 s; DBS^{ON} – EES^{ON}: 23.3 s). **i**, The pie charts report the accuracy of the decoder during DBS^{OFF} – EES^{ON} (n = 26 events) and DBS^{ON} – EES^{ON} (n = 29 events) while navigating the circuit measured during the online use of the neuroprosthesis. **j**, Bar plots reporting gains in balance measured using the ABC scale questionnaire and quality of life measured using the 39-item Parkinson's Disease Questionnaire (PDQ-39) after neurorehabilitation supported by the neuroprosthesis. **k**, Pie chart shows the daily independent use of the neuroprosthesis at home reported by P1 at his follow-up 1 year after the implantation. **l**, The chronophotograpy shows P1 using the neuroprosthesis for recreational walks in nature. *, ** and *** indicate significant difference at $P < 0.05$, $P < 0.01$ and $P < 0.001$, respectively, using two-sided Wilcoxon rank-sum test or the one-sided Monte Carlo permutation test. NS, not significant ($P \geq 0.05$) according to the same tests. Error bars, s.e.m., unless specified otherwise.

whether each gait pattern performed by P1 was more similar to gait patterns from people with PD or healthy people. When the neuroprosthesis was turned on, most steps performed by P1 were classified as gait patterns from healthy people (Fig. 6f).

Improvements were also observed when the DBS was turned off, albeit to a lesser extent (Fig. 6a–e and Extended Data Fig. 10c,d). Neurological assessments measured by Unified Parkinson's Disease Rating Scale (UPDRS)[49] scores highlighted the complementarity between the neuroprosthesis and DBS to alleviate locomotor deficits in P1 (Movement Disorder Society (MPS) UPDRS III score: DBS^{OFF} – EES^{OFF}: 65; DBS^{ON} – EES^{OFF}: 29; DBS^{ON} – EES^{ON}: 24; see gait subscores in Supplementary Table 10), as further confirmed by subjective assessments conducted by physical therapists (Fig. 6e) and by P1 (Extended Data Fig. 10d) using gait quality scores. As in NHPs, the neuroprosthesis maintained high

accuracy in the decoding of events associated with the activation of the hotspots, both with or without the use of DBS (Fig. 6c and Extended Data Fig. 10e).

The neuroprosthesis reduces freezing of gait

Freezing of gait refers to the episodically hampered ability to move the legs. Freezing of gait is one of the most debilitating locomotor deficits of PD, for which current treatment strategies are poorly effective[2,4,50,37]. Despite DBS and finely tuned dopaminergic replacement therapies, P1 exhibited frequent freezing-of-gait episodes that occurred when turning and when passing through narrow paths. These episodes led to multiple falls per day, which severely affected his quality of life. Although MPTP-treated NHPs and people with PD show similar gait impairments and balance problems, MPTP-treated NHPs rarely leads to freezing of gait[51]. Therefore, we had not been able to evaluate the benefits of our neuroprosthesis on freezing of gait in this model.

To quantify the impact of the neuroprosthesis on freezing of gait in P1, we designed a freezing circuit that involved frequent turns, crossing of obstacles and passing through narrow spaces (Fig. 6g). P1 experienced frequent freezing-of-gait episodes when navigating this environment. When the neuroprosthesis was turned on, freezing of gait nearly vanished, both with and without DBS (Fig. 6h). The closed-loop operations of the neuroprosthesis remained highly accurate despite the navigation through the complex environment of this task (Fig. 6i).

Rehabilitation supported by the neuroprosthesis improves gait

Many studies suggested that gait rehabilitation reduces locomotor deficits in people with PD and that the additional support of neuromodulation therapies may further augment the impact of rehabilitation. We, thus, sought to test this possibility in P1.

P1 followed a rehabilitation program augmented by the neuroprosthesis that involved a variety of exercises, including walking on basic and complex terrains, navigating outdoors in community settings, balance training and basic physical therapy. Rehabilitation sessions were conducted 2–3 times per week for a duration of 3 months.

Quantifications of locomotor deficits using well-established clinical scores and tests revealed improvements in endurance (Extended Data Fig. 10f) and balance (Fig. 6j and Extended Data Fig. 10g,h) combined with a reduction of freezing of gait (Extended Data Fig. 10h). Frequent use of the neuroprosthesis during gait rehabilitation translated into a reported increase in quality of life (Fig. 6j and Extended Data Fig. 10i).

The neuroprosthesis supports mobility in community settings

P1 was eager to integrate the neuroprosthesis in his daily life to support his activities of daily living. To enable the transition to community settings, we designed a user-friendly interface that allowed him to configure and operate the neuroprosthesis independently.

P1 has now been using the neuroprosthesis for nearly 2 years, for about 8 h per day (Fig. 6k), only switching the neuroprosthesis off when sitting for long periods of time or while sleeping. The neuroprosthesis enables P1 to enjoy recreational walks in nature over several kilometers without any additional assistance (Fig. 6l and Supplementary Movie 4).

Discussion

We developed a neuroprosthesis that reduced gait impairments, balance problems and freezing of gait due to PD. Moreover, gait rehabilitation augmented by the neuroprosthesis improved the neurological status of the participant, who reported improvement in his quality of life.

Although previous therapies focused on the regions of the brain that are directly affected by the loss of dopamine-producing cells, our neuroprosthesis targeted the region of the lumbosacral spinal cord that ultimately produces walking and is a priori not directly affected by PD. Central to the development of this neuroprosthesis was the understanding that EES modulates the activity of motor neuron pools involved in the production of walking by targeting large-diameter afferent fibers when they enter the spinal cord within the individual dorsal root entry zones. We translated this knowledge into a neuroprosthesis that modulates the activity of the lumbosacral spinal cord in real time to compensate for the abnormal activation of leg motor neurons due to PD.

We developed this neuroprosthesis in MPTP-treated NHPs but validated this therapeutic concept in only one person with PD. PD leads to a large spectrum of neurological profiles associated with distinct locomotor deficits. Consequently, it remains unclear whether the neuroprosthesis will be effective to alleviate gait impairments, improve balance and reduce freezing of gait across the entire population of people with PD. Future studies will, thus, have to identify the responders of this therapy.

Scaling up this therapy is contingent on purpose-built technologies that are optimized for the specific requirements of people with PD. First, the large-scale deployment of this therapy requires a library of electrode arrays that can target the ensemble of dorsal root entry zones involved in the control of leg motor neurons in each person with PD[25], combined with a neurostimulation platform for rapid, closed-loop control of EES. Second, the synchronization of the neuroprosthesis with motor intentions requires the identification of the optimal tradeoff among invasiveness, reliability and practicality of the technology used to detect motor intentions. Non-invasive wearable sensors are the preferred solution as long as the detections are reliable and the sensors practical to use in daily life. These signals were sufficient to operate the neuroprosthesis in our participant. Because PD induces a broad range of neurological deficits, it is possible that more severe conditions and/or locomotor deficits may require more precise signals based on invasive technologies. We showed here that motor intentions can be decoded from cortical activity using minimally invasive implants. We previously designed a digital bridge between the brain and spinal cord that restored natural walking in an individual with paralysis due to spinal cord injury[34]. The conceptual and technological feasibility of a brain-controlled neuroprosthesis is, thus, well established. Alternatively, one can take advantage of DBS electrodes to monitor neural activity from the subthalamic nucleus. We showed that normal and pathological gait events can be decoded in real time from these recordings in people with PD[52]. This methodology is attractive, because many people with PD receive DBS electrodes before experiencing untreatable locomotor deficits that would encourage them to be implanted with our neuroprosthesis.

We are committed to developing purpose-built technologies optimized for the specific requirements of people with PD, to identifying the patients who respond to this therapy and, thus, to informing the design of a pivotal trial to demonstrate the safety and efficacy of the neuroprosthesis for alleviating locomotor deficits of people with PD.

Online content

Any methods, additional references, Nature Portfolio reporting summaries, source data, extended data, supplementary information, acknowledgements, peer review information; details of author contributions and competing interests; and statements of data and code availability are available at https://doi.org/10.1038/s41591-023-02584-1.

References

1. Ge, H. L. et al. The prevalence of freezing of gait in Parkinson's disease and in patients with different disease durations and severities. *Chin. Neurosurg. J.* **6**, 17 (2020).
2. Stolze, H. et al. Prevalence of gait disorders in hospitalized neurological patients. *Mov. Disord.* **20**, 89–94 (2005).
3. Fasano, A., Canning, C. G., Hausdorff, J. M., Lord, S. & Rochester, L. Falls in Parkinson's disease: a complex and evolving picture. *Mov. Disord.* **32**, 1524–1536 (2017).

4. Snijders, A. H. et al. Physiology of freezing of gait. *Ann. Neurol.* **80**, 644–659 (2016).
5. Marsden, C. D. & Parkes, J. D. Success and problems of long-term levodopa therapy in Parkinson's disease. *Lancet* **1**, 345–349 (1977).
6. Funkiewiez, A. et al. Long term effects of bilateral subthalamic nucleus stimulation on cognitive function, mood, and behaviour in Parkinson's disease. *J. Neurol. Neurosurg. Psychiatry* **75**, 834–839 (2004).
7. Fasano, A., Aquino, C. C., Krauss, J. K., Honey, C. R. & Bloem, B. R. Axial disability and deep brain stimulation in patients with Parkinson disease. *Nat. Rev. Neurol.* **11**, 98–110 (2015).
8. Collomb-Clerc, A. & Welter, M. L. Effects of deep brain stimulation on balance and gait in patients with Parkinson's disease: a systematic neurophysiological review. *Neurophysiol. Clin.* **45**, 371–388 (2015).
9. Fuentes, R., Petersson, P., Siesser, W. B., Caron, M. G. & Nicolelis, M. A. Spinal cord stimulation restores locomotion in animal models of Parkinson's disease. *Science* **323**, 1578–1582 (2009).
10. Santana, M. B. et al. Spinal cord stimulation alleviates motor deficits in a primate model of Parkinson disease. *Neuron* **84**, 716–722 (2014).
11. Pinto de Souza, C. et al. Spinal cord stimulation improves gait in patients with Parkinson's disease previously treated with deep brain stimulation. *Mov. Disord.* **32**, 278–282 (2016).
12. de Lima-Pardini, A. C. et al. Effects of spinal cord stimulation on postural control in Parkinson's disease patients with freezing of gait. *eLife* **7**, e37727 (2018).
13. Nishioka, K. & Nakajima, M. Beneficial therapeutic effects of spinal cord stimulation in advanced cases of Parkinson's disease with intractable chronic pain: a case series. *Neuromodulation* **18**, 751–753 (2015).
14. Opova, K., Limousin, P. & Akram, H. Spinal cord stimulation for gait disorders in Parkinson's disease. *J. Parkinsons Dis.* **13**, 57–70 (2023).
15. de Andrade, E. M. et al. Spinal cord stimulation for Parkinson's disease: a systematic review. *Neurosurg. Rev.* **39**, 27–35 (2016). discussion 35.
16. Fuentes, R., Petersson, P. & Nicolelis, M. A. Restoration of locomotive function in Parkinson's disease by spinal cord stimulation: mechanistic approach. *Eur. J. Neurosci.* **32**, 1100–1108 (2010).
17. Thevathasan, W. et al. Spinal cord stimulation failed to relieve akinesia or restore locomotion in Parkinson disease. *Neurology* **74**, 1325–1327 (2010).
18. Hassan, S., Amer, S., Alwaki, A. & Elborno, A. A patient with Parkinson's disease benefits from spinal cord stimulation. *J. Clin. Neurosci.* **20**, 1155–1156 (2013).
19. Prasad, S. et al. Spinal cord stimulation for very advanced Parkinson's disease: a 1-year prospective trial. *Mov. Disord.* **35**, 1082–1083 (2020).
20. Capogrosso, M. et al. A computational model for epidural electrical stimulation of spinal sensorimotor circuits. *J. Neurosci.* **33**, 19326–19340 (2013).
21. Moraud, E. M. et al. Mechanisms underlying the neuromodulation of spinal circuits for correcting gait and balance deficits after spinal cord injury. *Neuron* **89**, 814–828 (2016).
22. Wenger, N. et al. Spatiotemporal neuromodulation therapies engaging muscle synergies improve motor control after spinal cord injury. *Nat. Med.* **22**, 138–145 (2016).
23. Capogrosso, M. et al. A brain–spine interface alleviating gait deficits after spinal cord injury in primates. *Nature* **539**, 284–288 (2016).
24. Wagner, F. B. et al. Targeted neurotechnology restores walking in humans with spinal cord injury. *Nature* **563**, 65–71 (2018).
25. Rowald, A. et al. Activity-dependent spinal cord neuromodulation rapidly restores trunk and leg motor functions after complete paralysis. *Nat. Med.* **28**, 260–271 (2022).
26. Kathe, C. et al. The neurons that restore walking after paralysis. *Nature* **611**, 540–547 (2022).
27. Bezard, E., Imbert, C., Deloire, X., Bioulac, B. & Gross, C. E. A chronic MPTP model reproducing the slow evolution of Parkinson's disease: evolution of motor symptoms in the monkey. *Brain Res.* **766**, 107–112 (1997).
28. Yin, M. et al. Wireless neurosensor for full-spectrum electrophysiology recordings during free behavior. *Neuron* **84**, 1170–1182 (2014).
29. Mignardot, J. B. et al. A multidirectional gravity-assist algorithm that enhances locomotor control in patients with stroke or spinal cord injury. *Sci. Transl. Med.* **9**, eaah3621 (2017).
30. Cappellini, G., Ivanenko, Y. P., Dominici, N., Poppele, R. E. & Lacquaniti, F. Migration of motor pool activity in the spinal cord reflects body mechanics in human locomotion. *J. Neurophysiol.* **104**, 3064–3073 (2010).
31. Guiho, T., Baker, S. N. & Jackson, A. Epidural and transcutaneous spinal cord stimulation facilitates descending inputs to upper-limb motoneurons in monkeys. *J. Neural Eng.* **18**, 046011 (2021).
32. Minev, I. R. et al. Biomaterials. Electronic dura mater for long-term multimodal neural interfaces. *Science* **347**, 159–163 (2015).
33. Barra, B. et al. Epidural electrical stimulation of the cervical dorsal roots restores voluntary upper limb control in paralyzed monkeys. *Nat. Neurosci.* **25**, 924–934 (2022).
34. Lorach, H. et al. Walking naturally after spinal cord injury using a brain–spine interface. *Nature* **618**, 126–133 (2023).
35. Milekovic, T. et al. Stable long-term BCI-enabled communication in ALS and locked-in syndrome using LFP signals. *J. Neurophysiol.* **120**, 343–360 (2018).
36. Capogrosso, M. et al. Configuration of electrical spinal cord stimulation through real-time processing of gait kinematics. *Nat. Protoc.* **13**, 2031–2061 (2018).
37. Milekovic, T., Truccolo, W., Grun, S., Riehle, A. & Brochier, T. Local field potentials in primate motor cortex encode grasp kinetic parameters. *Neuroimage* **114**, 338–355 (2015).
38. Milekovic, T. et al. An online brain–machine interface using decoding of movement direction from the human electrocorticogram. *J. Neural Eng.* **9**, 046003 (2012).
39. Burciu, R. G. & Vaillancourt, D. E. Imaging of motor cortex physiology in Parkinson's disease. *Mov. Disord.* **33**, 1688–1699 (2018).
40. Yu, H., Sternad, D., Corcos, D. M. & Vaillancourt, D. E. Role of hyperactive cerebellum and motor cortex in Parkinson's disease. *Neuroimage* **35**, 222–233 (2007).
41. Sabatini, U. et al. Cortical motor reorganization in akinetic patients with Parkinson's disease: a functional MRI study. *Brain* **123**, 394–403 (2000).
42. Eckert, T., Peschel, T., Heinze, H. J. & Rotte, M. Increased pre-SMA activation in early PD patients during simple self-initiated hand movements. *J. Neurol.* **253**, 199–207 (2006).
43. Catalan, M. J., Ishii, K., Honda, M., Samii, A. & Hallett, M. A PET study of sequential finger movements of varying length in patients with Parkinson's disease. *Brain* **122**, 483–495 (1999).
44. Turner, R. S., Grafton, S. T., McIntosh, A. R., DeLong, M. R. & Hoffman, J. M. The functional anatomy of parkinsonian bradykinesia. *Neuroimage* **19**, 163–179 (2003).
45. Milekovic, T., Ball, T., Schulze-Bonhage, A., Aertsen, A. & Mehring, C. Detection of error related neuronal responses recorded by electrocorticography in humans during continuous movements. *PLoS ONE* **8**, e55235 (2013).
46. Gilron, R. et al. Long-term wireless streaming of neural recordings for circuit discovery and adaptive stimulation in individuals with Parkinson's disease. *Nat. Biotechnol.* **39**, 1078–1085 (2021).

47. Bruel, A. et al. Investigation of neural and biomechanical impairments leading to pathological toe and heel gaits using neuromusculoskeletal modelling. *J. Physiol.* **600**, 2691–2712 (2022).
48. Prasanth, H. et al. Wearable sensor-based real-time gait detection: a systematic review. *Sensors* **21**, 2727 (2021).
49. Movement Disorder Society Task Force on Rating Scales for Parkinson's Disease. The Unified Parkinson's Disease Rating Scale (UPDRS): status and recommendations. *Mov. Disord.* **18**, 738–750 (2003).
50. Nutt, J. G. et al. Freezing of gait: moving forward on a mysterious clinical phenomenon. *Lancet Neurol.* **10**, 734–744 (2011).
51. Grabli, D. et al. Gait disorders in parkinsonian monkeys with pedunculopontine nucleus lesions: a tale of two systems. *J. Neurosci.* **33**, 11986–11993 (2013).
52. Thenaisie, Y. et al. Principles of gait encoding in the subthalamic nucleus of people with Parkinson's disease. *Sci. Transl. Med.* **14**, eabo1800 (2022).

Tomislav Milekovic[1,2,3,4,5,25], Eduardo Martin Moraud[2,3,4,25], Nicolo Macellari[1,2,3,4,26], Charlotte Moerman[2,3,4,26], Flavio Raschellà[1,6,26], Shiqi Sun[1,2,3,4,26], Matthew G. Perich[5,26], Camille Varescon[1,2,3,4], Robin Demesmaeker[1,2,3,4], Alice Bruel[7], Léa N. Bole-Feysot[1,2,3,4], Giuseppe Schiavone[1,8], Elvira Pirondini[2,3,9,10], Cheng YunLong[11,12,13], Li Hao[11,12,13], Andrea Galvez[1,2,3,4], Sergio Daniel Hernandez-Charpak[1,2,3,4], Gregory Dumont[1,2,3,4], Jimmy Ravier[1,2,3,4], Camille G. Le Goff-Mignardot[1,2,3,4], Jean-Baptiste Mignardot[1,2,3,4], Gaia Carparelli[1,2,3,4], Cathal Harte[1,2,3,4], Nicolas Hankov[1,2,3,4], Viviana Aureli[1,2,3,4], Anne Watrin[14], Hendrik Lambert[14], David Borton[1,2,3,4,15], Jean Laurens[1,16], Isabelle Vollenweider[1,2,3,4], Simon Borgognon[1,2,3,4], François Bourre[17,18], Michel Goillandeau[17,18], Wai Kin D. Ko[11,12,13], Laurent Petit[17,18], Qin Li[11,12,13], Rik Buschman[19], Nicholas Buse[19], Maria Yaroshinsky[20], Jean-Baptiste Ledoux[21], Fabio Becce[21], Mayté Castro Jimenez[22], Julien F. Bally[22], Timothy Denison[23], Dominique Guehl[17,18], Auke Ijspeert[7], Marco Capogrosso[1,2,3,4,9], Jordan W. Squair[1,2,3,4], Leonie Asboth[1,2,3,4], Philip A. Starr[20], Doris D. Wang[20], Stéphanie P. Lacour[6,8], Silvestro Micera[6,24], Chuan Qin[12], Jocelyne Bloch[1,2,3,4,27] ✉, Erwan Bezard[11,12,13,17,18,27] ✉ & G. Courtine[1,2,3,4,27] ✉

[1]NeuroX Institute, School of Life Sciences, Ecole Polytechnique Fédérale de Lausanne (EPFL), Geneva, Switzerland. [2]Department of Clinical Neurosciences, Lausanne University Hospital (CHUV) and University of Lausanne (UNIL), Lausanne, Switzerland. [3]NeuroRestore, Defitech Center for Interventional Neurotherapies, EPFL/CHUV/UNIL, Lausanne, Switzerland. [4]Department of Neurosurgery, CHUV, Lausanne, Switzerland. [5]Department of Fundamental Neuroscience, Faculty of Medicine, University of Geneva, Geneva, Switzerland. [6]NeuroX Institute, School of Bioengineering, EPFL, Lausanne, Switzerland. [7]Institute of Bioengineering, School of Engineering, EPFL, Lausanne, Switzerland. [8]Laboratory for Soft Bioelectronic Interfaces (LSBI), NeuroX Institute, EPFL, Lausanne, Switzerland. [9]Rehab and Neural Engineering Labs, University of Pittsburgh, Pittsburgh, PA, USA. [10]Department of Physical Medicine and Rehabilitation, University of Pittsburgh, Pittsburgh, PA, USA. [11]Motac Neuroscience, UK-M15 6WE, Manchester, UK. [12]China Academy of Medical Sciences, Beijing, China. [13]Institute of Laboratory Animal Sciences, Beijing, China. [14]ONWARD Medical, Lausanne, Switzerland. [15]School of Engineering, Carney Institute for Brain Science, Brown University, Providence, RI, USA. [16]Department of Neuroscience, Baylor College of Medicine, Houston, TX, USA. [17]Université de Bordeaux, Institut des Maladies Neurodégénératives, UMR 5293, Bordeaux, France. [18]CNRS, Institut des Maladies Neurodégénératives, UMR 5293, Bordeaux, France. [19]Medtronic, Minneapolis, USA. [20]Department of Neurological Surgery, University of California, San Francisco, San Francisco, CA, USA. [21]Department of Diagnostic and Interventional Radiology, CHUV/UNIL, Lausanne, Switzerland. [22]Department of Neurology, CHUV/UNIL, Lausanne, Switzerland. [23]Oxford University, Oxford, UK. [24]Department of Excellence in Robotics and AI, Biorobotics Institute, Scuola Superiore Sant'Anna, Pisa, Italy. [25]These authors contributed equally: Tomislav Milekovic, Eduardo Martin Moraud. [26]These authors contributed equally: Nicolo Macellari, Charlotte Moerman, Flavio Raschellà, Shiqi Sun, Matthew G. Perich. [27]These authors jointly supervised this work: Jocelyne Bloch, Erwan Bezard, G. Courtine. ✉e-mail: jocelyne.bloch@chuv.ch; erwan.bezard@u-bordeaux.fr; gregoire.courtine@epfl.ch

Methods

Animal husbandry

Experiments were approved by the Institutional Animal Care and Use Committee of Bordeaux (CE50, France) under license number 50120102-A and performed in accordance with the European Union directive of 22 September 2010 (2010/63/EU) on the protection of animals used for scientific purposes in a facility accredited by the Association for Assessment and Accreditation of Laboratory Animal Care International (Chinese Academy of Medical Sciences). Eleven male macaque monkeys, M1–M11 (10 *Macaca mulatta* and one *Macaca fascicularis*; Supplementary Table 1), aged between 4 years and 6 years and weighing between 4.1 kg and 7.1 kg (5.88 ± 0.72 kg), were housed individually in cages designed according to European guidelines (2 m × 1.6 m × 1.26 m). Environmental enrichment included toys and soothing music. Sex was not considered in the study design and analysis because all the monkeys were male.

Behavioral training of NHPs

The animals were trained to walk on a motorized treadmill, across a straight corridor and across a horizontal ladder course that consisted of a platform at the beginning and at the end of the course and seven equally spaced rungs in between. Plexiglas enclosures (treadmill: 110 cm × 40 cm × 70 cm; corridor/ladder: 300 cm × 35 cm × 70 cm) were used to keep the animals within the field of view of the cameras. Food pellets and fruits rewarded appropriate behavior. Additional food to complete daily dietary requirements was provided after training.

Preparation and assessment of the NHP model of PD

We administered MPTP in M1–11 according to the previously published protocol[53–59]. Animals were treated daily (7:00) with MPTP hydrochloride (0.2 mg kg^{-1}, intravenous, Sigma-Aldrich) dissolved in saline according to a previously described protocol[8]. This protocol describes a reproducible MPTP cumulative dosing regimen that leads to the first appearance of Parkinsonian clinical signs after 15 ± 1 injections (that is, a cumulative dose of 3.0 ± 0.2 mg kg^{-1}). Neurological deficits were evaluated every morning at 9:00 in home cages for 30 min. Two blinded observers who were not involved in the study quantified these deficits using a validated Parkinsonian Disability score[60] assessing general level of activity, body posture, vocalization, freezing, tremor and frequency/rigidity of arm movements. We stopped the injections when the deficits corresponded to late-stage Parkinsonism, defined by a Parkinsonian Disability score of 5 or higher. Injections were repeated if the monkeys displayed recovery of gait and balance. The kinetics of nigrostriatal degeneration in this model and the critical thresholds associated with the symptom appearance have been thoroughly investigated using several in vivo and postmortem endpoints[60,61].

Anatomical quantification of the impact of MPTP administration in NHPs

We analyzed the depletion of dopaminergic tissue in the six monkeys (M5, M6, M7, M8, M9 and M11) that were involved in primary motor cortex recordings after MPTP administration and in the experiments with the brain-controlled spinal cord neuroprosthesis. The monkeys were deeply anesthetized and perfused transcardially with a 4% solution of paraformaldehyde. Their brain was removed and stored at 4 °C in 0.1 M phosphate-buffered saline azide (0.03%). We counted, using an unbiased stereological method, the nigrostriatal dopaminergic neurons and quantified the density of dopaminergic fibers in the caudate and ventral and dorsal putamen as described previously[62]. In brief, tyrosine hydroxylase (TH) immunochemistry was performed using mouse anti-TH primary antibody (1:1,000, clone LNC1, catalog no. MAB318; Millipore/Chemicon International). Unbiased stereological counting of nigral TH^{ON} neurons as well as striatal optical density measurement were performed using Exploranova Mercator (Explora Nova). Technical reasons prevented quantification of dopaminergic fiber density in M5 and of all brain tissues in M11.

NHP surgical procedures

All surgical procedures were described in detail previously[23,36]. Surgical interventions were all performed under full anesthesia induced by atropine (0.04 mg kg^{-1}, intramuscular) and ketamine (10 mg kg^{-1}, intramuscular) and maintained under 1–3% isofluorane after intubation. A certified functional neurosurgeon (J.B.) supervised all surgical procedures. Surgical implantations were performed during one or two surgeries. M5–M7 were implanted with a 96-channel microelectrode array (Blackrock Microsystems, 1.5-mm pitch) into the leg area of the left primary motor cortex and a wireless system[23,63] to record EMG signals (T33F-4, Konigsberg Instruments) from the following leg muscles: gluteus medius (GLU), iliopsoas (IPS), rectus femoris (RF), semitendinosus (ST), gastrocnemius medialis (GM), tibialis anterior (TA), extensor digitorum longus (EDL) and flexor hallucis longus (FHL). M8–M11 were implanted with two 48-channel microelectrode arrays in the leg area of left and right primary motor cortex and a custom system that wired the EMG signals from right IPS, RF, ST, GM and TA and left GM and TA muscles to a skull-mounted titanium pedestal. In a second surgery, two epidural spinal arrays were inserted into the epidural space under the L2–L3 and L5–L6 vertebrae according to previously described methods[23,36]. We finely adjusted the rostro-caudal and medio-lateral position of the electrodes using intraoperative electrophysiological monitoring[23,36]. We anchored the implants to the spinous process of L3 and L6 vertebrae with a suture. The wires of each spinal implant were routed subcutaneously to an IPG (Activa RC, Medtronic) inserted between the intercostal muscles. All implantable devices were acquired from Medtronic, and research software was reused from previous work. The proper location of the microelectrode arrays and epidural spinal arrays with respect to gross anatomical landmarks was verified postmortem in all monkeys.

M9 was additionally implanted with two DBS mini-leads (four contacts per lead, 0.5-mm contact length, 0.5-mm inter-contact distance, 0.625-mm diameter, NuMED) in the right and left subthalamic nucleus. Stereotactic coordinates of each subthalamic nuclei were calculated based on ventriculography, as detailed previously[64]. First, we attached a hollow cannula (0.625-mm inner diameter) to a stereotactic frame to insert the probe into the brain until the tip was located at the computed coordinates. We then descended the leads into the brain through the cannula. After the descent, we verified the proper location of each implant using X-ray. We then removed the cannula and fixed the lead to the skull using surgical cement. We again confirmed the location of each lead after fixation using X-ray and then connected the leads with an implanted pulse generator (Activa RC, Medtronic) using quadripolar extension cables (Medtronic). We validated this connection by recording stimulation artifacts following stimulation through each DBS contact. We confirmed the placement of DBS leads postmortem using an MRI scan of the explanted brain.

The veterinary team continuously monitored the animals during the first hours after surgery and several times daily during the seven following days. A few hours after surgery, the animals could move around and feed themselves unaided. We used clinical rating and monitoring scales to assess postoperative pain. Ketophen (2 mg kg^{-1}, subcutaneous) and Metacam (0.2 mg kg^{-1}, subcutaneous) were administered once daily. Lidocaine cream was applied to surgical wounds twice per day. The ceftriaxone sodium antibiotic (100 mg kg^{-1}, intramuscular) was given immediately after surgery and then once daily for 7 d.

Design and fabrication of NHP epidural spinal arrays

According to our earlier modeling work[20,21,24,36], to recruit the proprioceptive fibers that access motor neuron pools located in the L2–L7 spinal segments, EES needs to target the dorsal roots projecting to these segments. For this purpose, we tailored epidural spinal arrays

to the anatomy and physiology of the vertebral and spinal columns, taking into account the electrochemical requirements related to the size of the electrodes and interconnect tracts that are connected to the IPG. To satisfy these limitations, we designed two implants: a rostral implant targeting the L2–L4 roots and a caudal implant targeting the L5–L7 roots. The epidural spinal arrays inserted in M8, M9 and M10 were produced by CorTec using AirRay Electrode Technology. We also fabricated the epidural spinal arrays using e-dura technology[32,33,65] (Supplementary Information), which was implanted in M11.

Data acquisition in NHP

Procedures to record kinematics and muscle activity were detailed previously[23,63,66]. We captured whole-body kinematics using the high-speed motion capture SIMI system (Simi Reality Motion Systems), combining 4–6 video cameras (100 Hz). We applied reflective white paint on the shaved skin of the animals overlying the following body landmarks: iliac crest (crest), greater trochanter (hip), lateral condyle (knee), lateral malleolus (ankle) and the fifth metatarsophalangeal (foot). We used the SIMI motion software to reconstruct the three-dimensional (3D) spatial coordinates of the markers. Joint angles were computed accordingly. In M5–M7, we used a custom-built system to receive the wirelessly emitted signals from the implanted T33F-4 devices (Konigsberg Instruments). In M8–M10, we used a W16 system (Triangle Biosystems) to acquire the wirelessly transmitted signals. In M11, the implanted EMG system failed soon after the surgery. Consequently, all subsequent analyses were performed using kinematic recordings. We wirelessly recorded neural signals using the Cereplex-W system[23,28] (Blackrock Microsystems). In M9, the skull-mounted pedestal used to connect the Cereplex-W system failed before we could test the efficacy of brain-controlled spinal cord stimulation on the ladder. Both EMG and neural wireless recording systems were connected to a Neural Signal Processor (NSP, Blackrock Microsystems) that synchronized EMG and neural signals sampled at 2 kHz and 22 kHz, respectively. The NSP band-pass filtered (500 Hz to 7.5 kHz) the neural signals and extracted multi-unit spikes as times when the signal crossed a threshold set to 3.5 times the root mean square of the signal[23]. This procedure resulted in spike times from each of the 96 electrodes. We used an additional NSP channel to record an analog trigger of the SIMI system used to synchronize the SIMI video recordings with the physiological signals. The NSP continuously broadcasted Used Datagram Protocol (UDP) packets containing neural, multi-unit spiking, EMG and trigger channel recordings over the local network. A dedicated storage computer received the UDP packets and saved the recordings on a hard drive using Cerebus Central Suite software (Blackrock Microsystems).

Analysis of NHP gait and balance deficits resulting from MPTP treatment

In monkeys M1–M9, we recorded gait kinematics before and after MPTP administration (Supplementary Table 2). We used two metrics as aggregate measures of performance: task time and crossing time. Similar to the instrumented timed-up-and-go (iTUG) assessment used to evaluate motor capacity of people with PD[67,68], task time is the period from the moment the animal stands up on one side of a corridor or a ladder to the moment it places the food reward in its mouth on the other side of the corridor. Because task time may vary due to differences in the time each animal spent reaching for the food, we also calculated the crossing time as the period necessary for the animals to cross the central portion of the corridor or ladder. To quantify locomotor performance, we applied a PC analysis on 83 gait parameters (Supplementary Table 3) calculated based on previously described methods[23,36,66]. We used three leading PCs of the space spanned by these parameters to visualize the differences between the gait cycles recorded before and after MPTP administration or across the experimental conditions (Extended Data Fig. 1). Next, we extracted the factor loading on each PC to identify the parameters that more robustly explained the differences between the conditions.

Analysis of gait impairments of people with PD

To compare gait deficits of people with PD to the gait deficits recorded from our MPTP NHP model, we organized gait recordings in people with PD and healthy controls as part of the PREDI-STIM clinical study (ClinicalTrials.gov ID: NCT02360683). The PREDI-STIM study was approved by the Nord Ouest IV Ethical Committee, France (2013-A00193-42) and was conducted in accordance with the Declaration of Helsinki. The inclusion criteria involved patients with PD receiving a pre-therapeutic assessment and monitoring for 1 year, 3 years and 5 years as part of the regular monitoring of the subthalamic nucleus DBS. The study involved 25 participants with PD (12 females and 13 males, mean age 60 ± s.d. 7.8) and nine participants without PD as controls (four females and five males, mean age 58.8 ± s.d. 4.5). Sex was self-reported. Sex was considered in the study design; the participants were enrolled to ensure a balanced sex distribution. Informed consent was obtained from all participants. The participants received no compensation for the study. The participants performed one or more sessions during which we recorded full-body kinematics. The study protocol can be made available upon reasonable request to the corresponding authors. The study outcomes are reported at https://classic.clinicaltrials.gov/ct2/show/NCT02360683.

Under the framework of the PREDI-STIM study, we recorded and analyzed the gait of $n = 25$ participants diagnosed with PD who exhibited debilitating gait deficits with various degrees of severity and $n = 9$ age-matched healthy controls. We recorded whole-body kinematics using a Vicon motion capture system (Vicon). We attached 34 reflective markers (26 on the legs, arms and trunk and eight on the head and wrists) on the surface of the skin of the participants to cover all key body joints (foot, ankle, knee, hip, shoulder, elbow, hand, neck and head as well as spinal vertebrae T10 and C7). We employed Nexus biomechanical software (Vicon) to triangulate the centroid of each joint in each timepoint. Putting the joint centroids together provided us with full-body kinematics. We developed custom software in the MATLAB environment (MathWorks) to derive the timing of gait events (heel strike/foot off) and calculate the walking parameters from full-body kinematics. We then used this software to discretize each gait cycle into $n = 65$ kinematic variables, which quantified the amplitude, speed or consistency of each step. To enable comparisons with NHP results, we restricted our analyses to the 35 kinematic variables related to leg movements (Supplementary Table 5). We then applied the PC analysis on this high-dimensional representation of gait across Parkinsonian and healthy study participants to identify the most relevant variables to explain changes in walking induced by the PD and potential improvements that can be brought in by a therapy.

Identification of hotspots from spatiotemporal maps of motor neuron activity

Video recordings were used to mark the right foot strike and right foot off gait events and, thus, calculate the average proportion of the stance and swing phases over all collected gait cycles. We transformed the EMG signals into activity of motor neuron pools using previously described methods[23,36]. The activity of motor neurons during each gait cycle was converted from time to gait phase coordinates. We then generated the spatiotemporal maps of motor neuron activity by averaging the activity of motor neurons over all the recorded gait cycles. We applied a Gaussian mixture model to these maps to identify the dominant hotspots of activity[69].

Decoding of hotspot initiation events from primary motor cortex neural activity of MPTP-treated NHPs

We implemented an algorithm that decoded the initiation of weight acceptance and leg lift hotspots from the neural activity. We used datasets with synchronized multi-unit spikes and gait events to calibrate the decoding algorithm, as done previously[23,33,36] and described in detail in the Supplementary Information. In brief, we used the spatiotemporal

maps of motor neuron activity to calculate the average temporal difference between the right foot off and foot strike gait events and the right weight acceptance and leg lift hotspot initiation events, respectively. We used these latencies to transform gait events into weight acceptance and leg lift hotspot initiation events. In the same dataset, we estimated multi-unit spike rates in each of the 96 channels by summing up the multi-unit spikes with a 150-ms history every 0.5 ms. We used these multi-unit rates and the hotspot initiation events to calibrate a multi-class rLDA decoder[23,33,35,36]. Based on a 300–500-ms history of neural activity, the decoder returned the probabilities of observing each of category of hotspot initiation events used to calibrate the decoder. The hotspot event types included (1) left weight acceptance, (2) left leg lift, (3) right weight acceptance and (4) right leg lift. When the probability of one of the hotspot initiation events crossed a threshold of 0.8, that event was detected. To verify the efficacy of our decoding approach after MPTP administration, we used the dataset collected from M6 and M7 and performed offline cross-validation of our decoding approach. We measured the temporal accuracy of the decoder in nine (M6) and eight (M7) sessions performed before and after MPTP administration.

Decoding of hotspot initiation events from epicortical signals of people with PD

We analyzed data of participants P2 and P3 of the 'Motor Network in Parkinson's Disease and Dystonia: Mechanisms of Therapy' clinical trial (ClinicalTrials.gov ID: NCT03582891). Both participants (male as self-reported, 40 years and 63 years old, respectively) provided written informed consent in accordance with the institutional review board and the Declaration of Helsinki. Sex and gender were considered in the study design: women and men were recruited in proportion to their numbers in the clinical population of the recruiting center. Nonetheless, because both participants included in our research were male, sex was not considered in the analysis. Patients were not compensated for participation but were offered reimbursement for transportation and parking when they came for the study visits. The period of recruitment and data collection for the two patients was from June 2019 to December 2019. The data were collected at the Human Performance Center at Mission Bay Campus at the University of California, San Francisco. The clinical trial outcomes are reported at https://classic.clinicaltrials.gov/ct2/show/NCT03582891.

The study procedures were previously described in detail[46]. In short, participants were recruited from a population referred for implantation of deep brain stimulators for PD. Before recruitment, they were evaluated by a movement disorders neurologist and met diagnostic criteria for PD[70] and by a neuropsychologist to exclude major cognitive impairment or untreated mood disorder. Inclusion criteria included motor fluctuations with prominent rigidity and bradykinesia in the off-medication state, baseline off-medication MDS UPDRS III scores between 20 and 80, greater than 30% improvement in MDS UPDRS III on medication than off medication and absence of substantial cognitive impairment (score of 20 or above on the Montreal Cognitive Assessment). The full IDE application (G180097) and study protocol have been shared with other researchers via the Open Mind initiative (https://openmind-consortium.github.io).

Study participants underwent bilateral placement of cylindrical quadripolar deep brain stimulator leads into the subthalamic nucleus (Medtronic model 3389; 1.5-mm contact length and 2.0-mm intercontact spacing), bilateral placement of quadripolar cortical paddles into the subdural space over the cortical area that included the motor cortex (Medtronic model 0913025; 4-mm contact diameter and 10-mm intercontact spacing) and bilateral placement of investigational sensing IPGs in a pocket over the pectoralis muscle (Medtronic Summit RC+S, model B35300R). The IPG on each side was connected to two leads by 60-cm lead extenders (Medtronic model 37087). The Summit RC+S IPG is a 16-channel device that, through the use of its application programming interface, allows researchers to record four bipolar time domain channels (250/500 Hz) or two channels at 1,000 Hz[71,72]. For all research functions, including configuring and initiating sensing and developing embedded or distributed adaptive DBS, investigators controlled the device by writing software in C# within the device API, accessed using a 'research development kit' (Medtronic model 4NR013) provided by the manufacturer. We wrote a software application to configure and initiate streaming data from two RC+S devices simultaneously (available at https://openmind-consortium.github.io). This software was written in compliance with the US Food and Drug Administration (FDA) code of federal regulation CFR 820.30, which specifies design controls for implantable human devices.

Here we have analyzed recordings collected with P2 and P3 during one session of overground walking in a corridor and with P2 during one session of walking on a treadmill. In those sessions, the participants were on their regular levodopa therapy, and their DBS was kept off. Cortical field potentials were sampled at 500 Hz. We simultaneously recorded video using a camera and full-body kinematics using a set of IMU sensors distributed across major anatomical landmarks.

Feature selection and decoding were performed according to previously published procedures[23,33,35,36,38,45]. In brief, we used the reconstructed kinematics of the ankle to identify left and right leg lift hotspot initiation events. These events match the events used to synchronize the spinal stimulation with the movement intentions of NHPs. We processed the epicortical signals using a high-pass filter at 0.5 Hz and then low-pass filtered with a second-order 0.25-s-long Savitzky–Golay filter[38,73]. The synchronized dataset of processed epicortical signals and gait events was then used to calibrate two rLDA decoders targeting, respectively, left and right leg lift hotspot initiation events. We evaluated the offline decoding accuracy for each side separately by performing cross-validation of the decoders (see 'Decoding performance' subsection).

Decoding performance

We derived the distribution of temporal differences between the decoded hotspot initiation events and the hotspot initiation events reconstructed from video recordings. We then quantified the performance of our decoders using temporal decoding accuracy, defined as the proportion of temporal differences falling within a window of 200 ms. Standard error was estimated using bootstrapping with 10,000 resamples.

Therapeutic approach

We aimed to re-establish the natural dynamics of motor neuron activation using EES protocols targeting the weight acceptance, propulsion and leg lift hotspots associated with the leg and right legs. This concept implied that EES had to be triggered (1) at the appropriate locations with amplitudes that reproduce the activation of these hotspots, (2) at the times when those hotspots should be active and (3) for the duration over which each hotspot is activated. The following three sections describe how we achieved these three requirements.

Identification of amplitude and duration to target each hotspot

In M8–M10, we recorded the electromyography from right leg muscles in response to single pulses of EES. For each of the 16 electrodes of the spinal implant, we recorded the muscle responses over a broad range of stimulation amplitude, ranging from subthreshold to saturation. We translated these recordings into a mapping among each electrode, EES amplitude and evoked muscle responses. We transferred the relative amplitude of the observed responses into spatial maps of motor neuron activity. We then identified the optimal combinations of electrodes and amplitudes that maximized the correlation between the targeted and elicited spatial map of motor neuron activity. Correlations were measured at the center of each hotspot. We, thus, obtained three

combinations of electrodes and amplitudes that targeted the weight acceptance, propulsion and leg lift hotspots. Because we recorded only two muscles on the left side, we could not follow the same procedure to determine EES protocols for the left hotspots. Consequently, we determined these combinations based on the observed kinematic responses to single-pulse stimulation. This procedure was applied for both sides in M11, because muscle activity could not be recorded in this animal. EES durations were set to the duration of the corresponding hotspots. In M11, the durations were determined by observing kinematic responses to stimulation during locomotion. We, thus, defined a set of 'stimulation protocols'—combinations of stimulation location, amplitude and duration designed to reinforce a specific hotspot.

Using detected hotspot initiation events to trigger spinal stimulation

We designed a real-time control system that used the decoding algorithm to trigger EES protocols at appropriate times. The control computer was connected to the local network and continuously received UDP packets containing neural recordings. We developed a C++ software application (Visual Studio 2010 and 2015) running on the control computer, which analyzed the neural signals in real time. Every 15 ms, the application used the decoding algorithm to calculate the probabilities. If one of the hotspot initiation events was detected, the application triggered the relevant EES sequence. We designed EES sequences as composite stimulation protocols that reinforce one or more of the ongoing or soon-to-be-active hotspots. Because these hotspots often overlapped, the sequences executed protocols in parallel to reinforce the natural dynamics of motor neuron activity. The wireless control of the stimulation had a mean transmission latency of 105 ms[23]. We accounted for this latency when translating gait events into hotspot initiation events (Extended Data Fig. 4a).

Tuning of EES sequences using brain-controlled spinal cord neuroprosthesis

Once the decoder was calibrated, we used the detected hotspot initiation events to trigger EES sequences that contained only one of the six protocols derived from the optimal combinations of electrode and amplitude targeting each hotspot. The animals walked while the brain-controlled spinal cord neuroprosthesis triggered these simple EES sequences. We then tuned the amplitudes and durations of EES protocols based on muscle and kinematic responses. We performed this procedure for all six protocols. We then designed 'left' and 'right' composite EES sequences containing either (1) left weight acceptance, right leg lift and left propulsion protocols or (2) right weight acceptance, left leg lift and right propulsion protocols, respectively. We then used the detected left or right weight acceptance events to trigger these sequences. To account for interaction of multiple EES protocols, we tuned the design of these composite EES sequences until we reached satisfying behavioral responses. This tuning process typically lasted for about 1 h during the first session. Subsequent sessions required only minor tuning that typically lasted 5–10 min.

Calibration procedure to account for stimulation-induced changes in neural signals

Due to sparsity of EES bursts using only one hotspot event (once over a 1–2-s-long gait cycle), the neural activity used to decode hotspot initiation events was not affected by the motor cortical response elicited by bursts of EES[23]. However, the repeated delivery of EES sequences that reinforce all six hotspots disrupted the decoder. We, thus, developed a procedure to ensure that the decoder would remain reliable during EES despite cortical responses to EES bursts. For this purpose, we implemented the previously developed two-step calibration procedure[23], which we optimized for PD. In brief, once we tuned the composite EES sequences, we recorded several trials along the corridor while only the left or right weight acceptance events triggered left or right composite sequence, respectively. We then calibrated a second decoder based on the data recorded with and without EES. This two-step decoder successfully compensated for stimulation-induced changes in motor cortex activity (Extended Data Fig. 4b).

Evaluation of the brain-controlled spinal cord neuroprosthesis in NHPs after MPTP administration

We evaluated the therapeutic efficacy of the brain-controlled spinal cord neuroprosthesis to alleviate gait and balance deficits in M8, M9 and M11. We applied all of the above procedures to calibrate the decoder and tune EES protocols. In M8, the decoders used in both reported sessions were calibrated using the data recorded 1 d or 2 d before. The same decoder was used to deliver EES sequences during locomotion along the ladder. We measured locomotor performance using task and crossing time, as explained above. M8 and M11 showed specific deficits. M8 developed occasional episodes of slowing of gait and freezing of gait. M11 displayed frequent falls when progressing along the ladder. To evaluate the improvement in these specific deficits with the neuroprosthesis, we calculated the proportion of trials along the corridor that contained episodes of slowing of gait or freezing of gait in M8 and the proportion of trials along the ladder in which M11 fell. We also quantified the impact of the neuroprosthesis on kinematics and muscle activity. We isolated all the gait cycles where all four decoded hotspot initiation events were within a window of 200 ms with respect to the reconstructed hotspot initiation events. In M8 and M9, we compared locomotor performance with and without using the neuroprosthesis for two different days of recordings before the MPTP administration as a reference to its healthy gait. We compared the effect of the neuroprosthesis on the variables that were identified as most relevant to account for gait and balance deficits resulting from MPTP administration: stride length, endpoint velocity of the foot and lateral hip displacement in the corridor task and stance duration and velocity in the ladder task. In M8 and M9, we applied a PC analysis on 83 gait parameters calculated for each gait cycle and visualized the impact of the experimental conditions in the plane defined by the first two PCs, according to previously described methods[23,36,66]. To quantify gait performance, we calculated the mean Euclidean distance between gait cycles in the entire 83-dimensional space of kinematic parameters, as described previously[23,66] and above.

Evaluation of synergistic effects between brain-controlled spinal cord neuroprosthesis and DBS in NHP

Monkey M9 was implanted with the spinal cord neuroprosthesis and a DBS implant. We first tuned and tested the spinal cord neuroprosthesis as described above. We then tuned and tested the effects of DBS. Finally, we tested the two therapies together. To tune DBS, we applied charge-balanced biphasic stimulation pulses (90 µs, 125 Hz, constant voltage mode) using each DBS contact at increasing amplitudes in steps of 0.2 V. We increased the amplitude until we observed stimulation-induced motor responses (for example, neck twitches) while the animal was sitting. We then reduced the amplitude, typically by 0.1–0.4 V, until these motor responses disappeared. To evaluate the effects of DBS, we turned on the stimulation at least 30 min before the experiments started to account for reported slow dynamics in the effects of DBS on gait[7]. When evaluating 20-Hz DBS, we increased the stimulation amplitude to compensate for frequency-related changes in induced charge according to previously published guidelines[74]. Motor changes induced by DBS additionally included observations in free behavior of the animal, which we quantified in terms of (1) number of corridor crossings within a 10-min interval, (2) number of corridor crossings completed without stopping and (3) average gait cycle duration during each crossing. These quantifications aimed to account for improvements in mobility and awareness, facility to turn and ambulate and locomotor speed.

STIMO-PARK study design and objectives

The experiments to evaluate the spinal cord neuroprosthesis were carried out as part of the ongoing clinical feasibility study STIMO-PARK (ClinicalTrials.gov ID: NCT04956770), which investigates the effects of lumbosacral EES to improve mobility in people with PD. The STIMO-PARK study was approved by the Swiss ethical authorities (Swissethics protocol no. 2021-0047) and the relevant regulatory authorities (Swissmedic protocol no. 100008) and was conducted following the Declaration of Helsinki. The inclusion criteria include (1) idiopathic PD with III–IV Hoehn–Yahr stage, (2) exhibiting severe gait difficulties and postural instability, (3) use of the Medtronic DBS implant and (4) receiving medication for PD. The study involved a pre-implantation assessment, surgical implantation of the spinal neurostimulation system, a 1-month period for configuration of EES protocols and a 3-month period of physiotherapist-assisted rehabilitation (3-h sessions, 2–3 times per week). The rehabilitation program is personalized based on the participants' needs and improvements. Study participation was not compensated, but all study-related costs incurred on the participants were reimbursed. The sex of participants was not considered in the clinical trial design. STIMO-PARK study protocol can be made available upon reasonable request to the corresponding authors. The trial outcomes are reported at https://classic.clinicaltrials.gov/ct2/show/NCT04956770.

P1 of the STIMO-PARK study

P1 was enrolled in the STIMO-PARK clinical study by signing a written informed consent. P1 also provided written informed consent for publication of identifiable images and video. He was a 61-year-old male (self-reported) at the time of enrollment. He had been diagnosed with PD at the age of 36 and was implanted with DBS at the age of 44. He is currently in stage 3 of the Hoen–Yahr scale. He experiences fluctuations in his gait pattern and lower limb symptoms typical of later stages of PD, including slowness, asymmetry, rigidity, small steps and flexed posture. Before being implanted with the EES system, during the Six-Minute Walk Test, P1 was able to cover 433 m with DBS turned on and during his regular levodopa intake and 224 m with DBS turned off and with the last levodopa intake the evening before. His MDS UPDRS motor examination scores (part III) in these two states were 20 and 47, respectively. He started to experience freezing of gait over the last decade, which greatly impacted his independence and quality of life. Before participation in the study, he reported four falls per day, on average, due to freezing of gait. After enrollment, we performed a CT scan of his torso and a structural MRI scan of his spine to generate a personalized anatomical model of his spine. After the pre-surgical assessments, P1 was implanted with the spinal EES neurostimulation system. After the surgery, P1 was transferred to the neurosurgery ward for recovery. P1 then went back to the hotel for a 1-week recovery period. After recovery, we successfully configured the EES protocols and sequences for P1 during the study configuration period. This study presents the analysis of seven sessions recorded during the study configuration period after the EES protocols and sequences were configured. P1 continued with the study procedures afterwards. All surgical and experimental procedures were performed at the Lausanne University Hospital (CHUV). The procedures are described in detail below.

P1 personalized neurobiomechanical model

To estimate the target for the immediate effects of our therapy, we sought to simulate the gait of P1 given his anatomy but in the absence of neurodegeneration. To this end, we generated a personalized musculoskeletal model of P1 by adapting the Lower Limb model[75] to P1's anatomy and by optimizing the reflex-based gait controller used to generate walking[76]. Similar methods have been used to reproduce gait of healthy individuals[77], gait of elderly affected by muscle weakness and reduced contraction speed[78] and gait adaptations due to ankle plantarflexor muscle weakness and contracture[47,76]. The musculoskeletal model included three planar degrees of freedom at the pelvis and another three for each leg: hip flexion, knee flexion and ankle flexion. These degrees of freedom are actuated by eight Hill-type muscle–tendon units[79] per leg corresponding to eight different leg muscles: (1) gluteus maximus, (2) hamstring muscles, (3) iliopsoas, (4) vastus muscles, (5) biceps femoris, (6) gastrocnemius, (7) soleus and (8) tibialis anterior. This model is scaled to P1 morphology derived from the motion tracking of P1 while standing using the OpenSim scaling tool[80]. We also scaled the muscular properties of the model using muscles' cross-sectional area segmented from P1's thigh CT scan. As the maximal voluntary force and cross-sectional area are significantly correlated through aging[81], we scaled the maximal isometric force of each Hill-type muscle–tendon unit to the ratio of the muscle cross-sectional area over the healthy reference from refs. 82,83. Due to the absence of the calf CT scans, we scaled the maximal isometric force of the calf muscles using the mean of the thigh muscle ratios. To obtain a more robust estimate of the muscle strengths, we averaged the scaling over both sides. The resulting scaling factors were 0.65 for the hamstrings group, 0.87 for the quadriceps group and 0.76 for the calf group. We then used SCONE software[84] to optimize the parameters of the reflex-based gait controller[76]. This controller is composed of phase-dependent reflexes providing muscle excitation based on muscle length, velocity or force feedback. We simulated P1 gait in the absence of neurodegeneration using the Covariance Matrix Adaptation Evolutionary Strategy (CMA-ES) [85] to optimize the controller parameters. We used a cost function penalizing falling, muscles' metabolic cost[86], joint angles out of healthy ranges and the head balance, with respective weights 100, 0.1, 0.1 and 0.05 balancing the competitive objectives. About 500 generations of CMA-ES were necessary to reach a stable gait initialization[76]. Once the parameters of the controller converged, we generated 200 steps of this neurobiomechanical model and extracted full kinematics of lower limbs and muscle activity. We then compared these simulation-generated kinematic and muscle activity signals with the signals recorded during the P1 study sessions.

Planning the surgical placement of the epidural spinal array in P1 using personalized anatomical model of the spine

We used P1's CT and MRI scans to generate a 3D anatomical model of his spine. First, we segmented the vertebral bones from the CT scan using a convolutional neural network (CNN)-based framework[87] trained on the VerSe 2019 and VerSe 2020 datasets[88]. We then segmented the spinal cord tissue from the MRI scan using nnU-Net[89] after pre-processing and with post-processing using the Spinal Cord Toolbox version 5.4 (ref. 90). The remainder of the array placement planning was performed in the Sim4Life software. We loaded the MRI scan images and the segmented spinal cord tissue and then identified the locations where spinal cord roots merge with the spinal cord—hereafter termed 'root merging point'. We then generated the trajectories of the spinal cord roots that follow the path from the root merging point to the entry of that root into the spinal canal. We defined the spinal cord segments as spinal cord tissue bounded by the midpoints between the two neighboring root merging points. We defined the root trajectory leading to the root merging point as the central rootlet and distributing four off-center rootlets across the segment. We then loaded the vertebral bones and disks segmented from the CT scan and aligned it to the spinal cord and roots. Next, we used this combined anatomical model to propose a placement of the array. We first loaded a 3D model of the array and placed it centered over the dorsal side of the spinal cord covering most of the L1–L5 spinal segments, which control the contraction of leg muscles. Position of the array with respect to the segmented vertebral column determined the insertion point of the array to be between L1 and T12 vertebrae.

Surgical implantation of the STIMO-PARK investigational spinal EES neurostimulation system in P1

During the surgery, we implanted P1 with a Specify SureScan MRI 5-6-5 16-electrode epidural spinal array (Medtronic) in the posterior epidural

space covering the lumbar spinal cord segments. This array is clinically approved for the treatment of chronic pain. We then connected the array by a cable to an Activa RC IPG (Medtronic), which is clinically approved as an IPG for DBS therapy. The IPG was first inserted into a subcutaneous pocket in the abdomen. The cables were then tunneled from one opening to the other and connected to the IPG. These combined elements and associated firmware constitute an investigational spinal EES neurostimulation system that was tested as part of this clinical study.

We identified the insertion level during surgery using fluoroscopy. To insert the array, we performed an approximately 5-cm midline skin incision. We opened the fascia, and the muscles retracted bilaterally. Excision of the midline ligamentous structures and T12/L1 flavectomy and partial laminectomy enabled the insertion of the array into the spinal epidural space. To perform the insertion, we placed the array over the midline of the exposed dura and advanced rostrally to the target location.

We used the ISIS Xpress monitoring and stimulation system (inomed Medizintechnik) to accurately adjust the medial and segmental position of the array. To this end, we delivered EES pulses with a pulse width of 300 µs at 0.5 Hz and at increasing amplitudes to elicit muscle responses that were recorded with subdermal (Neuroline Twisted Pair Subdermal, 12 × 0.4 mm, Ambu) or intramuscular needle electrodes (inomed SDN electrodes, 40 mm, inomed Medizintechnik). The lateral position of the array was adjusted so that the bottom electrodes selectively recruit the calf muscles while maintaining good activation of the hip flexor muscles using the top electrodes. The medial position of the array was adjusted to reach a similar side-specific muscle recruitment with the corner electrodes. The final location of the array overlaid lumbar and upper sacral segments. The surgery then finished, and P1 was transferred to the neurosurgery ward for recovery.

Reconstruction of the electrode position with respect to the patient spine was assessed from the postoperative CT scan. CT images enabled reconstructing the 3D geometry of vertebrae and the location of the array electrodes inside the vertebral column. The resulting 3D volume reconstruction of the spinal cord of the participant included the array with its electrodes, vertebral bodies, white matter, trajectory of dorsal spinal roots and rootlets.

P1 spinal cord neuroprosthesis

We delivered the EES of the lumbar spinal cord by controlling the delivery of current though the 16 IPG header channels, each connected to one of 16 electrodes of the epidural spinal array, or through the IPG case. The IPG was modified from its clinical version with an investigational firmware that enabled real-time communication with NEUWalk Research Programmer Application (NRPA) software (Medtronic model 09103) running on an external computer. The NRPA acted as a relay between the G-Drive Plus control software (described below) and the IPG. The NRPA communicated wirelessly with the IPG through the following communication chain: the NRPA sent commands via a virtual COM port corresponding to a Bluetooth adapter; a custom wireless bridge consisting of a nano computer (Raspberry Pi) received this command and forwarded it to a virtual COM port corresponding to a USB adapter; and a USB to infrared adapter (ACT-IR224UN-LN115-LE, ACTiSYS) transformed this command into infrared signals that were then read by a modified Medtronic patient's programmer (Sensing Programmer Telemetry Module (SPTM), Medtronic), which finally transmitted the command to the patient's IPG by electromagnetic induction through the skin.

G-Drive Plus software for configuration and control of the spinal cord neuroprosthesis in P1

We developed a custom G-Drive Plus software application to configure and control the spinal cord neuroprosthesis[25]. G-Drive Plus runs on a desktop computer, laptop or tablet and interfaces with the stimulation system (through NRPA) and collects the signals from different sensors that can be used for closed-loop stimulation. The sensors include the wireless Next Generation Inertial Measurement Units (NGIMU, X-IO Technologies) and the Trigno Research+ System using wireless Trigno Avanti sensors that can record both the IMU and EMG signals simultaneously. G-Drive Plus includes a graphical user interface (GUI) that enables rapid personalization of EES protocols, each of which is parametrized by a set of cathodes and anodes to deliver the stimulation, the amplitude of the stimulation current and the stimulation frequency. G-Drive Plus GUI also includes a stimulation scheduler that enables rapid personalization of sequences of EES protocols. Once defined, these EES protocols and sequences can be uploaded to the IPG. To enable closed-loop controlled stimulation, the execution of EES sequences is linked to specific events detected from data collected by the sensors. On detection of an event, G-Drive Plus sends a wireless command to the IPG to execute the linked sequence. After 105 ms, on average, the currently running stimulation sequence is interrupted, and the commanded sequence is initiated. The following command can be sent only after 200 ms, on average, once the IPG has sent back the confirmation that the previous command has been received and executed. G-Drive Plus can also trigger acquisition from video cameras and emit standardized synchronization pulses. During recording sessions, these functionalities allow us to use G-Drive Plus to visualize and immediately assess the effects of the EES protocols and EES sequences on muscle activity and whole-body kinematics. All the acquired data, including the delivery of EES protocols synchronized with the kinematics and muscle activity, are saved for offline analysis.

Calibration of EES protocols in P1

In an EES calibration session, we used single-pulse EES to identify electrode configurations that recruit the six targeted hotspots of spinal activity: left and right weight acceptance, propulsion and leg lift hotspots. Weight acceptance roughly corresponds to knee extension, propulsion to ankle extension and leg lift to co-activated hip flexion and ankle flexion, respectively. The participant was lying relaxed in the supine position on an examination table. We recorded EMG activity from left and right iliopsoas (IL), rectus femoris (RF), vastus lateralis (VLat), semitendinosus (ST), tibialis anterior (TA), medial gastrocnemius (MG) and soleus (Sol) muscles using Trigno wireless EMG sensors (Delsys). We applied Nuprep abrasive paste on the skin (Weaver) to reduce electrode–skin resistance and improve EMG signal quality. We then mapped the muscle responses to single-pulse EES (300-µs pulse width) delivered using monopolar configurations (one array electrode as cathode and case as anode) at currents ranging from 0.1 mA to 3.5 mA. We systematically tested all possible monopolar configurations. For each configuration, the EES current was gradually increased until all muscle responses reached saturation or until P1 reported discomfort. We recorded three repetitions for each amplitude. We then used recorded EMG responses to compute spinal map activations for each monopolar configuration across a range of amplitudes. We then identified eight monopolar configurations that each generate a spinal map activation with the highest correlation with one of the identified hotspot spinal activations. If the muscle activation selectivity of one of these configurations was not satisfactory, we refined that EES protocol with multipolar electrode configurations, which use additional anodes to steer the electrical field toward the targeted posterior roots. We then tuned the frequency and amplitude of each of the EES protocols. Because our intention was to finally generate EES sequences with multiple overlapping EES protocols, the limitation of the Activa RC IPG allowed the use of only a single stimulation frequency. Extensor muscles are more responsive to low-frequency stimulation (for example, <40 Hz), whereas the flexor muscles respond better to higher frequencies (for example, >80 Hz). Because our EES protocols targeted both the flexor and extensor muscles, our tuning

identified 60 Hz as the most effective stimulation frequency overall. We then tuned the current amplitude for each EES protocol by asking the participant to walk while triggering that protocol and observing the muscle responses. We selected the amplitudes that generated a clear enhancement of gait and were below P1's discomfort threshold. We found that continuous stimulation using both the left and the right knee extension EES protocols clearly enhances the gait. We, therefore, defined two of left and right knee extension EES protocols, a knee extension 'boost' EES protocol with a higher amplitude to coincide with the natural activation of the knee extension hotspot and another with a lower amplitude active during the remainder of the gait cycle (Supplementary Table 6).

Calibration of EES sequences in P1

In an EES calibration session, we assembled the EES protocols into two EES sequences: 'Left Foot Off' and 'Right Foot Off'. These were designed to be initiated in synchrony with the beginning of the left and right leg lift hotspot, respectively. We tuned the duration of each protocol in the sequence by asking P1 to walk overground while we delivered the EES sequences. We used G-Drive Plus to look at the overlap of EES protocols and activation of muscles targeted by those protocols. We modified the sequences until all the misalignments were removed (Supplementary Table 7). With NHPs, whose gait cycle typically lasted more than 1 s, we used four EES sequences. With the help of EES, the gait cycle of P1 was often below 0.8 s. Due to the communication chain between G-Drive Plus and the IPG, we can send only one command to the IPG every 200 ms, Therefore, using more than one EES sequence per side generated delays in the execution of EES sequences, which made the neuroprosthesis ineffective.

P1 corridor and freezing circuit sessions

These sessions tested the synergistic effects of DBS and EES therapies through four conditions: DBS^{OFF} - EES^{OFF}, DBS^{ON} - EES^{OFF}, DBS^{OFF} - EES^{ON} and DBS^{ON} - EES^{ON}. Because the effect of DBS takes time to wash out, we could only test either the DBS^{OFF} or DBS^{ON} conditions in a single session. For the DBS^{OFF} sessions, we instructed P1 to turn his DBS therapy off in the morning before the session. P1 maintained the same daily regime of levodopa intake during the trial protocol. To ensure balanced comparison between the conditions tested on different days, sessions always started at the same time, thus ensuring roughly the same levedopa levels at the beginning of each session. During these sessions, we first equipped P1 with up to 16 wireless Trigno Avanti sensors with bipolar surface electrodes over the muscles of the left and right legs: iliopsoas, rectus femoris, adductors, vastus lateralis, semitendinosus, tibialis anterior, medial gastrocnemius and soleus. We also attached two NGIMU sensors on the surface of the left and right shank. Additionally, we attached 14 infrared reflective markers on the following anatomical landmarks: left and right toe, ankle, knee, hip and shoulder and two on each wrist. For the remainder of these sessions, P1 walked within the instrumented space of our gait laboratory as we recorded his EMG activity and kinematics and controlled his spinal EES. We acquired the EMG and IMU signals using the Trigno Avanti sensors with a 1,259-Hz and a 148-Hz sample rate, respectively, and additional IMU signals from NGIMU sensors at 30 Hz. We obtained the kinematic recordings using a Vicon 3D motion capture system, consisting of 14 infrared cameras, each set to record the reflection of infrared-reflective markers at 100 frames per second. The Vicon system covered a 12 m × 4 m × 2.5 m workspace. We also captured chronophotographic images of participants using a high-definition camera (FUJIFILM X-T2, 5 images per second, ISO 6400, shutter speed 1/250 s). As he walked, P1 was always followed by a physiotherapist to prevent falls in the case of freezing. During the corridor sessions, on the mark of the experimenter, we asked P1 to stand up from his chair, walk from before one floor marker to beyond another floor marker in a straight line, turn around and come back again in a straight line and to repeat this a second time. Once he finished the task, P1 was free to sit down and rest. We defined an epoch starting with P1 passing the marker on one side of the gait lab and ending with P1 passing the marker on the other side of the gait lab as a trial. We defined the time to complete a trial as task time. The epoch between P1 standing to walk on the experimenter's mark and him finishing the task was defined as a 'trial set'. During the freezing circuit sessions, we built a circuit consisting of narrow corridors with obstacles. On the mark of the experimenter, we asked P1 to stand up from his chair and walk across the floor marker and through the circuit across the obstacles until he reached the floor marker on the other side of the gait lab. Once he finished the task, P1 was asked to walk around the circuit to the initial position, sit down and rest. We defined each crossing of an obstacle as a trial, during which P1 either froze or not. We defined one passing of the entire circuit as a trial set. In both types of sessions, P1 and the physiotherapist were not informed on whether the EES was on or off during that trial set. In the corridor sessions, after each trial, we asked P1 to comment on and score the quality of his gait on a scale from 0 to 5 with 0.25 increments. After P1 finished with the scoring, we asked the physiotherapist to also comment on and score the quality of P1's gait on the same scale.

Kinematically controlled spinal cord neuroprosthesis in P1

The process to calibrate the closed-loop control of EES for P1 followed the procedure based on our earlier work to decode sparse events from motor cortical spiking activity in NHPs[23,33,36] and people[35] and from motor cortical ECoG activity in people[38,45] and employed earlier in the study for the NHPs and people with PD (Extended Data Fig. 4). On a day preceding the first overground walking session, we recorded a dataset in which P1 walked straight while being equipped with the NGIMU sensors and the Trigno Research+ system and recorded by cameras. He walked first in the DBS^{ON} EES^{OFF} condition. We used these trial sets to calibrate thresholds on the pitch angles acquired from the NGIMU sensors positioned on the left and right leg shanks. We then asked P1 to again walk straight, now in the DBS^{ON} EES^{ON} condition where the Left Foot Off and Right Foot Off EES sequences were triggered by left and right leg shank pitch angles, respectively, passing their thresholds. We then labeled the gait events of both the DBS^{ON} EES^{OFF} and DBS^{ON} EES^{ON} dataset using a custom-developed MATLAB program through visual inspection of the video frames. We used these labeled datasets to calibrate rLDA decoders that detected the initiation of the left leg lift and right leg lift hotspot initiation events. The decoder used accelerations and angular velocities acquired by the Trigno Avanti sensors low-pass filtered with a second-order 0.25-s-long Savitzky–Golay filter[38,73] as inputs. To enable closed-loop control of EES sequences in real time, we developed a DecodingGate C++ software application (Visual Studio 2010, 2015 and 2017) that acquired the Trigno Avanti sensors recordings from G-Drive Plus, processed those recordings, applied the rLDA decoding algorithms and, upon detection of hotspot initiation events, sent the commands to the G-Drive Plus to initiate the relevant EES sequence. G-Drive Plus then relayed these commands to the IPG. DecodingGate ran on a separate computer and exchanged data with G-Drive Plus via UDP packets through a local network. While calibrated from data recorded during straight walking in the DBS^{ON} conditions, the decoders remained accurate in the DBS^{OFF} conditions and when used in the freezing circuit task (Fig. 6 and Extended Data Fig. 10).

Assessment of gait impairments in P1

After each corridor trial, the physiotherapists attributed a general gait quality score according to predefined criteria (Supplementary Table 8). We processed the motion tracking of P1's legs into kinematic variables that were used to quantify key deficits of Parkinsonian gait. We quantified gait speed by task time and stride length and gait asymmetry for temporal and spatial parameters by the ratio of gait phases and step

lengths between the left and right legs[91]. Gait is more symmetric as these ratios approach zero.

$$Gait\ Phase\ asymmetry = 100 \times \left| \log \left(\frac{\frac{Swingduration_R}{Stanceduration_R}}{\frac{Swingduration_L}{Stanceduration_L}} \right) \right|$$

$$Step\ length\ asymmetry = 100 \times \left| \log \left(\frac{Steplength_R}{Steplength_L} \right) \right|$$

We also quantified the variability of gait patterns using stride time coefficient of variation, which has been associated with gait instability and risk of fall in PD[92,93]. The coefficient of variation is defined as the ratio between the s.d. and the mean and increases with variability.

We quantified the gait upper body control by measuring the arm swing angle[92].

Assessment of balance problems in P1

We evaluated the impact of the spinal cord neuroprosthesis and DBS therapies on balance problems by using the standard Mini-BESTest clinical evaluation[94] and using the Activities-specific Balance Confidence (ABC) scale questionnaire[95–97].

Assessment of freezing of gait in P1

We evaluated the impact of the spinal cord neuroprosthesis and DBS therapies on freezing of gait by having a trained neurologist observe the videos of each of the freezing circuit trials and label freezing-of-gait epochs with 100-ms resolution. We then calculated the fraction of the time P1 spent traversing the circuit that he spent under a freezing-of-gait epoch.

Blinding

No statistical methods were used to predetermine sample size. The P1 and NHP experimental sessions were not randomized. However, different trials during the NHP experimental sessions and trial sets during the P1 sessions were randomly interleaved. The investigators were not blinded to allocation during experiments and outcome assessment because they controlled the use of the stimulation. Experienced technicians working at the NHP facility and not part of the study were blinded during their assessments of Parkinsonian Disability scores. They were unaware of the MPTP administration protocol or any of the details related to our experiments. The PREDI-STIM participants and participants of the Motor Network in Parkinson's Disease and Dystonia: Mechanisms of Therapy clinical trial were recorded in only one condition. Therefore, blinding and randomization were not applicable. We performed all data analyses, except for the semi-automatic kinematic reconstruction in the SIMI software, Vicon software and marking of gait events from video recordings, using automatic computer routines.

Statistical procedures

All computed parameters were quantified and compared within each animal and patient. All data are reported as mean values and s.e.m. Significance was analyzed using the non-parametric two-sided Wilcoxon rank-sum and signed-rank tests, Student's *t*-test, bootstrapping or a one-sided Monte Carlo approach, as indicated for each test.

Reporting summary

Further information on research design is available in the Nature Portfolio Reporting Summary linked to this article.

Data availability

Data that support the findings and software routines developed for the data analysis will be made available upon reasonable request to the corresponding authors at: jocelyne.bloch@chuv.ch or gregoire.courtine@epfl.ch. Third party datasets used in our study are available under the Creative Commons Public License: VerSe 2019 (https://osf.io/nqjyw/) and VerSe 2020 (https://osf.io/t98fz/).

Code availability

Code developed for the data analysis will be made available upon reasonable request to the corresponding authors at: jocelyne.bloch@chuv.ch or gregoire.courtine@epfl.ch.

References

53. Ahmed, M. R. et al. Lentiviral overexpression of GRK6 alleviates L-dopa-induced dyskinesia in experimental Parkinson's disease. *Sci. Transl. Med.* **2**, 28ra28 (2010).
54. Bezard, E. et al. The mGluR5 negative allosteric modulator dipraglurant reduces dyskinesia in the MPTP macaque model. *Mov. Disord.* **29**, 1074–1079 (2014).
55. Bezard, E. et al. Attenuation of levodopa-induced dyskinesia by normalizing dopamine D3 receptor function. *Nat. Med.* **9**, 762–767 (2003).
56. Fasano, S. et al. Inhibition of Ras-guanine nucleotide-releasing factor 1 (Ras-GRF1) signaling in the striatum reverts motor symptoms associated with L-dopa-induced dyskinesia. *Proc. Natl Acad. Sci. USA* **107**, 21824–21829 (2010).
57. Porras, G. et al. PSD-95 expression controls L-DOPA dyskinesia through dopamine D1 receptor trafficking. *J. Clin. Invest.* **122**, 3977–3989 (2012).
58. Shen, W. et al. M4 muscarinic receptor signaling ameliorates striatal plasticity deficits in models of L-DOPA-induced dyskinesia. *Neuron* **88**, 762–773 (2015).
59. Urs, N. M. et al. Targeting β-arrestin2 in the treatment of L-DOPA-induced dyskinesia in Parkinson's disease. *Proc. Natl Acad. Sci. USA* **112**, E2517–E2526 (2015).
60. Bezard, E. et al. Relationship between the appearance of symptoms and the level of nigrostriatal degeneration in a progressive 1-methyl-4-phenyl-1,2,3,6-tetrahydropyridine-les ioned macaque model of Parkinson's disease. *J. Neurosci.* **21**, 6853–6861 (2001).
61. Meissner, W. et al. Time-course of nigrostriatal degeneration in a progressive MPTP-lesioned macaque model of Parkinson's disease. *Mol. Neurobiol.* **28**, 209–218 (2003).
62. Rosenblad, C. et al. Vector-mediated l-3,4-dihydroxyphenylalanine delivery reverses motor impairments in a primate model of Parkinson's disease. *Brain* **142**, 2402–2416 (2019).
63. Courtine, G. et al. Kinematic and EMG determinants in quadrupedal locomotion of a non-human primate (Rhesus). *J. Neurophysiol.* **93**, 3127–3145 (2005).
64. Tass, P. A. et al. Coordinated reset has sustained aftereffects in Parkinsonian monkeys. *Ann. Neurol.* **72**, 816–820 (2012).
65. Schiavone, G. et al. Soft, implantable bioelectronic interfaces for translational research. *Adv. Mater.* **32**, e1906512 (2020).
66. Baufreton, J. et al. Inhaling xenon ameliorates L-dopa-induced dyskinesia in experimental parkinsonism. *Mov. Disord.* **33**, 1632–1642 (2018).
67. Zampieri, C. et al. The instrumented timed up and go test: potential outcome measure for disease modifying therapies in Parkinson's disease. *J. Neurol. Neurosurg. Psychiatry* **81**, 171–176 (2010).
68. Palmerini, L., Mellone, S., Avanzolini, G., Valzania, F. & Chiari, L. Quantification of motor impairment in Parkinson's disease using an instrumented timed up and go test. *IEEE Trans. Neural Syst. Rehabil. Eng.* **21**, 664–673 (2013).
69. McLachlan, G. J. & Peel, D. *Finite Mixture Models* (Wiley, 2000).
70. Postuma, R. B. et al. MDS clinical diagnostic criteria for Parkinson's disease. *Mov. Disord.* **30**, 1591–1601 (2015).

71. Stanslaski, S. et al. A chronically implantable neural coprocessor for investigating the treatment of neurological disorders. *IEEE Trans. Biomed. Circuits Syst.* **12**, 1230–1245 (2018).
72. Kremen, V. et al. Integrating brain implants with local and distributed computing devices: a next generation epilepsy management system. *IEEE J. Transl. Eng. Health Med.* **6**, 2500112 (2018).
73. Pistohl, T., Ball, T., Schulze-Bonhage, A., Aertsen, A. & Mehring, C. Prediction of arm movement trajectories from ECoG-recordings in humans. *J. Neurosci. Methods* **167**, 105–114 (2008).
74. Moreau, C. et al. STN-DBS frequency effects on freezing of gait in advanced Parkinson disease. *Neurology* **71**, 80–84 (2008).
75. Delp, S. L. et al. An interactive graphics-based model of the lower extremity to study orthopaedic surgical procedures. *IEEE Trans. Biomed. Eng.* **37**, 757–767 (1990).
76. Ong, C. F., Geijtenbeek, T., Hicks, J. L. & Delp, S. L. Predicting gait adaptations due to ankle plantarflexor muscle weakness and contracture using physics-based musculoskeletal simulations. *PLoS Comput. Biol.* **15**, e1006993 (2019).
77. Geyer, H. & Herr, H. A muscle-reflex model that encodes principles of legged mechanics produces human walking dynamics and muscle activities. *IEEE Trans. Neural Syst. Rehabil. Eng.* **18**, 263–273 (2010).
78. Song, S. & Geyer, H. Predictive neuromechanical simulations indicate why walking performance declines with ageing. *J. Physiol.* **596**, 1199–1210 (2018).
79. Thelen, D. G. Adjustment of muscle mechanics model parameters to simulate dynamic contractions in older adults. *J. Biomech. Eng.* **125**, 70–77 (2003).
80. Seth, A. et al. OpenSim: simulating musculoskeletal dynamics and neuromuscular control to study human and animal movement. *PLoS Comput. Biol.* **14**, e1006223 (2018).
81. Häkkinen, K. & Häkkinen, A. Muscle cross-sectional area, force production and relaxation characteristics in women at different ages. *Eur. J. Appl. Physiol. Occup. Physiol.* **62**, 410–414 (1991).
82. Goodpaster, B. H. et al. Attenuation of skeletal muscle and strength in the elderly: the Health ABC Study. *J. Appl Physiol.* **90**, 2157–2165 (2001).
83. Cotofana, S. et al. Correlation between single-slice muscle anatomical cross-sectional area and muscle volume in thigh extensors, flexors and adductors of perimenopausal women. *Eur. J. Appl. Physiol.* **110**, 91–97 (2010).
84. Geijtenbeek, T. SCONE: open source software for predictive simulation of biological motion. *J. Open Source Softw.* **4**, 1421 (2019).
85. Hansen, N. & Kern, S. Evaluating the CMA evolution strategy on multimodal test functions. In *Parallel Problem Solving from Nature - PPSN VIII* (eds Yao, X. et al.) 282–291 (Springer, 2004).
86. Wang, J. M., Hamner, S. R., Delp, S. L. & Koltun, V. Optimizing locomotion controllers using biologically-based actuators and objectives. *ACM Trans. Graph.* **31**, 25 (2012).
87. Altini, N. et al. Segmentation and identification of vertebrae in CT scans using CNN, *k*-means clustering and *k*-NN. *Informatics* **8**, 40 (2021).
88. Sekuboyina, A. et al. VerSe: a vertebrae labelling and segmentation benchmark for multi-detector CT images. *Med. Image Anal.* **73**, 102166 (2021).
89. Isensee, F., Jaeger, P. F., Kohl, S. A. A., Petersen, J. & Maier-Hein, K. H. nnU-Net: a self-configuring method for deep learning-based biomedical image segmentation. *Nat. Methods* **18**, 203–211 (2021).
90. De Leener, B. et al. SCT: Spinal Cord Toolbox, an open-source software for processing spinal cord MRI data. *Neuroimage* **145**, 24–43 (2017).
91. Patterson, K. K., Gage, W. H., Brooks, D., Black, S. E. & McIlroy, W. E. Evaluation of gait symmetry after stroke: a comparison of current methods and recommendations for standardization. *Gait Posture* **31**, 241–246 (2010).
92. Horak, F. B. & Mancini, M. Objective biomarkers of balance and gait for Parkinson's disease using body-worn sensors. *Mov. Disord.* **28**, 1544–1551 (2013).
93. Lord, S., Galna, B. & Rochester, L. Moving forward on gait measurement: toward a more refined approach. *Mov. Disord.* **28**, 1534–1543 (2013).
94. Franchignoni, F., Horak, F., Godi, M., Nardone, A. & Giordano, A. Using psychometric techniques to improve the Balance Evaluation Systems Test: the mini-BESTest. *J. Rehabil. Med.* **42**, 323–331 (2010).
95. Dal Bello-Haas, V., Klassen, L., Sheppard, M. S. & Metcalfe, A. Psychometric properties of activity, self-efficacy, and quality-of-life measures in individuals with Parkinson disease. *Physiother. Can.* **63**, 47–57 (2011).
96. Powell, L. E. & Myers, A. M. The Activities-specific Balance Confidence (ABC) Scale. *J. Gerontol. A Biol. Sci. Med. Sci.* **50A**, M28–M34 (1995).
97. Franchignoni, F., Giordano, A., Ronconi, G., Rabini, A. & Ferriero, G. Rasch validation of the Activities-specific Balance Confidence Scale and its short versions in patients with Parkinson's disease. *J. Rehabil. Med.* **46**, 532–539 (2014).

Acknowledgements

Funding was obtained from the Defitech Foundation, the Roger de Spoelberch Prize, ONWARD Medical, CAMS Innovation Fund for Medical Sciences grant 2021-1-I2M-034, National Natural Science Foundation of China grants 81941012 and 82161138027, PDWALK ERANET JP cofunND 2-NT (ANR, FNS, ZonMw), the Parkinson Schweiz Foundation, the European Community's Seventh Framework Program (NeuWalk), a Consolidator Grant from the European Research Council, the Wyss Center for Bio- and Neuroengineering, the Bertarelli Foundation, a Marie Curie fellowship to D.A.B., Marie Curie COFUND EPFL fellowships to T.M. and G.S., a Morton Cure Paralysis Fund fellowship to T.M., a Whitaker Foundation fellowship to M.G.P. and the Swiss National Science Foundation, including the National Center of Competence in Research in Robotics, the Sino-Swiss Science and Technology Cooperation (IZLCZ3_156331), the NanoTera.ch program (SpineRepair) and the Sinergia program (CRSII3_160696).

Author contributions

T.M., E.M.M., N.M., C.M., F.R., S.S., M.G.P., R.J.D., A.B., G.S., C.H., N.H., L.A., D.B., F.B., M.C., P.A.S., T.D., D.W. and S.P.L.: technological framework. M.G.P., C.Y.L., L.H., D.B., Q.L., E.B., D.W., J.B. and G.C.: surgeries. T.M., E.M.M., N.M., C.M., F.R., S.S., M.G.P., C.V., R.J.D., A.B., L.N.B.-F., Y.J., C.H., D.B., J.L., I.V., S.B., F.B., M.G., C.Y.L., L.H., L.P., M.Y., F.B., M.C., D.D.W., J.B. and G.C. performed experiments. T.M., E.M.M., N.M., C.M., F.R., S.S., M.G.P., R.J.D., A.B., A.G., S.D.H.-C., G.D., J.R., C.G.L.G.-M., J.S.Q., J.-B.M., G.C. and J.L.: data analysis. Y.J., C.Y.L., L.H., Q.L., F.B., M.G., M.C.J., J.F.B., P.A.S. and D.G.: neurological evaluations. T.M., E.M.M., N.M., C.M., F.R., S.S., M.G.P., R.J.D., G.S., A.G. and J.R. generated figures. A.W., H.L., S.B., W.K.D.K., Q.L., C.Q., J.B., E.B. and G.C.: regulatory affairs. T.M., E.M.M., F.R., R.D., L.A., D.B., W.K.D.K., Q.L., M.C., P.A.S., T.D., D.G., A.I., D.D.W., S.P.L., S.M., C.Q., J.B., E.B. and G.C.: conception and supervision. G.C. wrote the paper, with T.M., E.M.M., F.R., M.G.P., G.S., J.B. and E.B.

Competing interests

The authors declare the following competing financial interests: G.C., J.B., R.D., S.M., S.L., T.M., E.M.M. and M.C. hold various patents or applications in relation to the present work. G.C. and J.B. are consultants for ONWARD Medical. G.C., J.B., S.M., S.L., H.L. are founders and minority shareholders of ONWARD Medical, a company with potential commercial interest in the presented work. E.B. reports

personal fees from Motac Neuroscience Ltd UK and is a shareholder of Motac Holding UK and Plenitudes SARL France. The remaining authors declare no competing interests.

Additional information

Extended data is available for this paper at https://doi.org/10.1038/s41591-023-02584-1.

Supplementary information The online version contains supplementary material available at https://doi.org/10.1038/s41591-023-02584-1.

Correspondence and requests for materials should be addressed to Jocelyne Bloch, Erwan Bezard or G. Courtine.

Peer review information *Nature Medicine* thanks the anonymous reviewers for their contribution to the peer review of this work. Primary Handling Editor: Jerome Staal, in collaboration with the *Nature Medicine* team.

https://doi.org/10.1038/s41591-023-02584-1

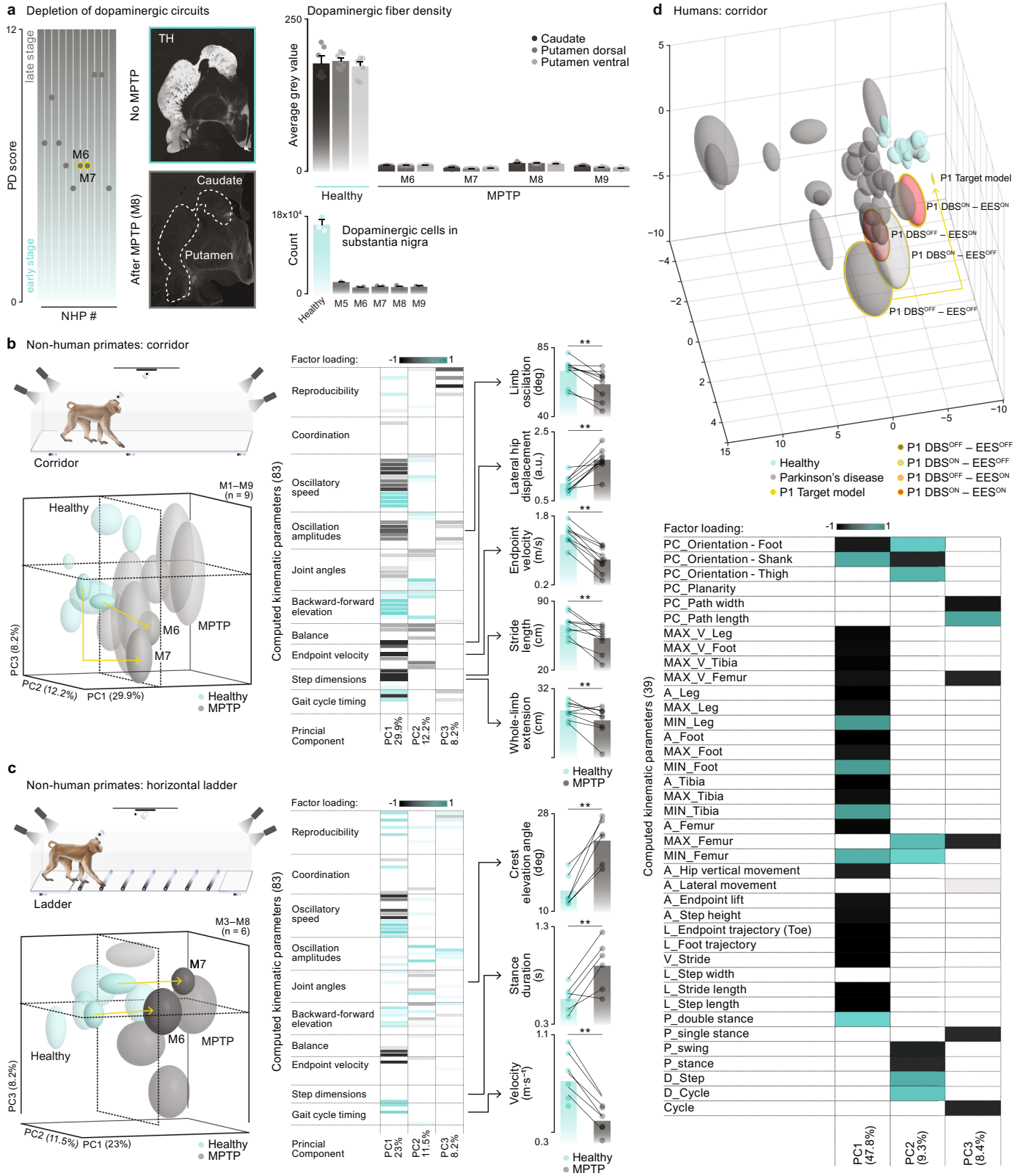

Extended Data Fig. 1 | See next page for caption.

https://doi.org/10.1038/s41591-023-02584-1

Extended Data Fig. 1 | Objective quantification of gait impairments and balance problems in the NHP MPTP model of Parkinson's disease and in people with PD. a, Scatter plot shows the rounded mean of PD scores for each monkey across sessions recorded after MPTP administration. Photographs show the dopaminergic projections labelled with tyrosine hydroxylase (TH) in the putamen and caudate of a healthy monkey and in M8. The bar plots show the density of TH-labelled projections in the putamen and caudate (n = Healthy: M6: 6, M7: 6, M8: 4, M9: 6) and count of dopaminergic cells in substantia nigra (n = Healthy: 3, M5: 1, M6: 2, M7:2, M8: 2, M9: 2) in healthy monkeys and in monkeys after the MPTP administration. **b-c**, The NHPs were trained to walk across a 3m-long corridor (M1-9, n = 9) and along the rungs of a 3m-long horizontal ladder (M3-8, n = 6). Both runways were embedded within Plexiglass enclosures that allowed the NHPs to behave freely and untethered while anatomical landmarks painted on the joints were filmed using 4 or 6 cameras in order to reconstruct whole-body kinematics in 3D. We used these kinematic recordings to compute 83 variables from each gait cycle that quantified kinematic features of monkeys' locomotor patterns (Supplementary Table 3). This dataset was arranged in a matrix with variables as the matrix columns and each row representing one gait cycle. Data collected from different conditions (before and after MPTP administration) and different monkeys were pooled together in a single matrix and z-scored across columns. Two different tasks, corridor (a) and ladder (b), were analysed separately. We then applied PCA on this dataset and visualized the outcome by plotting the dataset in a new space spanned by the three leading PCs. The data for each monkey and condition is represented by a balloons – ellipsoids with the centre and principal semi-axis as the mean and standard deviation calculated across all the gait cycles for that condition and monkey (number of gait cycles in corridor: before MPTP: M1: 4, M2: 6, M3: 18, M4: 13, M5: 14, M6: 22, M7: 14, M8: 95, M9: 49; after MPTP: M1: 28, M2: 8, M3: 16, M4: 22, M5: 11, M6: 6, M7:9, M8: 48, M9: 59; ladder: before MPTP: M3: 12, M4: 25, M5: 23, M6: 19, M7: 9, M8: 40; after MPTP: M3: 18, M4: 7, M5: 24, M6: 31, M7: 24, M8: 14). Since the variance in the dataset is driven by the changes in gait parameters between the healthy and MPTP conditions consistent across monkeys, the parameters that best capture gait and balance deficits after MPTP administration have the highest loading factors in leading principal components (PCs). The colorplot shows the loading factors for the three leading PCs. The bar plots report the mean values of the parameters with the highest factor loadings. These parameters reflect gait and balance deficits commonly observed in people with PD. **d**, Healthy subjects (H; n = 9) and subjects with PD (PD; n = 25) walked straight overground as we recorded their full-body kinematics in 3D using the Vicon multi-camera system. We used these kinematic recordings to compute 35 variables from each gait cycle that quantified kinematic features of human locomotor patterns (Supplementary Table 5). As for the monkeys, we arranged this dataset in a gait parameters x gait cycles matrix, applied PCA on this dataset and visualized the outcome by plotting the distribution balloons for each subject in a space spanned by the three leading PCs (number of gait cycles: H1: 37, H2: 36, H3: 33, H4: 44, H5:42, H6: 38, H7: 45, H8: 33, H9: 39; PD1: 28, PD2: 30, PD3: 54, PD4: 53, PD5: 81, PD6: 47, PD7: 69, PD8: 37, PD9: 8, PD10: 100, PD11: 32, PD12: 22, PD13: 48, PD14: 25, PD15: 69, PD16: 70, PD17: 33, PD18: 61, PD19: 40, PD20: 29, PD21: 82, PD22: 8, PD23: 66, PD24: 33, PD25: 29). The colorplot shows the loading factors for the three leading PCs. *, ** significant difference at $p < 0.05$ and $p < 0.01$, respectively, using two-sided Wilcoxon signed rank test. Error bars, sem.

https://doi.org/10.1038/s41591-023-02584-1

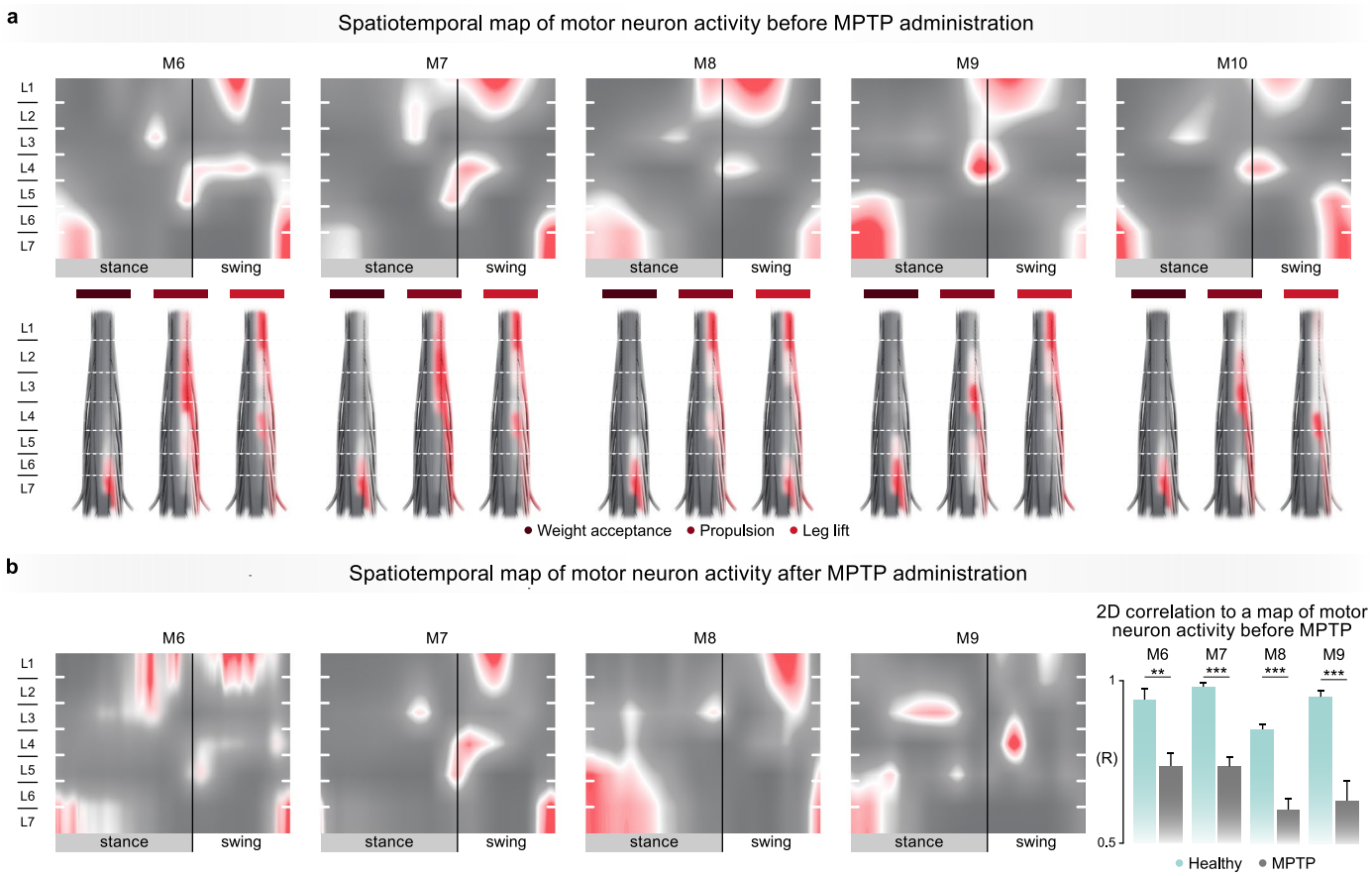

Extended Data Fig. 2 | Design of EES protocols based on spatiotemporal maps of motor neuron activity. a, Colorplots showing the average spatiotemporal map of motor neuron activity underlying locomotion in M6 (n = 12 gait cycles), M7 (n = 10), M8 (n = 20), M9 (n = 32) and M10 (n = 13) before MPTP administration (Healthy). We identified the hotspots of motor neuron activity using Gaussian Mixture Modelling. The spatial maps of motor neuron activity corresponding to the time at which each hotspot reached a maximum (centre) are laid over the schematics of the spinal cord. **b**, Colorplots show the spatiotemporal maps of motor neuron activity underlying locomotion in M6 (n = 55 gait cycles), M7 (n = 44), M8 (n = 17) and M9 (n = 11) after MPTP administration (MPTP). Bar plots compare the surface correlation between two maps calculated before MPTP administration and between a map calculated before MPTP administration and a map calculated after the MPTP administration. **, *** significant difference at $p < 0.01$, $p < 0.001$, respectively, using non-parametric one-sided Monte Carlo permutation test. Error bars show sem.

https://doi.org/10.1038/s41591-023-02584-1

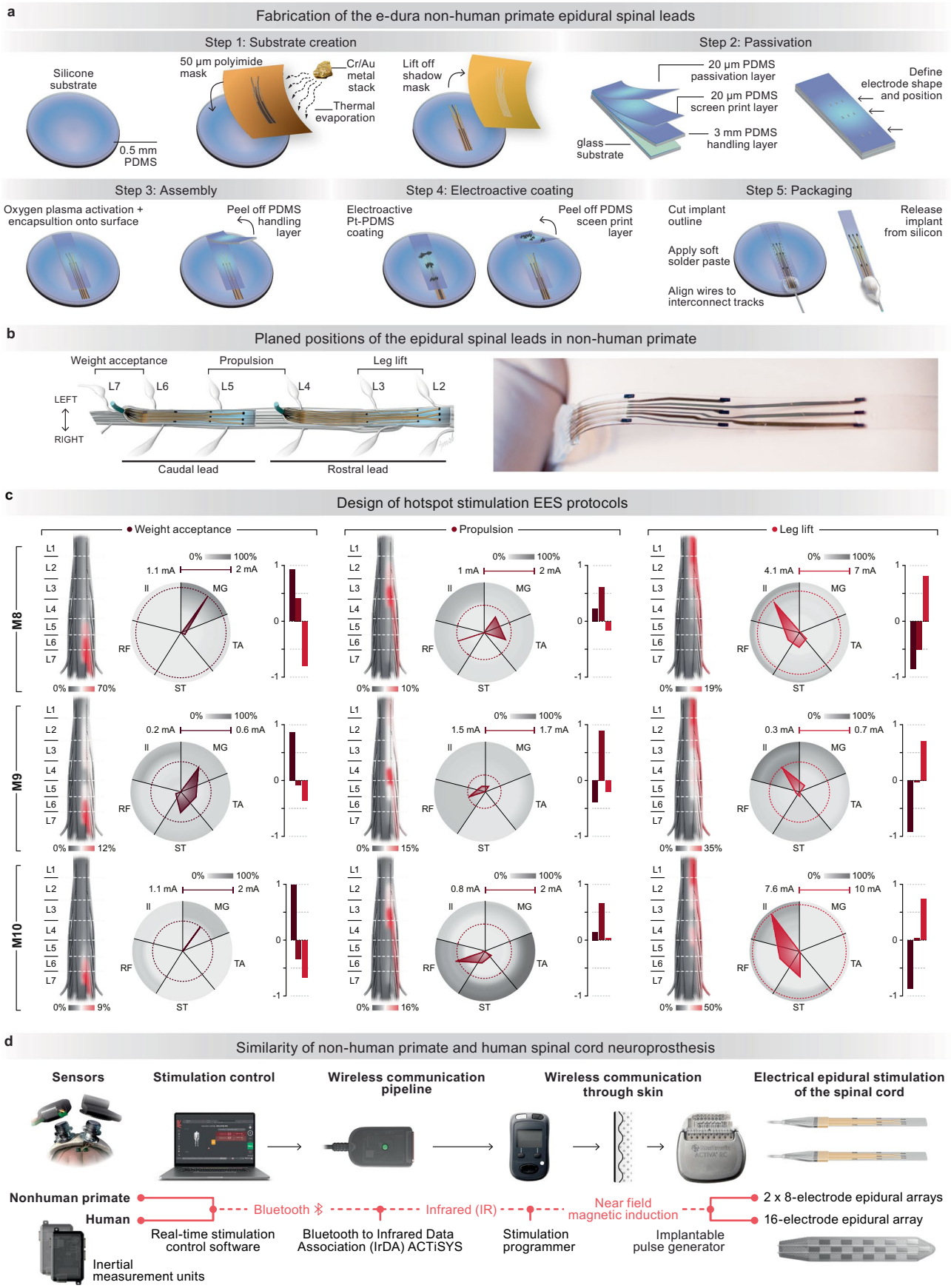

Extended Data Fig. 3 | See next page for caption.

https://doi.org/10.1038/s41591-023-02584-1

Extended Data Fig. 3 | Brain-controlled spinal cord neuroprosthesis technology. a, We developed a fabrication process to manufacture the non-human primate epidural spinal arrays used in M11 using *e-dura* technology (see Methods). **Step 1:** Substrate creation. We used 4' silicon wafers as substrate to prepare the arrays. (top) A polystyrene sulfonic acid layer is spin coated on the carrier to provide a water-release layer for the substrate stack. A PDMS layer is subsequently cast on the substrate until reaching a thickness of approximately 500 µm. (middle) A laser-machined, 50 µm thick polyimide mask is then manually laminated on the PDMS surface, and the carriers are then mounted in a thermal evaporation chamber. A stack of chromium and gold is thermally evaporated on the carriers through the polyimide masks, at a thickness of 5 nm (Cr) and 55 nm (Au). The chromium acts as adhesion promoter for the gold interconnect on PDMS. (bottom) The polyimide shadow mask is then peeled off the surface, revealing the interconnect design patterned in the metal stack. **Step 2**: Passivation. (top) A 3 mm thick PDMS handling layer is cast in a Petri dish. Once cured, the top surface is exposed to an oxygen plasma and a vapour-phase 1H,1H,2H,2H-perfluorooctyltriethoxysilane layer is applied in a vacuum chamber. This process inhibits the adhesion of the silicone to subsequent PDMS layers deposited on the surface. Two subsequent 20 µm thick PDMS layers are spin-coated and cured on the thick PDMS, separated by the same adhesion inhibiting layer. A slab of this triple PDMS stack (3 mm, 20 µm, 20 µm in cross section) is then cut with a blade and mounted on a glass slide. (bottom) A mechanical catheter puncher is used to make holes through the two thin PDMS layers and into the thick handling layer, in order to machine the passivation stack with through-vias. Each via is created by punching a series of 4 round holes of 690 µm diameter with 400 µm centre-to-centre spacing. **Step 3:** Assembly. (top) The top surfaces of the substrate and triple stack encapsulation are exposed to oxygen plasma, then mounted on an alignment rack, with the two treated surfaces facing one another. The vias machined in the encapsulation are aligned with the interconnect patterned on the substrate, and the two parts are then put into contact in order to form a covalent bond between the silicone layers. (bottom) Once bonded, the thick PDMS handling layer is peeled off the substrate, leaving the interconnect encapsulated by two 20 µm thick PDMS layers with openings corresponding to the position of the electrodes. **Step 4:** Electroactive coating. (top) The electroactive coating is prepared as a composite material obtained by dispersing microscale platinum particles (3.5 µm maximum particle size) within a polydimethylsiloxane (PDMS) matrix. This creates a conductive paste that offers a balance between the charge injection properties of platinum and the mechanical properties of PDMS. The composite paste is applied on the encapsulation through the screen print PDMS layer, filling the openings to make an electrical contact with the interconnect. (bottom) The screen print layer is then peeled off to remove the excess coating and define the active stimulation sites. **Step 5:** Packaging. (top) The assembled implant is manually cut while still on wafer to the desired shape using a blade. Electrical wires are threaded in a PDMS guiding piece through holes that are machined at the same pitch as the gold tracks on the substrate. This soft connector is aligned and placed onto the interconnect with wires close to the ends of the gold tracks. Conductive Silver paste is then pressure dispensed to form individual electrical connections between the wires and the gold tracks. Once all electrical connections are made, a bolus of room temperature vulcanisation sealant (one component silicone sealant 734, Dow Corning) is applied over the connector to mechanically secure the assembly. (bottom) After the sealant is cured, the implant is released from the silicon carrier by dissolving the PSS layer under the PDMS substrate with DI water. All silicone layers are prepared by mixing polydimethylsiloxane using a weight ratio of 10:1 between pre-polymer and cross-linker. The deposited layers are cured for a minimum of 3 hours in a temperature-controlled oven set to 80 °C. Photographs show a fabricated *e-dura* spinal implant, including a zoom on the electrode contacts. **b**, We exploited our fabrication process to produce epidural spinal arrays that embedded laterally-located electrodes targeting the left and right posterior roots of the lumbar spinal cord, as well as midline-located electrodes targeting the ascending fibres within the dorsal column. The shown spinal cord was reconstructed from a magnetic resonance imaging scan of a rhesus macaque onto which we represented the planed locations of the rostral and caudal spinal arrays. **c**, Circular plots reporting the amplitude (grey scale) of muscle responses recorded from leg muscles when delivering single-pulse EES at increasing amplitudes (radial axis). Red circles highlight the optimal amplitude while the polygon quantifies the muscular selectivity at this amplitude. Spatial map of motor neuron activity corresponding to optimal EES amplitudes are laid over the schematics of the spinal cord for each hotspot. Bar plots report the correlation between each maximal-selectivity spatial map of motor neuron activity and the spatial map corresponding to the targeted hotspot. Muscle responses were normalized to the maximum amplitudes observed across all the recording sessions. **d**, The scheme illustrates the similarity between non-human primate and human implementation of the spinal cord neuroprosthesis. In both implementations, sensors collected physiological signals that are wirelessly acquired by the control computer running a stimulation control software. This software processed the sensor signals and used a rLDA algorithm to detect hotspot initiation events. On detection of an event, the stimulation control software sent a command to the implanted pulse generator via a wireless communication pipeline that featured electromagnetic induction though the users' skin. On reception of the command, the implanted pulse generator modified the EES sequence to promote the activity of the detected hotspot and, therefore, reinforce the intended movements. Modified EES was delivered over the posterior spinal cord by the epidural spinal arrays. Between non-human primate and human implementations, only the sensors and the spinal arrays differed. Non-human primate implementation relied on recordings from neurosensors featuring microelectrode arrays implanted into the leg area of the motor cortex; and on custom spinal arrays designed for Rhesus macaque spinal anatomy. Human implementation relied on recordings from wearable non-invasive IMU sensors distributed across major anatomical landmarks; and on clinically-approved epidural spinal arrays. The remainder of the spinal cord neuroprosthesis implementation was identical.

https://doi.org/10.1038/s41591-023-02584-1

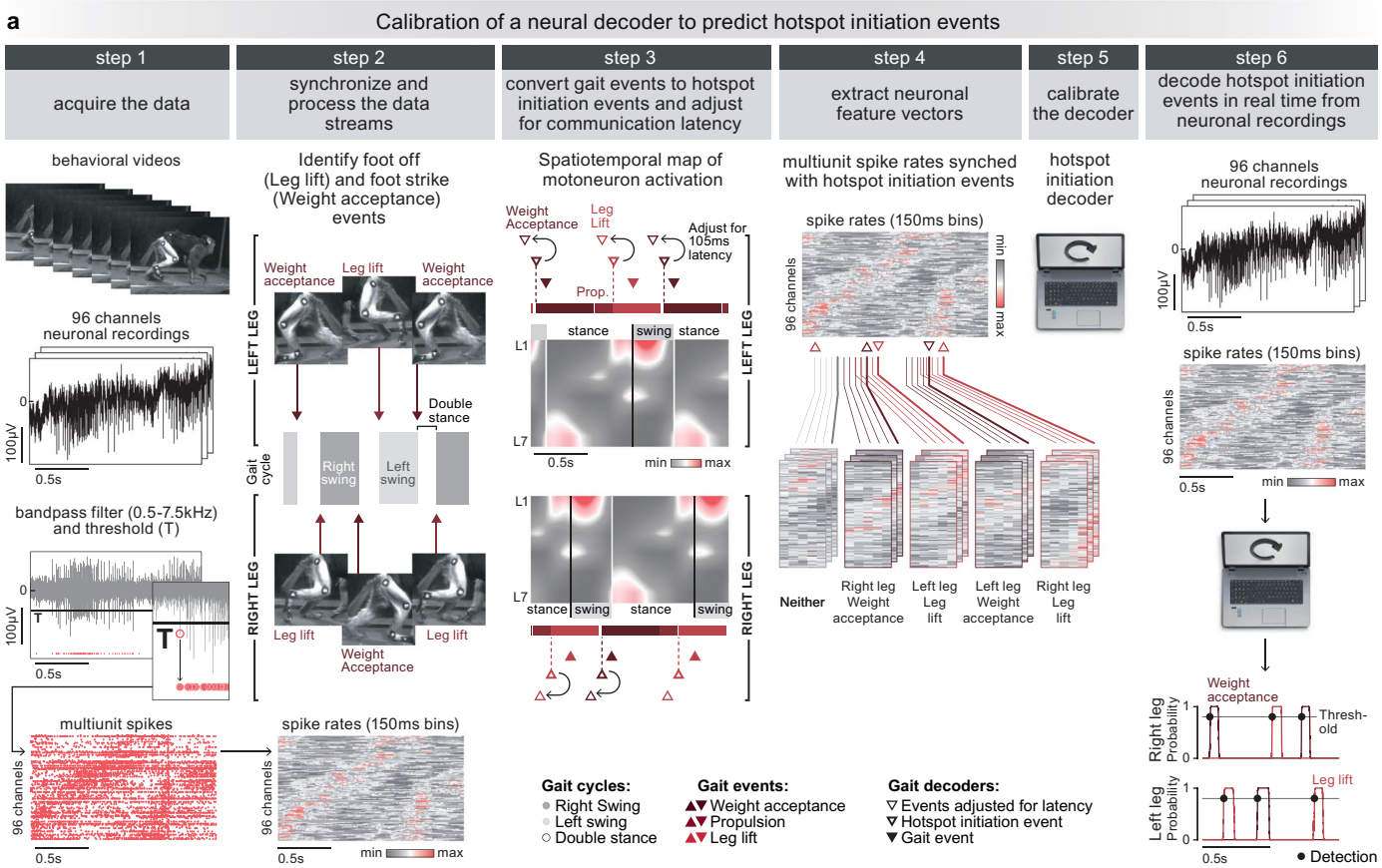

Extended Data Fig. 4 | See next page for caption.

https://doi.org/10.1038/s41591-023-02584-1

Extended Data Fig. 4 | Calibration of neural decoders for real-time detection of hotspot initiation events. a. Step 1: Hindlimb kinematics and MI activity were recorded during locomotion. The neural signals were band-pass filtered (0.5-7.5 kHz), and multiunit spike events were collected based on a threshold set at 3.5 times the standard deviation. **Step 2:** We marked video frames containing left and right foot off and foot strike events. We estimated multiunit spike rates from overlapping 150 ms bins that were updated every 0.5 ms. **Step 3:** We identified the right weight acceptance and right leg lift hotspots initiation events from the spatiotemporal map of motor neuron activity by aligning the gait events to the derived map of spatiotemporal motor neuron activity. The left hotspot initiation events were derived using the same process, assuming symmetry between both legs. The hotspot events were adjusted to account for the stimulation latency of 105 ms. **Step 4:** We extracted feature vectors that originated at hotspot events and assigned them to respective hotspot classes. We assigned all other feature vectors to the 'neither' class. **Step 5:** We used these feature vector classes to calibrate a regularized linear discriminant analysis decoder. **Step 6:** The decoder was uploaded into our real-time analysis software application running on the control computer. Neural data was collected in real-time, processed into multiunit spike rates, and passed through the decoder that calculated the probabilities of hotspot events. When one of the hotspot event probabilities crossed a threshold of 0.8, a wireless command was sent to the implanted pulse generator to trigger the respective stimulation sequences. These sequences were composed of one or more stimulation protocols, each designed to reinforce one of six hotspots: left and right weight acceptance, propulsion and leg lift hotspots. **b**. Two-step decoder calibration. **Step 1:** Data are acquired without EES to calibrate the first-step decoder as shown in a. **Step 2:** An additional set of data is acquired during which the first step decoder trigger composite stimulation sequences once per gait cycle. This sparse triggering mitigates the ability of EES to influence the neural activity used to detect the hotspot events that trigger EES. The composite EES sequences contain either left weight acceptance, left propulsion and right leg lift; or right weight acceptance, right propulsion and left leg lift EES protocols. **Step 3:** A second step decoder is then calibrated using all the acquired datasets. Since the decoder is calibrated on neural activity that is non-affected and affected by EES, the decoder maintains high accuracy regardless of the presence or absence of EES.

https://doi.org/10.1038/s41591-023-02584-1

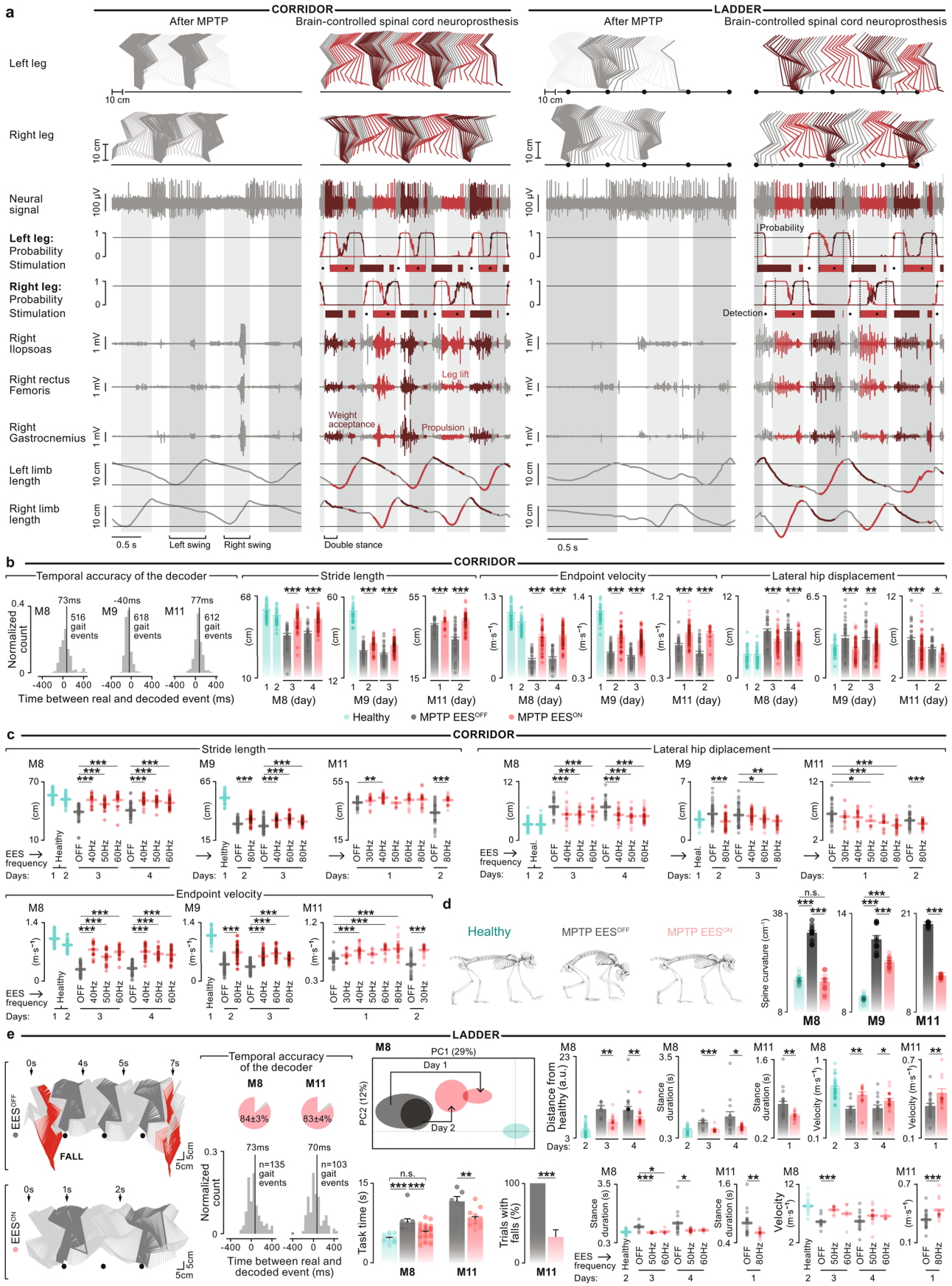

Extended Data Fig. 5 | See next page for caption.

https://doi.org/10.1038/s41591-023-02584-1

Extended Data Fig. 5 | The brain-controlled spinal cord neuroprosthesis improves basic and skilled locomotion after MPTP administration. **a**, Examples of locomotor execution along the corridor (3.3 s) and ladder (2.4 s) without stimulation (left columns) and when using the brain-controlled spinal cord neuroprosthesis in M8 after MPTP administration. From top to bottom: stick diagram decompositions of left and right leg movements; neural recording from a single channel; probability of left and right weight acceptance events; detected hotspot events (broken vertical lines), periods of stimulation through the electrodes targeting the left and right weight acceptance, propulsion and leg lift hotspots; electromyographic signals; whole-limb extension calculated as distance from the hip to the ankle joint. The white, light grey and dark grey backgrounds correspond to double stance, left and right swing gait phases, respectively. **b**, The histogram plots show the distributions between hotspot initiation events measured from kinematic recordings (ground truth) and hotspot initiation events decoded during locomotion with the brain-controlled spinal cord neuroprosthesis (n = 516, 618 and 612 events for M8, M9 and M11, respectively). Bar plots report key parameters associated with gait and balance deficits commonly observed in people with PD (n = 26, 51, 27, 81, 50 and 45 steps for M8, 63, 62, 45, 140 and 55 steps for M9, and 25, 87, 33 and 19 steps for M11 across conditions from left to right). M8's gait was recorded in two days before the MPTP treatment (days 1 and 2) and two days after the treatment (days 3 and 4). M9's gait was recorded in one day before the MPTP treatment (day 1) and two days after the treatment (days 2 and 3). M11's gait was recorded in two days after the treatment (days 1 and 2). The statistical significance is shown only for comparison of between the MPTP EES^{OFF} dataset and MPTP EES^{ON} datasets recorded on the same day. **c**, Changes in EES frequency between 30 and 80 Hz modulate gait parameters but has minimal impact on the efficacy of the therapy. The plots report the mean stride length, endpoint velocity and lateral hip displacement during locomotion along the corridor (n = 50, 45, 26, 16, 17, 18, 27, 26, 22 and 33 steps for M8, 55, 63, 62, 45, 58, 43 and 39 steps for M9, and 25, 11, 29, 10, 19, 26, 33 and 19 steps for M11 across conditions from left to right) under different EES frequencies with the brain-controlled spinal cord neuroprosthesis. Small circles, individual gait cycles; lines, mean across all gait cycle for each condition. Recording days and presentation of statistical significance same as in (c). **d**, Body posture reconstructed from body kinematics using a whole-body skeletal model. Bar plots show the spine curvature measured from these reconstructions (n = 12, 12 and 12 samples for M8, 12, 12 and 12 samples for M9, and 10 and 10 samples for M11 across conditions from left to right). **e**, Brain-controlled spinal cord neuroprosthesis immediately improves locomotor performance when traversing a horizontal ladder. Stick diagrams show right leg kinematics during walking along the horizontal ladder of M11 after MPTP administration without and with brain-controlled spinal cord neuroprosthesis. Pie charts report the temporal accuracy of the decoder (n = 135 and 103 events for M8 and M11 respectively) measured during the online use of the neuroprosthesis. The histogram plots show the distributions between hotspot initiation events measured from kinematic recordings (ground truth) and hotspot initiation events decoded during locomotion with the brain-controlled spinal cord neuroprosthesis (n = 135 and 103 events for ladder for M8 and M11, respectively). Bar plots repot 'task' time needed to complete the task (n = 11, 9, 30 trials for M8 and 6, 14 trials for M11 across conditions from left to right) and the occurrence of falls (n = 30 trials). Balloons show mean ± standard deviation of all gait cycles for a given condition in space defined by PC1 and PC2, which explained 41% of all the variance. Bar plots report the Euclidean distance in the full 83-dimensional space of gait parameters between each gait cycle and the mean values across all the gait cycles recorded during two independent sessions before MPTP administration; as well as key parameters associated with gait and balance deficits commonly observed in people with PD (Ladder: n = 10, 13, 14, 19 and 40 steps for M8, and 20 and 12 steps for M11 across conditions from left to right). Changes in EES frequency between 30 and 80 Hz modulates gait parameters but has minimal impact on the efficacy of the therapy in the ladder. The plots report the stance duration and velocity during locomotion along the ladder (n = 40, 10, 8, 5, 14, 14 and 5 steps for M8, and 20 and 12 steps for M11 across conditions from left to right) under different EES frequencies with the brain-controlled spinal cord neuroprosthesis. Small circles, individual gait cycles; thick lines, mean across all gait cycle for each condition. Recording days and presentation of statistical significance same as in (c). *, **, *** significant difference at $p < 0.05$, $p < 0.01$ and $p < 0.001$, respectively using two-sided Wilcoxon rank sum test or the one-sided Monte Carlo permutation test. n.s., not significant ($p \geq 0.05$) according to the same tests. Error bars show sem.

https://doi.org/10.1038/s41591-023-02584-1

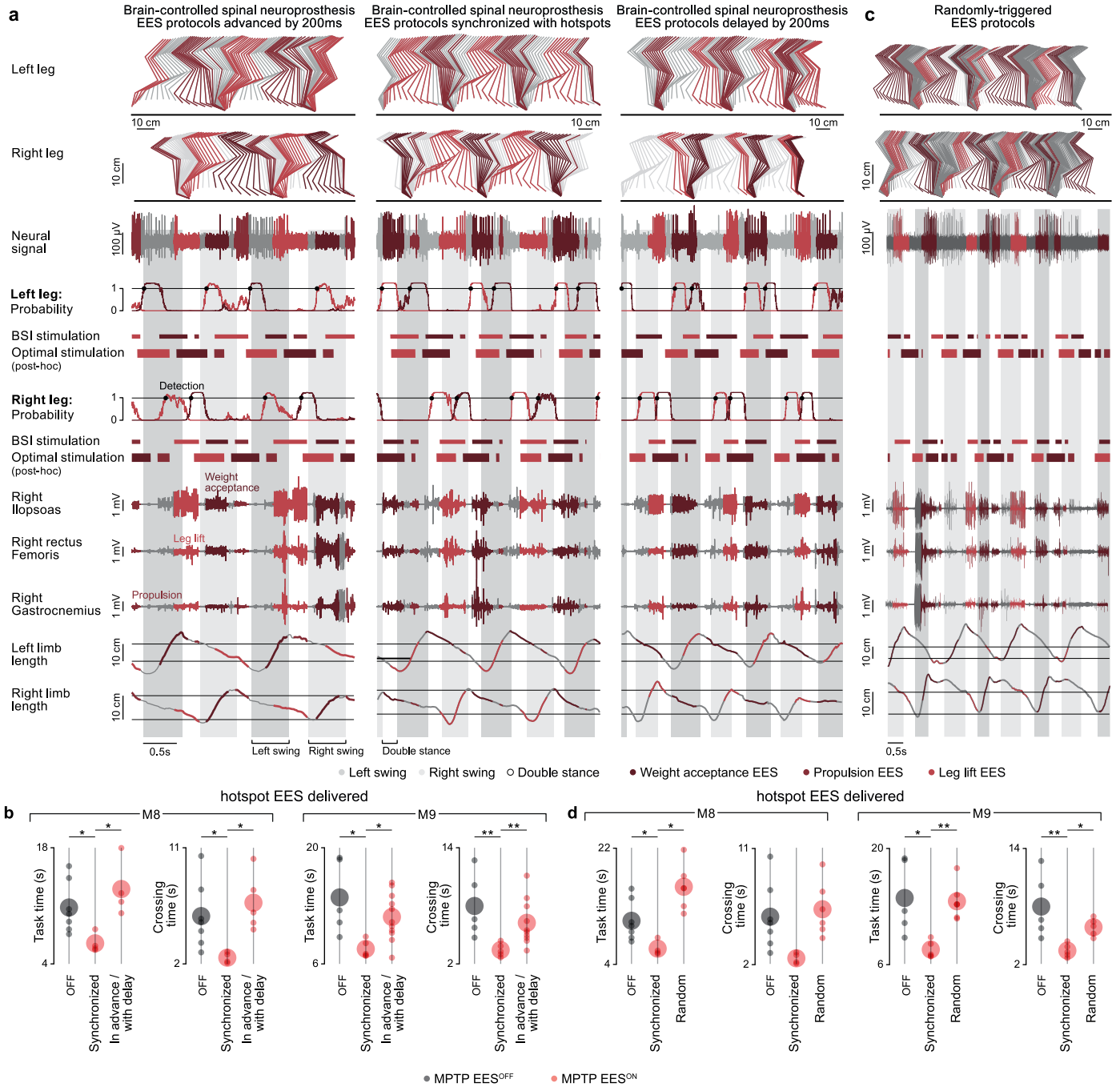

Extended Data Fig. 6 | EES protocols must be synchronized precisely with hotspot initiation events for maximum efficacy of the brain-controlled spinal cord neuroprosthesis. a, Examples showing 3.3 s of locomotion across the corridor using the brain-controlled spinal cord neuroprosthesis with three different decoding models (M8). From left to right: hotspot stimulation protocols initiated 200 ms before their initiation, hotspot stimulation protocols synchronized with hotspot initiation, hotspot stimulation protocols initiated 200 ms after their initiation. Conventions are the same as in Extended Data Fig. 5a. **b**, Dot plots showing the task time and crossing time without stimulation and when using the brain-controlled spinal cord neuroprosthesis delivering synchronized, advanced or delayed EES (task time: n = 7, 4 and 4 trials for M8 and 5, 5 and 11 trials for M9; crossing time: n = 7, 4 and 5 trials for M8 and 5, 5 and 11 trials for M9 for conditions from left to right, respectively). c, Example showing 7.16 s of locomotion across the corridor during the randomly triggered stimulation protocols. Conventions are the same as in Extended Data Fig. 5a. d, Dot plots showing the task time and crossing time without stimulation, when using the brain-controlled spinal cord neuroprosthesis to deliver synchronized EES, and random delivery of EES (task time: n = 7, 4 and 5 trials for M8 and 5, 5 and 5 trials for M9; crossing time: n = 7, 4 and 5 trials for M8 and 5, 5 and 5 trials for M9 for conditions from left to right, respectively). *, ** significant difference at $p < 0.05$ and $p < 0.01$, respectively, using two-sided Wilcoxon rank sum test.

https://doi.org/10.1038/s41591-023-02584-1

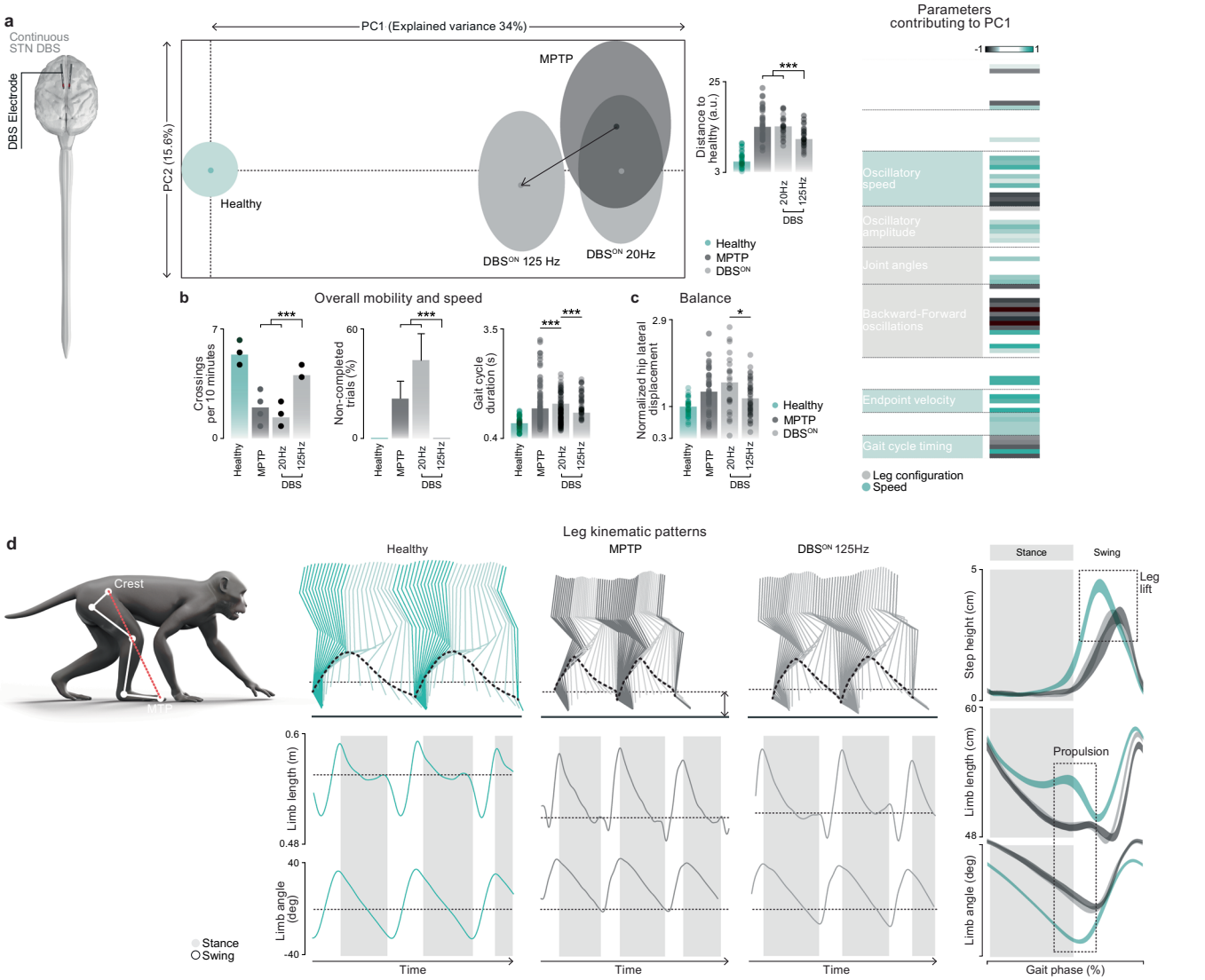

Extended Data Fig. 7 | DBS reduces bradykinesia in an NHP MPTP model of PD. a, We implanted monkey M9 with mini-DBS electrodes in the left and right subthalamic nucleus after the MPTP treatment to test the effect of low frequency (20 Hz) and high frequency (125 Hz) DBS during corridor walking. We evaluated the locomotor performance for the following conditions: before MPTP administration (Healthy) and after MPTP administration with stimulation off (MPTP), using 20 Hz DBS (DBS^{ON} 20 Hz), and using 125 Hz DBS (DBS^{ON} 125 Hz). Balloons show mean ± SD of all gait cycles for each condition in the space spanned by two leading PCs (number of gait cycles: Healthy: 39; MPTP: 47; DBS^{ON} 20 Hz: 27; DBS^{ON} 125 Hz: 37). The bar plot inset reports the Euclidean distance in the full 83-dimensional gait space between each gait cycle and the mean values across all the gait cycles recorded before MPTP administration. To identify the MPTP-induced locomotor deficits affected the most by the DBS, we identified the parameters with the highest loading factors on PC1. This analysis revealed a strong influence of DBS on parameters related to gait velocity and size, but reduced impact of limb configuration values (leg lift, propulsion) during gait. **B**, As reported in Parkinson's disease patients, high frequency DBS increases the overall mobility and mediates a moderate increase on gait speed, while the low frequency DBS fails to improve locomotion and impairs awareness. The bar plots show the number of corridor crossings within 10 minutes (number of trials: Healthy: 24; MPTP: 19; DBS^{ON} 20 Hz: 12; DBS^{ON} 125 Hz: 17), percentage of uncompleted trials, and gait cycle duration (number of gait cycles: Healthy: 50; MPTP: 160; DBS^{ON} 20 Hz: 49; DBS^{ON} 125 Hz: 137). **C**, High frequency DBS moderately improves the balance locomotor deficits. The bar plot shows the mean lateral displacement of the hip during gait (number of gait cycles same as in a). **d**, DBS failed to correct for the lack of propulsion and leg lift induced by MPTP. The plots show examples of three successive gait cycles recorded before MPTP (left column), and after MPTP without using stimulation (middle column) or using 125 Hz DBS (right column). The plots show mean ± SD of left leg step height, limb length and limb angle across the gait cycle (number of gait cycles same as in a). *, **, *** reflect a significant difference at $p < 0.05$, $p < 0.01$, $p < 0.001$ respectively, using two-sided Wilcoxon ranksum test or the one-sided Monte Carlo permutation test. Error bars show sem.

https://doi.org/10.1038/s41591-023-02584-1

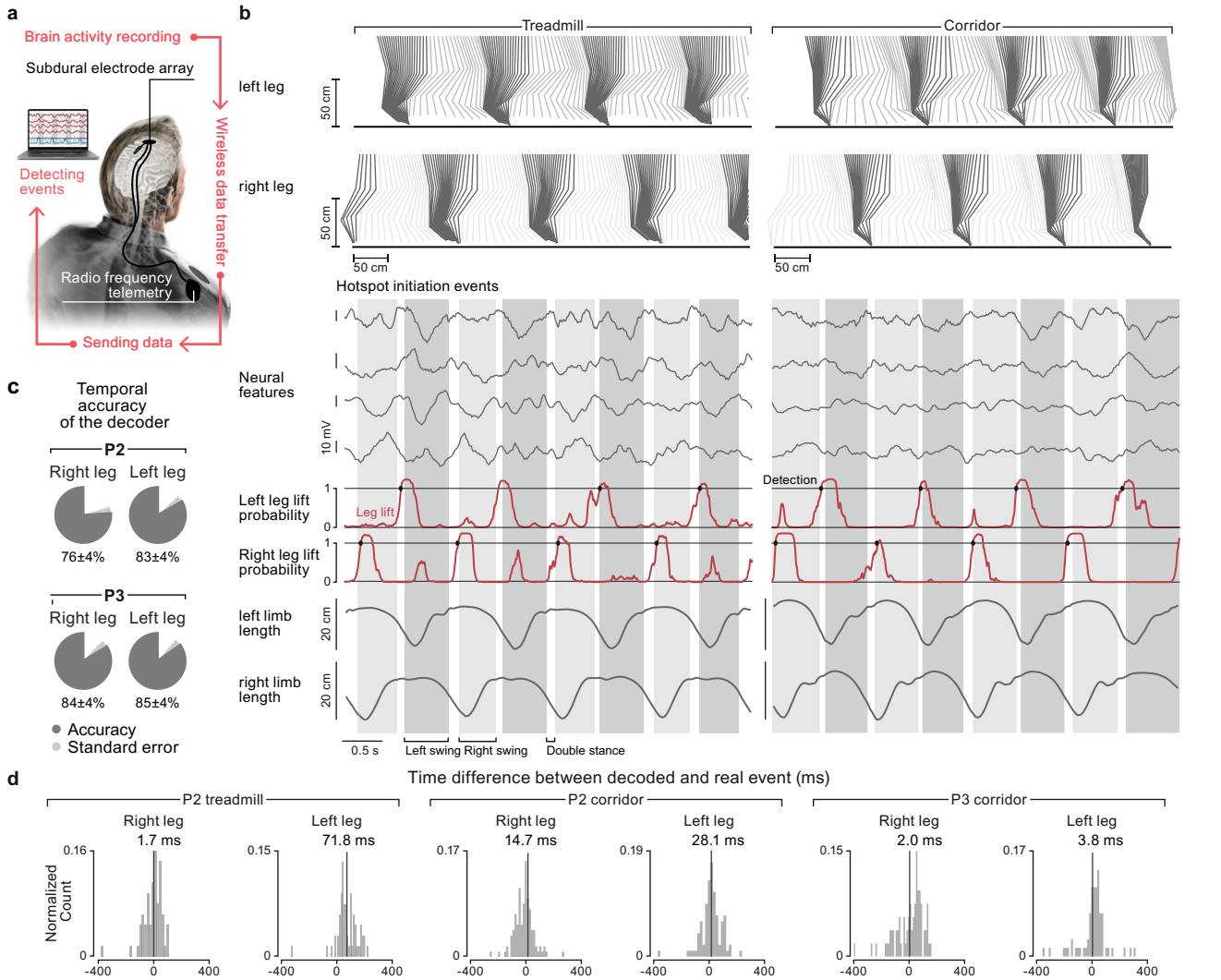

Extended Data Fig. 8 | EcoG signals collected from the surface of the motor cortex of people with Parkinson's disease enable accurate detection of hotspot initiation events during locomotion. a, Two people with Parkinson's disease, P2 and P3, were implanted with quadripolar cortical paddles inserted subdurally over the motor cortex. Each paddle was connected to an implanted Medtronic Summit RC + S device to acquire epicortical ECoG signals wirelessly. **b**, Examples of locomotor execution along the treadmill (5 s) and corridor (5 s) of participant P2. From top to bottom: stick diagram decompositions of left and right leg movements; neural features (low-pass filtered ECoG signal) from all four recorded channels; probability of left and right leg lift events with detected hotspot events (black dots); left and right limb length calculated as distance from the hip to the ankle joint. The white, light grey and dark grey backgrounds correspond to double stance, left and right swing gait phases, respectively. **c**, Decoding remains accurate for both tasks in P2 and for P3. The pie charts show the mean ± sem accuracy of the detections for P2 (events: left: 64; right: 62) and P3 (events: left: 70; right: 74) calculated by offline analysis using cross-validation. **d**, Histogram plots show the distribution of the temporal differences between real and detected events (events: P1 treadmill: left: 92; right: 118; P1 corridor: left: 64; right: 62; P2 corridor: left: 70; right: 74) calculated by offline analysis using cross-validation. Median temporal difference is provided and marked by a vertical black line.

https://doi.org/10.1038/s41591-023-02584-1

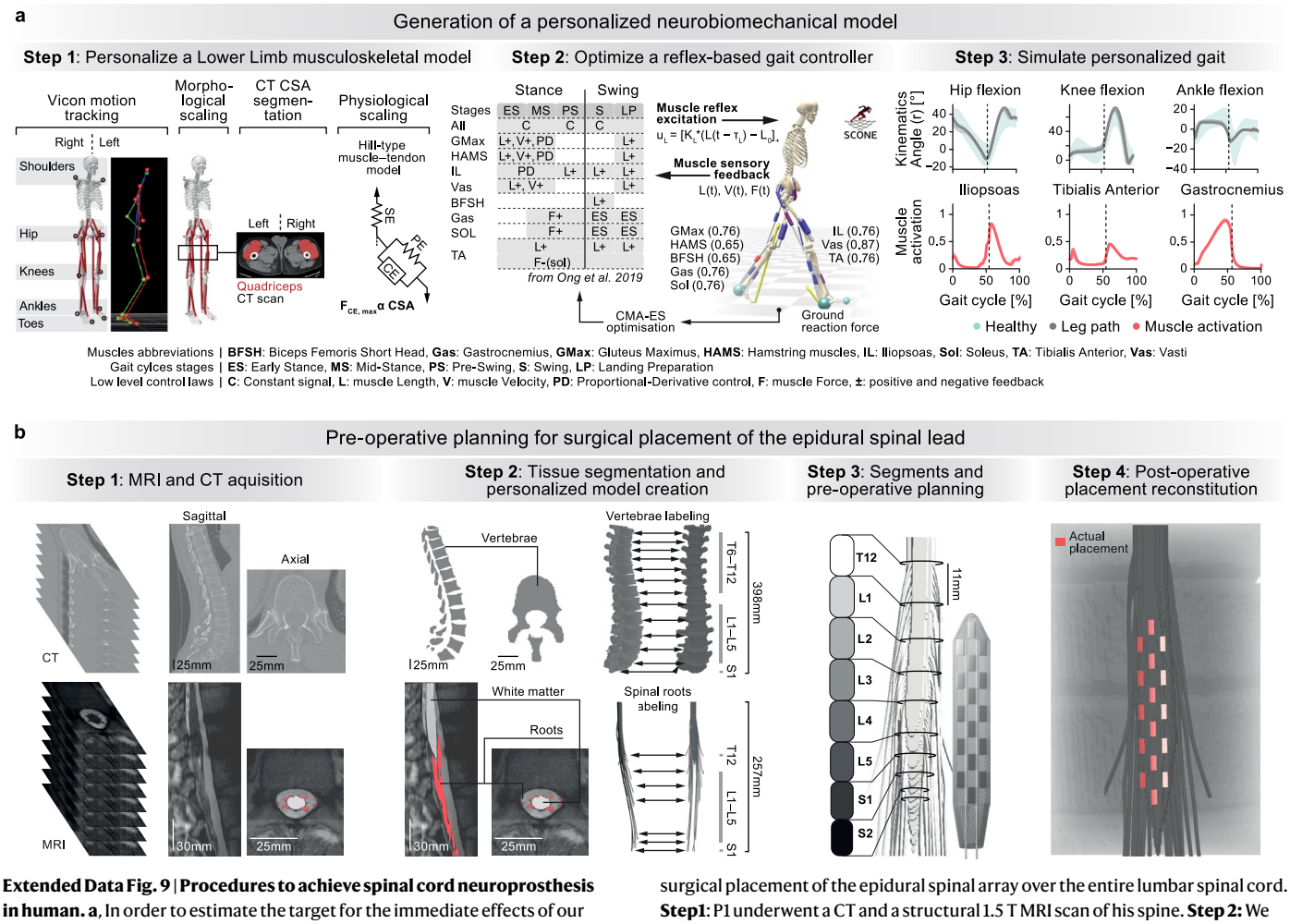

Extended Data Fig. 9 | Procedures to achieve spinal cord neuroprosthesis in human. a, In order to estimate the target for the immediate effects of our therapy, we sought to simulate the gait of P1 given his anatomy but in the absence of neurodegeneration. To this end, we generated a personalized neurobiomechanical model of P1. **Step1:** We personalized the Lower Limb model[1] to P1's anatomy using morphological and physiological scaling. We performed the morphological scaling based on full-body motion tracking using the Vicon system. We then implemented the physiological scaling based on segmentation of muscles' cross-sectional area (CSA) from CT images. **Step2:** We optimized the reflex-based gait controller using the SCONE software[2,3]. This controller is composed of phase dependent reflexes providing muscle excitation based on muscle length, velocity or force feedback. **Step3:** We simulated P1 gait in the absence of neurodegeneration using Covariance Matrix Adaptation Evolutionary Strategy (CMA-ES)[4] to optimize controller parameters. About 500 generations of CMA-ES were necessary to reach a stable gait from initialization. Once the parameters of the controller have converged, we generated 200 steps of this model and extracted full kinematics of lower limbs and muscle activity. The graphs show the mean with tubes showing the mean +/- standard deviation range of values. **b**, We used the P1's CT and MRI scans to generate a three-dimensional anatomical model of the spine, which we then used to plan the surgical placement of the epidural spinal array over the entire lumbar spinal cord. **Step1**: P1 underwent a CT and a structural 1.5 T MRI scan of his spine. **Step 2:** We segmented the vertebral bones and disks from the CT scan, and segmented the spinal cord tissues (spinal cord, spinal cord roots and cerebrospinal fluid) from the MRI scan. We co-registered the tissues segmented from the two different scans, and combined them into a 3D anatomical model of the P1 spine. **Step 3:** We loaded a 3D model of the spinal array and placed it centred over the dorsal side of the spinal cord covering the L1-L5 spinal segments. Position of the array with respect to the segmented vertebral column determined the insertion point of the array to be between L1 and T12 vertebra. During the surgery, we opened the access to the surface of the dura by small incisions and a T12/L1 flavectomy, placed the tip of the array over the midline of the exposed dura and advanced the array rostrally to the target location. We accurately adjusted the medial and segmental position of the paddle array by monitoring the muscle responses to single-pulse EES delivered by different array electrodes**. Step 4:** After the surgery, we performed a post-operative CT scan to reconstruct the position of the spinal array with respect to the patient spine. The actual placement of the array was within 1 cm of the preoperative plan, as expected due to segmentation and co-registration inaccuracies.

https://doi.org/10.1038/s41591-023-02584-1

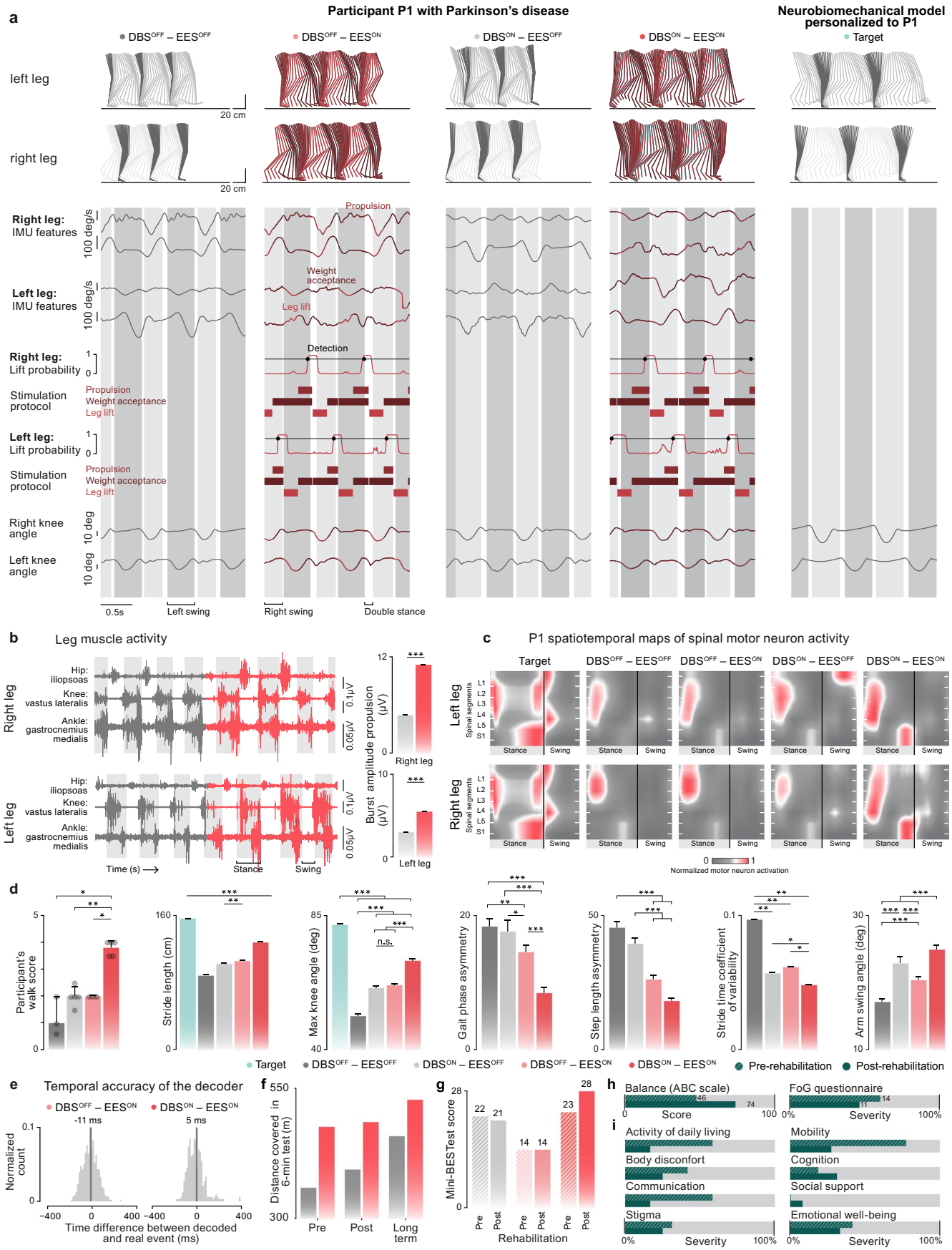

Extended Data Fig. 10 | See next page for caption.

https://doi.org/10.1038/s41591-023-02584-1

Extended Data Fig. 10 | Spinal cord neuroprosthesis delivering spinal EES in synchrony with attempted movements alleviates gait deficits of PD alone and synergistically with DBS of the subthalamic nucleus. a, Examples show 3 s of P1's locomotor execution along the corridor in four combinations of using or not the kinematically-controlled spinal cord neuroprosthesis (marked 'EES') and DBS of the subthalamic nucleus, and of the personalized neurobiomechanical model of P1. From top to bottom: stick diagram decompositions of left and right leg movements; four IMU features used to control the EES; probability of left and right weight acceptance events; detected hotspot events (broken vertical lines), periods of stimulation using a combination of 10 EES protocols targeting the left and right weight acceptance, propulsion and leg lift hotspots; and left and right knee angles. The white, light grey and dark grey backgrounds correspond to double stance, left swing and right swing gait phases, respectively. **b**, The plots showing EMG of left and right hip (iliopsoas), knee (gastrocnemius medialis) and ankle (vastus lateralis) leg muscles when transitioning from DBS^{ON} - EES^{OFF} into DBS^{ON} - EES^{ON} conditions illustrate the change in muscle activation. Bar plots show the burst amplitude of left and right gastrocnemius medialis muscle during the propulsion phase of gait in DBS^{ON} - EES^{OFF} (gait cycles: left: 79; right: 72) and DBS^{ON} - EES^{ON} (gait cycles: left: 136; right: 134) conditions. **c**, With the progressive use of spinal cord neuroprosthesis and DBS therapies, the motor neuron activation dynamics became more similar to that of the P1 neurobiomechanical model. The colorplots show the Target spatiotemporal spinal map derived from the P1 neurobiomechanical model, and the left and right leg spatiotemporal spinal maps of P1 in four combinations of using or not the kinematically-controlled spinal cord neuroprosthesis and DBS of the subthalamic nucleus (number of gait cycles: Target: 168; left leg: DBS^{OFF} - EES^{OFF}: 130; DBS^{ON} - EES^{OFF}: 67; DBS^{OFF} - EES^{ON}: 119; DBS^{ON} - EES^{ON}: 95; right leg: DBS^{OFF} - EES^{OFF}: 131; DBS^{ON} - EES^{OFF}: 66; DBS^{OFF} - EES^{ON}: 118; DBS^{ON} - EES^{ON}: 91). Surface correlation between the Target and therapy spatiotemporal spinal maps are shown on Fig. 5d. **d**, Bar plots show measures of gait quality, efficacy and symmetry, as well as balance: participants walk score (number of trials: DBS^{OFF} - EES^{OFF}: 2; DBS^{ON} - EES^{OFF}: 2; DBS^{OFF} - EES^{ON}: 5; DBS^{ON} - EES^{ON}: 5), stride length (number of gait cycles: P1 target model: 335, DBS^{OFF} - EES^{OFF}: 239; DBS^{ON} - EES^{OFF}: 120; DBS^{OFF} - EES^{ON}: 297; DBS^{ON} - EES^{ON}: 209), max knee angle (number of gait cycles: Target: 336; DBS^{OFF} - EES^{OFF}: 328; DBS^{ON} - EES^{OFF}: 175; DBS^{OFF} - EES^{ON}: 431; DBS^{ON} - EES^{ON}: 339), gait phase asymmetry (number of gait cycles: DBS^{OFF} - EES^{OFF}: 119; DBS^{ON} - EES^{OFF}: 60; DBS^{OFF} - EES^{ON}: 148; DBS^{ON} - EES^{ON}: 103), step length asymmetry as measured by the ratio between lengths of the left and right steps (number of gait cycles: P1 Target model: 167; DBS^{OFF} - EES^{OFF}: 119; DBS^{ON} - EES^{OFF}: 60; DBS^{OFF} - EES^{ON}: 148; DBS^{ON} - EES^{ON}: 103), stride time coefficient of variability (number of gait cycles same as for stride length), and arm swing angle (number of gait cycles: DBS^{OFF} - EES^{OFF}: 328; DBS^{ON} - EES^{OFF}: 175; DBS^{OFF} - EES^{ON}: 431; DBS^{ON} - EES^{ON}: 339). **e**, Decoding of hotspot initiation events from IMU signals to control the spinal cord neuroprosthesis remains accurate both when DBS is on or off. Histogram plots show the distribution of the temporal differences between real and detected events (events: DBS^{OFF} - EES^{ON}: 462; DBS^{ON} - EES^{ON}: 328) when using the brain-controlled spinal cord neuroprosthesis. Median temporal difference is provided and marked by a vertical line. **f**, The bar plots show improvements in endurance, as measured by the distance covered during a 6-minute walking test, after the three-month rehabilitation supported by the spinal cord EES and 1-year after (n = 1 test in each condition). **g**, The bar plots show the gains in balance, as measured using the Mini-BESTest, after the three-month rehabilitation supported by the spinal cord EES (n = 1 test in each condition). **h**, Improvements in balance and freezing of gait, as measured by the ABC questionnaire and FoG questionnaire, prior and post-rehabilitation (n = 1 filled-out questionnaire in each condition). **i**, The bar plots show the sub-categories of the quality of life PDQ-39 questionnaire scores before and after the three-month rehabilitation supported by the spinal cord EES (n = 1 filled-out questionnaire in each condition). *, **, *** significant difference at $p < 0.05$, $p < 0.01$, $p < 0.001$, respectively, using two-sided Wilcoxon rank sum test or the one-sided Monte Carlo permutation test. n.s., not significant ($p \geq 0.05$) according to the same tests. Error bars show sem.

nature portfolio

Corresponding author(s): Gregoire Courtine

Last updated by author(s): 07/07/2023

Reporting Summary

Nature Portfolio wishes to improve the reproducibility of the work that we publish. This form provides structure for consistency and transparency in reporting. For further information on Nature Portfolio policies, see our Editorial Policies and the Editorial Policy Checklist.

Statistics

For all statistical analyses, confirm that the following items are present in the figure legend, table legend, main text, or Methods section.

n/a	Confirmed
☐	☒ The exact sample size (*n*) for each experimental group/condition, given as a discrete number and unit of measurement
☐	☒ A statement on whether measurements were taken from distinct samples or whether the same sample was measured repeatedly
☐	☒ The statistical test(s) used AND whether they are one- or two-sided *Only common tests should be described solely by name; describe more complex techniques in the Methods section.*
☒	☐ A description of all covariates tested
☒	☐ A description of any assumptions or corrections, such as tests of normality and adjustment for multiple comparisons
☐	☒ A full description of the statistical parameters including central tendency (e.g. means) or other basic estimates (e.g. regression coefficient) AND variation (e.g. standard deviation) or associated estimates of uncertainty (e.g. confidence intervals)
☐	☒ For null hypothesis testing, the test statistic (e.g. *F*, *t*, *r*) with confidence intervals, effect sizes, degrees of freedom and *P* value noted *Give P values as exact values whenever suitable.*
☒	☐ For Bayesian analysis, information on the choice of priors and Markov chain Monte Carlo settings
☒	☐ For hierarchical and complex designs, identification of the appropriate level for tests and full reporting of outcomes
☒	☐ Estimates of effect sizes (e.g. Cohen's *d*, Pearson's *r*), indicating how they were calculated

Our web collection on statistics for biologists contains articles on many of the points above.

Software and code

Policy information about availability of computer code

Data collection

We collected data from 11 macaque monkeys, 34 human participants of the PREDI-STIM clinical study, two participants of the "Motor Network in Parkinson's Disease and Dystonia: Mechanisms of Therapy" clinical trial, and one participant of the STIMO-PARK clinical trial,as follows: 1) Non-human primate data: behavioral, motion tracking, electromyographic, intracortical neurophysiological and histological data. 2) Human data: self-reported and observational behavioral, motion tracking, electromyographic, epicortical neurophysiological and medical imaging data, as well as data from clinically-established questionnaires on motor capacity and quality of life.

All softwares and software versions used to acquire data: G-Drive Plus software suite by EPFL, DecodingGate software application by EPFL, Neural Research Programmer v5.2.999 and later by Medtronic, NEUWalk Research Programmer Application 09103 by Medtronic, Research Development Kit 4NR013 by Medtronic, Cerebus Central Suite v6 and later by Blackrock Neurotech, Simi Motion software v8 and later by Simi Reality Motion Systems, Nexus 1.8.5 by Vicon, and ISIS XPress by inomed

The methods, procedures and devices to to collect data are described in the man text of the manuscript and in the Method section of the relevant paragraphs.

Data analysis	All softwares and software versions used to analyze data : Matlab v2018a and later by Mathworks, Sim4Life v7.0 by ZMT, Cerebus Central Suite v6 and later by Blackrock Neurotech, Simi Motion software v8 and later by Simi Reality Motion Systems, Nexus 1.8.5 by Vicon, OpenSim software suite v4.2 and later by SimTK, SCONE software v2.0.0 and later, ISIS XPress by inomed, Neurolucida image analysis software v2019.1.1 and later by MBF Bioscience, Spinal Cord Toolbox v5.4 These are described in the Method section at the relevant paragraphs.

For manuscripts utilizing custom algorithms or software that are central to the research but not yet described in published literature, software must be made available to editors and reviewers. We strongly encourage code deposition in a community repository (e.g. GitHub). See the Nature Portfolio guidelines for submitting code & software for further information.

Data

Policy information about availability of data

All manuscripts must include a data availability statement. This statement should provide the following information, where applicable:

- Accession codes, unique identifiers, or web links for publicly available datasets
- A description of any restrictions on data availability
- For clinical datasets or third party data, please ensure that the statement adheres to our policy

Data that supports the findings and software routines developed for the data analysis will be made available upon reasonable request to the corresponding authors. Third party datasets used in our study are available under the Creative Commons Public License: VerSe 2019 (https://osf.io/nqjyw/) and VerSe 2020 (https://osf.io/t98fz/).

Human research participants

Policy information about studies involving human research participants and Sex and Gender in Research.

Reporting on sex and gender	We comply with the sex and gender guidelines.
Population characteristics	PREDI-STIM clinical study The study involved 25 participants with PD (12 female, 13 male, mean age 60 +/- std 7.8) and 9 participants without PD as controls (4 female, 5 male, mean age 58.8 +/- std 4.5). Sex was self-reported. Sex was considered in the study design – the participants were enrolled to ensure a balanced sex distribution. Informed consent was obtained for all participants. The participants received no compensation for the study. Key inclusion criteria for people with Parkinson's disease: o Diagnosed with Parkinson's disease o Receiving a pre-therapeutic assessment and monitoring for one, three and five years as part of the regular monitoring of the subthalamic nucleus deep brain stimulation. Motor Network in Parkinson's Disease and Dystonia: Mechanisms of Therapy clinical trial Key inclusion criteria for people with Parkinson's disease: o Ability to give informed consent for the study. o Movement disorder symptoms that are sufficiently severe, in spite of best medical therapy, to warrant surgical implantation of deep brain stimulators according to standard clinical criteria. o Patient has requested surgical intervention with deep brain stimulation for their disorder. o No MR abnormalities that suggest an alternative diagnosis or contraindicate surgery. o Absence of significant cognitive impairment (score of 20 or greater on the Montreal Cognitive Assessment - MoCA). o Signed informed consent. o Ability to comply with study follow-up visits for brain recording, testing of adaptive stimulation, and clinical assessment. o Age 21-75 (for STN patients, minimum age is 25). o Diagnosis of idiopathic PD with duration of motor symptoms for 4 years or greater. o Patient has undergone appropriate therapy with oral medications with inadequate relief as determined by a movement disorders neurologist, and has had stable doses of antiparkinsonian medications for 30 days prior to baseline assessment. o UPDRS-III score off medication between 20 and 80 and an improvement of at least 30% in the baseline UPDRS-III on medication score, compared to the baseline off-medication score, and motor fluctuations with at least 2 hours per day of on time without dyskinesia or with non-bothersome dyskinesia, or Patients with tremor-dominant PD (a tremor score of at least 2 on a UPDRS-III sub-score for tremor), treatment resistant, with significant functional disability despite maximal medical management. Key exclusion criteria: o Coagulopathy, anticoagulant medications, uncontrolled hypertension, history of seizures, heart disease, or other medical conditions considered to place the patient at elevated risk for surgical complications. o Evidence of a psychogenic movement disorder: Motor symptoms that remit with suggestion or "while unobserved", symptoms that are inconsistent over time or incongruent with clinical condition, plus other manifestation such as "false" signs, multiple somatizations, or obvious psychiatric disturbance. o Pregnancy: all women of child bearing potential will have a negative urine pregnancy test prior to undergoing their surgical procedure. o Significant untreated depression (BDI-II score >20) History of suicidal attempt or active suicidal ideation (Yes to #2-5 on C-SSRS). o Any personality or mood symptoms that study personnel believe will interfere with study requirements. o Subjects who require ECT, rTMS or diathermy.

o Implanted stimulation systems such as; cochlear implant, pacemaker, defibrillator, neurostimulator or metallic implant.
o Previous cranial surgery.
o Drug or alcohol abuse.
o Meets criteria for Parkinson's disease with mild cognitive impairment (PD-MCI). These criteria are: performance of more than two standard deviations below appropriate norms, for tests from two or more of these five cognitive domains: attention, executive function, language, memory, and visuospatial tests.

STIMO-PARK clinical trial
STIMO-PARK is an ongoing clinical feasibility study (clinicaltrials.gov ID: NCT04956770) that investigates the effects of lumbosacral EES to improve mobility in people with Parkinson's disease. Study participation was not compensated, but all the study-related costs incurred on the participants were reimbursed. The sex of participants was not considered in the clinical trial design as not a relevant criterium to evaluate in this feasibility case study. The inclusion criteria include idiopathic Parkinson's disease with III-IV Hoehn-Yahr stage, exhibiting severe gait difficulties and postural instability, use of the Medtronic DBS implant and receiving medication for Parkinson's disease. The study involves assessments before the implantation surgery for the spinal EES neurostimulation system, the surgical implantation of the neurostimulation system, a 1-month period for configuration of EES protocols and sequences, and a 3-month period of physiotherapist-assisted rehabilitation during 1–3-hour sessions taking place 2 to 3 times per week. The rehabilitation program is personalized based on the participants' needs and improvements.

Key inclusion criteria:
o Diagnosed with idiopathic Parkinson's disease with III-IV Hoehn-Yahr stage, exhibiting severe gait difficulties and postural instability.
o Implanted with Medtronic DBS implant and receiving medication for Parkinson's disease.
o Aged 18 to 80 years.
o Stable medical, physical and psychological condition as considered by the Investigators in accordance with treating physician and treating neurologist.
o Must agree to comply in good faith with all conditions of the study and to attend all required study training and visit
o Must provide and sign the study's Informed Consent prior to any study-related procedures.

Key exclusion criteria:
o Severe or chronic medical disorder pre-existing PD diagnosis affecting rehabilitation.
o Active oncological disease requiring heavy treatments and frequent MRI controls.
o Having an implanted device that is active (e.g., pacemaker, implantable cardiac defibrillator) whose interference with the investigational system's neurostimulator (Activa RC) is not confirmed safe by the CE-mark of the device, or having an indication that might lead to implantation of such device.
o Inability to follow study procedures, e.g. due to language problems, psychological disorders, dementia as considered by the Investigators in accordance with treating physician and treating neurologist.
o Hematological disorders with an increased risk of hemorrhagic event during surgical interventions.
o Life expectancy of less than 12 months.
o Pregnant or breast feeding.
o Participation in another interventional study.

Recruitment

PREDI-STIM clinical study
This article describes the analysis of data collected from 25 people with Parkinson's disease and 9 age-matched healthy controls that were enrolled in the PREDI-STIM clinical study, conducted at the Bordeaux University Hospital. People with Parkinson's disease were recruited among all the pool of patients being followed within the Neurology Dpt. Participation in the study was proposed to all patients as they were being followed in the clinic, until filling the sex / gender distribution. The controls were recruited by adds.

Motor Network in Parkinson's Disease and Dystonia: Mechanisms of Therapy clinical trial
This article described the analysis of data collected from two people with Parkinson's disease that were enrolled in the clinical trial. They were recruited from a population referred for implantation of deep brain stimulators for PD. Before recruitment, they were evaluated by a movement disorders neurologist and met diagnostic criteria for PD and by a neuropsychologist to exclude major cognitive impairment or untreated mood disorder. Inclusion criteria included motor fluctuations with prominent rigidity and bradykinesia in the off-medication state, baseline off-medication MDS-UPDRS-III scores between 20 and 80, greater than 30% improvement in MDS-UPDRS-III on medication than off of medication and absence of significant cognitive impairment (score of 20 or above on the Montreal Cognitive Assessment). The full IDE application (G180097) and study protocol have been shared with other researchers via the Open Mind initiative (https://openmind-consortium.github.io). After enrollment, participants underwent bilateral placement of cylindrical quadripolar deep brain stimulator leads into the STN (Medtronic model 3389; 1.5-mm contact length and 2.0-mm intercontact spacing), bilateral placement of quadripolar cortical paddles into the subdural space over the cortical area that included the motor cortex (Medtronic model 0913025; 4-mm contact diameter and 10-mm intercontact spacing) and bilateral placement of investigational sensing IPGs in a pocket over the pectoralis muscle (Medtronic Summit RC+S model B35300R). The IPG on each side was connected to two leads by 60-cm lead extenders (Medtronic model 37087). The Summit RC+S IPG is a 16-channel device that, through the use of its application programming interface, allows researchers to record four bipolar time domain channels (250/500 Hz) or two channels at 1,000 Hz62,63. For all research functions, including configuring and initiating sensing and developing embedded or distributed adaptive DBS, investigators controlled the device by writing software in C# within the device API, accessed using a 'research development kit' (RDK; Medtronic model 4NR013) provided by the manufacturer. We wrote a software application to configure and initiate streaming data from two RC+S devices simultaneously (available at https://openmind-consortium.github.io).

STIMO-PARK clinical trial
This article describes the analysis of data collected from P1, the first and only participant enrolled in the STIMO-PARK study by February 2022. Recruitment was performed through referral from Neurology clinics in the consortium. P1 was a 61-year-old male at time of enrollment. He has been diagnosed with Parkinson's Disease at the age of 36 and implanted with DBS at the age of 44. He is currently in stage 3 of the Hoen-Yahr scale. He experiences fluctuations in his gait pattern and lower limb

symptoms typical of later stages of PD, including slowness, asymmetry, rigidity, small steps, flexed posture. Before being implanted with the EES system, during the 6-minute walk test P1 was able to cover 433 meters with DBS turned on and during his regular levodopa intake, and 224 meters with DBS turned off and with the last levodopa intake the evening before. His MDS-UPDRS motor examination scores (part III) in these two states were 20 and 47, respectively. He started to experience freezing-of-gait over the last decade, which greatly impacted his independence and quality of life. Before participation in the study, he reported 4 falls per day on average due to freezing-of-gait. Following the enrolment, we performed a CT scan of his torso and a structural MRI scan of his spine to generate a personalized anatomical model of his spine. Following the pre-surgical assessments, P1 was implanted with the spinal EES neurostimulation system. After the surgery, P1 was transferred to the neurosurgery ward for recovery. P1 then went back to the hotel for a one-week recovery period. After recovery, we successfully configured the EES protocols and sequences for P1 during the study configuration period.

Ethics oversight

PREDI-STIM clinical study
The study was approved by the Nord Ouest-IV Ethical Committee, France (2013- A00193-42) and was conducted in accordance with the Declaration of Helsinki (clinicaltrials.gov ID: NCT02360683).

Motor Network in Parkinson's Disease and Dystonia: Mechanisms of Therapy clinical trial
The study was approved by the University of California, San Francisco IRB and was conducted in accordance with the Declaration of Helsinki (clinicaltrials.gov ID: NCT03582891).

STIMO-PARK clinical trial
The study was approved by the Swiss ethical authorities (Swissethics protocol number 2021-0047) and is conducted following the Declaration of Helsinki (clinicaltrials.gov ID: NCT04956770).

Note that full information on the approval of the study protocol must also be provided in the manuscript.

Field-specific reporting

Please select the one below that is the best fit for your research. If you are not sure, read the appropriate sections before making your selection.

☒ Life sciences ☐ Behavioural & social sciences ☐ Ecological, evolutionary & environmental sciences

For a reference copy of the document with all sections, see nature.com/documents/nr-reporting-summary-flat.pdf

Life sciences study design

All studies must disclose on these points even when the disclosure is negative.

Sample size

No power calculation was used to determine the sample size.
- Data from 9 non-human primates was used to characterize gait deficits developed by the MPTP-treated macaque model. This sample size is larger than most studies that study locomotor deficits in nonhuman primate models of PD.
- Data from 25 people with Parkinson's disease and 9 healthy age-matched controlled was used to characterize gait deficits of Parkinson's disease. This sample size is in line with most studies that study motor deficits in people with PD in a clinical settings, as this sample size is enough for statistical power, while ensuring feasibility and maximizing adherence (due to the difficulty of inviting patients of an advanced age to the hospital)
- Data from 5 rhesus macaques was used to count the dopaminergic fiber density in Caudate and Putamen after the use of our MPTP-treatment protocol. This sample size is larger than most studies that study histology in nonhuman primate models of PD.
- Data from 4 rhesus macaques was used to count dopaminergic cells in substantia nigra. This sample size is larger than most studies that study histology in nonhuman primate models of PD.
- Data from 4 rhesus macaques was used to evaluate the impact of the MPTP treatment on the spatiotemporal maps of spinal cord motor neuron activity. This sample size is larger than most studies that study locomotor deficits in nonhuman primate models of PD.
- Data from 3 rhesus macaques was used to characterize the spinal motor neuron activity evoked by epidural electrical stimulation of the lumbar spinal cord. This sample size is larger than most studies that study locomotor deficits in nonhuman primate models of PD.
- Data from 3 rhesus macaques was used to longitudinally quantify the accuracy of detecting gait events from the activity of motor cortical neural ensembles after the MPTP treatment. This sample size is larger than most studies that study neural correlates of locomotor deficits in nonhuman primate models of PD.
- Data from two people with Parkinson's disease was used to quantify the accuracy of detecting gait events from the epicortical brain signals collected over the motor cortex. This sample size is in line with studies that report on epicortical neural correlates of locomotor deficits in people with PD.
- Data from 3 macaques was used to evaluate the efficacy of spinal cord neuroprosthesis to alleviate parkinsonian locomotor deficits after the MPTP treatment. This sample size is larger than most studies that report on the efficacy of a neuroprosthesis in nonhuman primates.
- Data from 3 rhesus macaques was used to quantify the accuracy of detecting gait events from the activity of motor cortical neural ensembles after the MPTP treatment during the use of spinal cord neuroprosthesis.
- Data from 3 rhesus macaques was used to characterize the motor responses to electrical epidural stimulation of the lumbar spinal cord at different frequencies. This sample size is larger than most studies that report the efficacy of a neuroprosthesis in nonhuman primates.
- Data from 2 macaques was used to demonstrate that lack of synchrony between the spinal cord stimulation and the motor intention causes the loss of efficacy of the spinal cord neuroprosthesis in alleviating parkinsonian locomotor impairments. This sample size is in line with most studies that report on the efficacy of a neuroprosthesis in nonhuman primates.
- Data from 1 macaque was used to evaluate the efficacy of spinal cord neuroprosthesis to alleviate parkinsonian locomotor impairments synergistically with the deep brain stimulation of the substantia nigra after the MPTP treatment. This sample size is in line with studies that report on the efficacy of a neuroprosthesis in nonhuman primates.
- Data from one person with Parkinson's disease was used to evaluate the efficacy of spinal cord neuroprosthesis to alleviate parkinsonian

	locomotor deficits synergistically with the deep brain stimulation of the substantia nigra and the levedopa treatment. This N=1 sample size corresponds to a feasibility case study and is in line with studies that report on the use of neuroprosthesis in people with neurological disorders.
Data exclusions	None.
Replication	The analysis of kinematic, electromyography and neurophisiological datasets of non-human primates was performed on multiple sessions, each recorded on a different day. Detailed list is provided in Supplementary Table 2. Replication numbers for analysis of human data are provided in detail in figure captions.
Randomization	Different trials during the non-human primate experimental sessions and trial sets during the P1 sessions were randomly interleaved. PREDI-STIM data and data from P2 and P3 were collected in only one conditions, therefore randomization was not applicable.
Blinding	The investigators operating the stimulation could not blinded to allocation during experiments and outcome assessment. However: 1) In NHP: Experienced technicians working at the non-human primate facility and not part of the study were blinded during their assessments of PD scores. They were unaware of the MPTP administration protocol or any of the details related to our experiments. 2) In P1: all evaluations from physiotherapists and clinicians were performed blinded to the therapy being delivered. All data analyses, except for the semi-automatic kinematic reconstruction in the Simi Motion software, Vicon software and marking of gait events from video recordings were performed "blindly" using automatic computer routines. 3) In PREDI-STIM: data were collected in only one conditions, therefore blinding was not applicable. 4) In Motor Network in Parkinson's Disease and Dystonia: Mechanisms of Therapy clinical trial: data were collected in only one conditions, therefore blinding was not applicable.

Reporting for specific materials, systems and methods

We require information from authors about some types of materials, experimental systems and methods used in many studies. Here, indicate whether each material, system or method listed is relevant to your study. If you are not sure if a list item applies to your research, read the appropriate section before selecting a response.

Materials & experimental systems

n/a	Involved in the study
☐	☒ Antibodies
☒	☐ Eukaryotic cell lines
☒	☐ Palaeontology and archaeology
☐	☒ Animals and other organisms
☐	☒ Clinical data
☒	☐ Dual use research of concern

Methods

n/a	Involved in the study
☒	☐ ChIP-seq
☒	☐ Flow cytometry
☐	☒ MRI-based neuroimaging

Antibodies

Antibodies used	Tyrosine hydroxylase (TH) immunochemistry was performed using mouse anti-TH primary antibody (1:1000; clone LNC1; catalog MAB318, Millipore/Chemicon International, Technology, Billerica, MA, USA). Unbiased stereological counting of nigral THON neurons as well as striatal optical density measurement were performed using Exploranova Mercator (Explora Nova, La Rochelle, France).
Validation	We used commercial antibodies. All of them were quality controlled by the manufacturer. They are extensively validated in the NHP as referenced already in the mansucript (refs 62-65) Merck website reports more than 85 papers reporting its use.

Animals and other research organisms

Policy information about studies involving animals; ARRIVE guidelines recommended for reporting animal research, and Sex and Gender in Research

Laboratory animals	Data from 10 rhesus macaques and one fascicularis macaque (aged 4-6 yo)
Wild animals	None.
Reporting on sex	All the animals were males.
Field-collected samples	No field collected samples were used in the study
Ethics oversight	Experiments were approved by the Institutional Animal Care and Use Committee of Bordeaux (CE50, France) under the license number 50120102-A and performed in accordance with the European Union directive of 22 September 2010 (2010/63/EU) on the protection of animals used for scientific purposes in an AAALAC-accredited facility.

Note that full information on the approval of the study protocol must also be provided in the manuscript.

Clinical data

Policy information about clinical studies

All manuscripts should comply with the ICMJE guidelines for publication of clinical research and a completed CONSORT checklist must be included with all submissions.

Clinical trial registration	PREDI-STIM clinical study: clinicaltrials.gov ID NCT02360683 Motor Network in Parkinson's Disease and Dystonia: Mechanisms of Therapy clinical trial: clinicaltrials.gov ID NCT03582891 STIMO-PARK clinical trial: clinicaltrials.gov ID NCT04956770
Study protocol	PREDI-STIM clinical study: clinicaltrials.gov/ct2/show/NCT02360683 Motor Network in Parkinson's Disease and Dystonia: Mechanisms of Therapy clinical trial: clinicaltrials.gov/ct2/show/NCT03582891 STIMO-PARK clinical trial: clinicaltrials.gov/ct2/show/NCT04956770
Data collection	PREDI-STIM clinical study Patient recruitment and data collection took place between Sept 2015 and January 2019 at the Neurology Dpt of the Bordeaux University Hospital. We recorded whole-body kinematics using a Vicon motion-capture system (Vicon, Oxford, UK). We attached 34 reflective markers (26 on the legs, arms and trunk, and 8 on the head and wrists) on the surface of the skin of the participants to cover all key body joints (foot, ankle, knee, hip, shoulder, elbow, hand, neck and head, as well as spinal vertebrae T10 and C7). Motor Network in Parkinson's Disease and Dystonia: Mechanisms of Therapy clinical trial The period of recruitment and data collection for the two patients were from June 2019 – December 2019. The data were collected at the Human Performance Center at Mission Bay Campus at the University of California San Francisco. Data was collected from two people with Parkinson's disease that were enrolled in the clinical trial. They were recruited from a population referred for implantation of deep brain stimulators for PD. Before recruitment, they were evaluated by a movement disorders neurologist and met diagnostic criteria for PD and by a neuropsychologist to exclude major cognitive impairment or untreated mood disorder. Inclusion criteria included motor fluctuations with prominent rigidity and bradykinesia in the off-medication state, baseline off-medication MDS-UPDRS-III scores between 20 and 80, greater than 30% improvement in MDS-UPDRS-III on medication than off of medication and absence of significant cognitive impairment (score of 20 or above on the Montreal Cognitive Assessment). The full IDE application (G180097) and study protocol have been shared with other researchers via the Open Mind initiative (https://openmind-consortium.github.io). After enrollment, participants underwent bilateral placement of cylindrical quadripolar deep brain stimulator leads into the STN (Medtronic model 3389; 1.5-mm contact length and 2.0-mm intercontact spacing), bilateral placement of quadripolar cortical paddles into the subdural space over the cortical area that included the motor cortex (Medtronic model 0913025; 4-mm contact diameter and 10-mm intercontact spacing) and bilateral placement of investigational sensing IPGs in a pocket over the pectoralis muscle (Medtronic Summit RC+S model B35300R). The IPG on each side was connected to two leads by 60-cm lead extenders (Medtronic model 37087). The Summit RC+S IPG is a 16-channel device that, through the use of its application programming interface, allows researchers to record four bipolar time domain channels (250/500 Hz) or two channels at 1,000 Hz62,63. For all research functions, including configuring and initiating sensing and developing embedded or distributed adaptive DBS, investigators controlled the device by writing software in C# within the device API, accessed using a 'research development kit' (RDK; Medtronic model 4NR013) provided by the manufacturer. We wrote a software application to configure and initiate streaming data from two RC+S devices simultaneously (available at https://openmind-consortium.github.io). We have analysed recordings collected with P2 and P3 during one session of overground walking in a corridor, and with P2 during one session of walking on a treadmill. In those sessions, the participants were on their regular levodopa therapy and their DBS was kept off. Cortical field potentials were sampled at 500 Hz. We simultaneously recorded video using a camera and full body kinematics using a set of IMU sensors distributed across major anatomical landmarks. STIMO-PARK clinical trial Recruitment and data analyses ranged between August 2021 and Dec 2022. Data collected from P1, the first and only participant, was enrolled in the study by October 2021. He was a 61-year-old male at time of enrollment. He has been diagnosed with Parkinson's Disease at the age of 36 and implanted with DBS at the age of 44. He is currently in stage 3 of the Hoen-Yahr scale. He experiences fluctuations in his gait pattern and lower limb symptoms typical of later stages of PD, including slowness, asymmetry, rigidity, small steps, flexed posture. Before being implanted with the EES system, during the 6-minute walk test P1 was able to cover 433 meters with DBS turned on and during his regular levodopa intake, and 224 meters with DBS turned off and with the last levodopa intake the evening before. His MDS-UPDRS motor examination scores (part III) in these two states were 20 and 47, respectively. He started to experience freezing-of-gait over the last decade, which greatly impacted his independence and quality of life. Before participation in the study, he reported 4 falls per day on average due to freezing-of-gait. Following the enrolment, we performed a CT scan of his torso and a structural MRI scan of his spine to generate a personalized anatomical model of his spine. Following the pre-surgical assessments, P1 was implanted with the spinal EES neurostimulation system. After the surgery, P1 was transferred to the neurosurgery ward for recovery. P1 then went back to the hotel for a one-week recovery period. After recovery, the study protocol continued with a 1-month period for configuration of EES protocols and sequences, and a 3-month period of physiotherapist-assisted rehabilitation during 1–3-hour sessions taking place 2 to 3 times per week. The rehabilitation program is personalized based on the participants' needs and improvements. We collected data from P1 through the entire duration of the study protocol.
Outcomes	PREDI-STIM clinical study Primary Outcome Measures : - Improve of quality of life on PDQ39>20% [Time Frame: 1 year] Secondary Outcome Measures : - Percentage of motor score MDS-UPDRS III improve under stimulation [Time Frame: 1 year] - Socio-familial evolution (institutionalization) [Time Frame: 1, 3 and 5 years] - Clinical Global Impression of Patient by 7-point scale with the CGI-scale [Time Frame: 1, 3 and 5 years]

- Clinical Global Impression of doctor by 7-point scale with the CGI-scale [Time Frame: 1, 3 and 5 years]
- Death [Time Frame: 1, 3 and 5 years]
- Cognitive function with a neuropsychological examination with Mattis scale, Wisconsin Card Sorting test, Stroop test, , verbal episodic memory test with 16 items, phonemic and semantic verbal fluency, Boston naming test (15 items), clock drawing and Benton line orientation task [Time Frame: 1, 3 and 5 years]
- Behavior test [Time Frame: 1, 3 and 5 years]
- ECMP scale of Ardouin 2009, Hamilton depression scale, Anxiety Hamilton scale, Lille Apathy Rating Scale, QUIP questionnaire, Billieux Impulsivity Scale, Hallucination questionnaire of Miami
- Motor response rates to Levodopa with the difference of the motor handicap measured by MDS UPDRS part III before and after an acute L-dopa challenge [Time Frame: 1, 3 and 5 years]
- Non-motor functions evaluated by a numerical evaluation scale [Time Frame: screening and at 1, 3 and 5 years]

Motor Network in Parkinson's Disease and Dystonia: Mechanisms of Therapy clinical trial
Primary Outcome Measures :
- Duration of 'on' stimulation time without dyskinesia from motor diaries in adaptive compared to standard open loop stimulation. (Parkinson's disease patients) [Time Frame: Comparison will use data from the testing of open and closed-loop stimulation during chronic adaptive DBS testing at home.]
- Karolinska Sleepiness Scale [Time Frame: Through study completion, up to 4 years]
- Psychomotor vigilance task (PVT) [Time Frame: Through study completion, up to 4 years]
- Positive and Negative Affect Schedule (PANAS-SF) [Time Frame: Through study completion, up to 4 years]

Secondary Outcome Measures :
- The Unified Parkinsons Disease Rating Scale (UPDRS) III scores off of medication in adaptive compared to standard open-loop stimulation. [Time Frame: Comparison will use data from the testing of open and closed-loop stimulation during chronic adaptive DBS testing at home.]
- Schwab England scale in adaptive compared to standard open loop stimulation. [Time Frame: Comparison will use data from the testing of open and closed-loop stimulation during chronic adaptive DBS testing at home.]
- Hoehn and Yahr Staging in the medication 'on' state in adaptive compared to standard open loop stimulation.
[Time Frame: Comparison will use data from the testing of open and closed-loop stimulation during chronic adaptive DBS testing at home.]
- The patient' quality of life report (PDQ-39) in adaptive compared to standard open loop stimulation. The PDQ39 yields a score between 0 to 100, where a higher score indicates more health problems. [Time Frame: Comparison will use data from the testing of open and closed-loop stimulation during chronic adaptive DBS testing at home.]
- Patient's Global Impression of Change (PGIC) in adaptive compared to standard open loop stimulation. [Time Frame: Comparison will use data from the testing of open and closed-loop stimulation during chronic adaptive DBS testing at home.]
- Total Electric Energy Delivered (TEED) by the pulse generator in adaptive compared to standard open loop stimulation.
[Time Frame: Comparison will use data from the testing of open and closed-loop stimulation during chronic adaptive DBS testing at home.]
- Resting state EEG Recording [Time Frame: Through study completion, up to 4 years]

STIMO-PARK clinical trial
Primary Outcome Measures :
- Occurence of all SAEs and AEs deemed or related to study procedure or to the study investigational system [Time Frame: Through study completion, an average of 6 months]

Secondary Outcome Measures :
- EMG measurements of muscle recruitment in response to stimulation of increasing amplitudes for different contact configurations [Time Frame: At baseline and during the 5-month TESS-supported rehabilitation phase]
- Maximum voluntary contraction (MVC) of single joints [Time Frame: At baseline and during the 5-month TESS-supported rehabilitation phase]
- Muscle Fatigue Test [Time Frame: At baseline and during the 5-month TESS-supported rehabilitation phase]
- 10-meter walk test [Time Frame: At baseline and during the 5-month TESS-supported rehabilitation phase]
- 6 minute walk test [Time Frame: At baseline and during the 5-month TESS-supported rehabilitation phase]
- Timed up and Go test and its cognitive version, as custom-made FOG circuit [Time Frame: At baseline and during the 5-month TESS-supported rehabilitation phase]
- Kinematic analysis [Time Frame: At baseline and during the 5-month TESS-supported rehabilitation phase]
- Mini Balance Evaluation Systems Test (mini-BESTest) [Time Frame: At baseline and during the 5-month TESS-supported rehabilitation phase]
- Movement Disorders Society Unified Parkinson's Disease Rating Scale (MDS-UPDRS) [Time Frame: At baseline and during the 5-month TESS-supported rehabilitation phase]

Magnetic resonance imaging

Experimental design

Design type	Participant P1 was positioned supine with arms at their side.
Design specifications	Resting state structural MRI.
Behavioral performance measures	The participant did not perform any behavioral experiment while being scanned (no fMRI was acquired on the human participant). The MRI scan was an anatomical structural volume image with participant at rest.

Acquisition

Imaging type(s)	Structural MRI
Field strength	1.5T
Sequence & imaging parameters	2D sagittal T2-weighted turbo spin-echo
Area of acquisition	Thoracolumbar spine

Diffusion MRI ☐ Used ☒ Not used

Preprocessing

Preprocessing software	MRI image acquisition did not require a preprocessing software. No preprocessing software was used.
Normalization	MRI image acquisition did not require normalization. Normalization was not used.
Normalization template	MRI image acquisition did not require a normalization template. Normalization template was not used.
Noise and artifact removal	MRI image acquisition did not require neither noise nor artifact removal. Neither noise nor artifact removal was used.
Volume censoring	MRI image acquisition did not require volume censoring. Volume censoring was not used.

Statistical modeling & inference

Model type and settings	We did not perform any functional MRI experiments. Therefore, neither statistical modeling nor inference was carried out.
Effect(s) tested	We did not perform any functional MRI experiments. Therefore, neither statistical modeling nor inference was carried out.

Specify type of analysis: ☐ Whole brain ☐ ROI-based ☐ Both

Statistic type for inference (See Eklund et al. 2016)	We did not perform any functional MRI experiments. Therefore, neither statistical modeling nor inference was carried out.
Correction	We did not perform any functional MRI experiments. Therefore, neither statistical modeling nor inference was carried out.

Models & analysis

n/a	Involved in the study
☒	☐ Functional and/or effective connectivity
☒	☐ Graph analysis
☒	☐ Multivariate modeling or predictive analysis